The University of Maine
DigitalCommons@UMaine

Electronic Theses and Dissertations | Fogler Library

Spring 4-20-2022

Optimization of Synthetic Mooring Systems for Floating Offshore Wind Turbines

William M. West
University of Maine, william.west@maine.edu

Follow this and additional works at: https://digitalcommons.library.umaine.edu/etd

 Part of the Ocean Engineering Commons

Recommended Citation

West, William M., "Optimization of Synthetic Mooring Systems for Floating Offshore Wind Turbines" (2022). *Electronic Theses and Dissertations*. 3578.
https://digitalcommons.library.umaine.edu/etd/3578

This Open-Access Thesis is brought to you for free and open access by DigitalCommons@UMaine. It has been accepted for inclusion in Electronic Theses and Dissertations by an authorized administrator of DigitalCommons@UMaine. For more information, please contact um.library.technical.services@maine.edu.

OPTIMIZATION OF SYNTHETIC MOORING SYSTEMS FOR FLOATING OFFSHORE WIND TURBINES

By

William West

B.S. University of Maine, 2017

M.S. University of Maine, 2019

A DISSERTATION

Submitted in Partial Fulfillment of the

Requirements for the Degree of

Doctor of Philosophy

(in Mechanical Engineering)

The Graduate School

The University of Maine

May 2022

Advisory Committee:

Dr. Andrew Goupee, Donald A. Grant Associate Professor of Mechanical Engineering, Advisor

Dr. Anthony Viselli, Chief Engineer Offshore Energy Programs, Co-Advisor

Dr. Habib Dagher, Director of the Advanced Structures and Composites Center, Bath Iron Works Professor of Civil Engineering

Dr. Richard Kimball, Presidential Professor in Ocean Engineering and Energy

Dr. Matthew Hall, Senior Engineer, National Renewable Energy Laboratory

© 2022 William West

All Rights Reserved

OPTIMIZATION OF SYNTHETIC MOORING SYSTEMS FOR FLOATING OFFSHORE WIND TURBINES

By William West

Dissertation Advisors: Dr. Andrew Goupee and Dr. Anthony Viselli

An Abstract of the Dissertation Presented
in Partial Fulfillment of the Requirements for the
Degree of Doctor of Philosophy
(in Mechanical Engineering)
May 2022

As the floating offshore wind industry matures it has become increasingly important for researchers to determine the next generation materials and processes that will allow platforms to be deployed in intermediate (50-85 m) water depths which challenge the feasibility of traditional catenary chain mooring systems and fixed-bottom jacket structures. One such technology, synthetic ropes, has in recent years come to the forefront of this effort. A significant challenge of designing synthetic rope moorings is capturing the complex physics of the materials which exhibit viscoelastic and nonlinear elastic properties. Currently numerical tools for modeling the dynamic behavior of floating offshore wind turbines (FOWTs) are limited to mooring materials that lack these strain-rate dependent properties and have a linear tension-strain response. To address this limitation, a mooring modelling module, MoorDyn, which operates within the popular FOWT design and analysis program, OpenFAST, was modified to allow for nonlinear elastic mooring materials to add additional capabilities in the numerical tools. Simulations from the modified OpenFAST tool were then compared with 1:52-scale test data for a 6-MW FOWT Semi-submersible platform in 55m of water subjected to representative design load cases. A strong correlation between the simulations and test data was observed.

In addition to reducing the cost of the mooring systems, synthetic systems can also reduce the footprint compared to a chain catenary system which frees areas around the turbine

for other maritime uses such as commercial fishing. Both the mooring systems component cost and footprint are pertinent design criteria that lend themselves naturally to a multi-objective optimization routine. A new approach for efficiently screening the design space for plausible mooring systems that balance component cost and footprint using a multi-objective genetic algorithm is presented. This method uses a tiered-constraint method to avoid performing computationally expensive time-domain simulations of mooring system designs that are infeasible. Performance metrics for assessing the constraints of candidate designs are performed using open-source software such as Mooring Analysis Program (MAP++), OpenFAST and MoorDyn. A case study is presented providing a Pareto-optimal design front for a taut synthetic mooring system of a 6-MW floating offshore wind turbine.

As the wind industry develops larger turbines for offshore deployment the problems with stationkeeping systems are exacerbated. While turbines increase in size so do the loads on the turbine. Meanwhile the offshore sites available for leasing in the intermediate water depth are still available to developers regardless of turbine and platform size. This complicates the process of designing mooring systems for these larger systems and emphasizes the importance of having a good methodology for automating this process. The final portion of this dissertation presents a method for mapping objectives for a multi-objective genetic algorithm to obtain the relationship between mooring system minimum cost and mooring radius. This work implements and expands on the aforementioned tiered-constraint evaluation scheme. These techniques are used to find the most cost-effective mooring designs for a 15-MW FOWT with a semi-taut mooring system over a range of mooring radii. New components and constraints are added to the system to allow the optimizer to find realistically deployable designs with reasonably accurate cost estimates.

ACKNOWLEDGEMENTS

There are a lot of people who were instrumental in my education thus far. First is my father Donald West who has continuously preached the importance of education to me. Without his encouragement I likely would not have pursued this path, so his support from my childhood has been exceedingly important.

Along this journey there have been many staff at the Advanced Structures and Composites Center who have provided assistance. The funding for many, if not all, of the projects I have worked on are due to the leadership of Dr. Anthony Viselli and Dr. Habib Dagher. I have also been privileged to work with many talented engineers at the center over the last 5 years including Chris Allen, Dr. Jacob Ward, Hannah Allen, and Dr. Spencer Hallowell.

Over the past 9 years I have been privileged to learn theory and fundamentals from great instructors in both the Mechanical Engineering and Civil Engineering Departments at the University of Maine. Originally it was instructors like Professor Senthil Vel who encouraged me to consider graduate school. During my graduate career instructors like Professor Bill Davids, Professor Krish Thiagarajan and Professor Richard Kimball have all taught courses related to numerical modelling and offshore design that have assisted with my research. I would also like to thank Dr. Matthew Hall for volunteering to be the external reader on my committee.

Last but certainly not least I would like to recognize my academic advisor Dr. Andrew Goupee. Andy has always had his door open for me to drop by any time, and is willing to assist in any way that he can. I cannot imagine having a better mentor over the last five years.

TABLE OF CONTENTS

LIST OF TABLES

LIST OF FIGURES

CHAPTER 1

INTRODUCTION

Overall, this dissertation aims to further the knowledge of synthetic mooring systems which may be key for floating offshore wind turbine (FOWT) installations moving forward. As many governments have set goals for zero net emissions in the 2050's and 2060's it has become clear that wind energy is going to be a big part of the solution. Wind energy capacity worldwide is 778 GW and at this point of time offshore wind is only 36.2 GW, a small percentage of the overall global capacity [1]. However, as time goes on offshore wind is projected to grow rapidly. In 2019 the total installed offshore wind capacity in the United States was 30 MW. In the next ten years that number is projected to grow to between 19,000 MW and 25,000 MW [2].

One of the major reasons offshore wind has gained so much interest among academia and industry is the quality of the wind resource. Figure 1.1 shows the windspeed at an elevation of 100m for the continental United States [3][4]. It can be observed from this figure that the offshore wind resource is significantly better than the land-based resource. The northeastern United States has one of the best resources for offshore wind. Unfortunately, many lease areas are in the so-called transitional water depth from 45m – 85m [5]. Figure 1.2 shows one such lease site located off the coast of Massachusetts [6]. The average water depth over this entire lease site is 50m which is firmly within the transitional water depth.

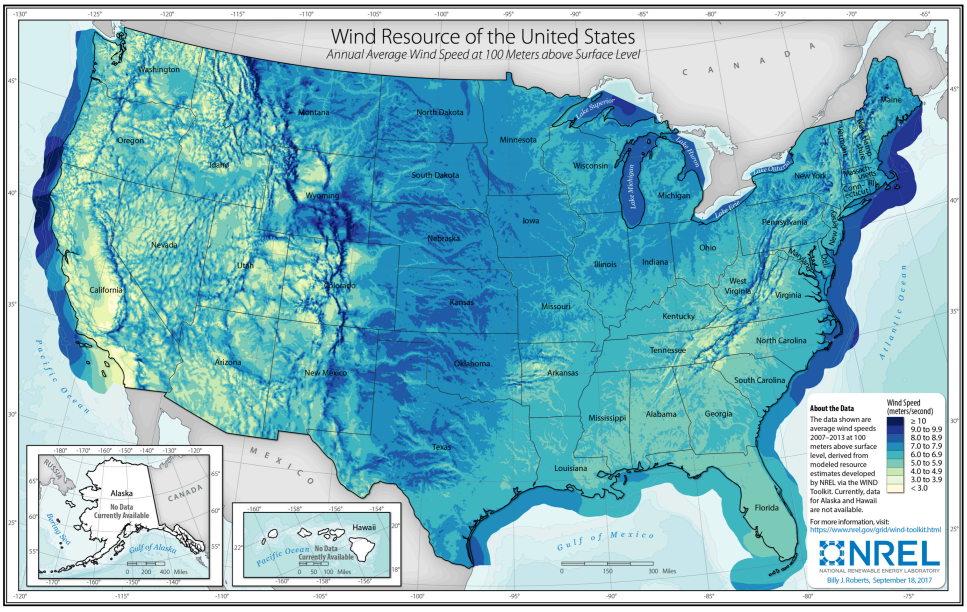

Figure 1.1. United States Wind Resource at 100m Elevation [3][4]

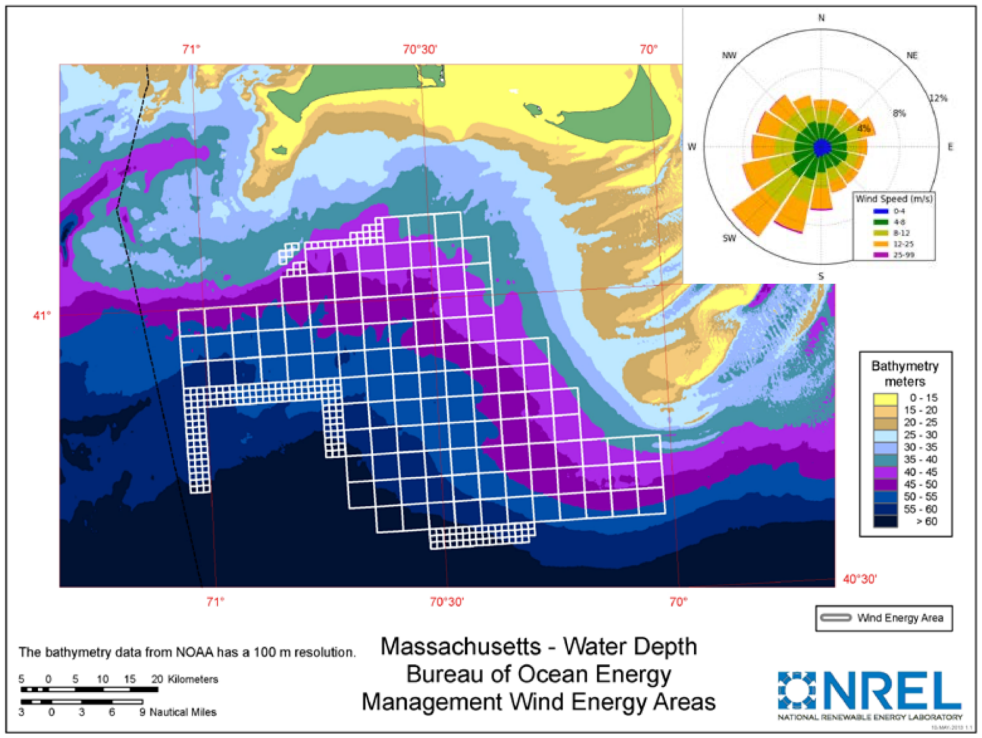

Figure 1.2. Bathymetry for a Lease Area off the Massachusetts Coast [6]

The transitional depth presents unique engineering challenges. In shallow water depths up to around 25 m traditional fixed bottom technology such as monopiles or truss structures can be used [5]. When the water depth becomes deeper the cost to engineer a fixed bottom structure becomes cost prohibitive. The technology of choice for water depths greater than about 85 m are floating platforms with a chain catenary system to keep the vessel in place. Traditional chain catenary systems provide a restoring force due to the weight of the chain. For these systems to be effective in shallow waters there needs to be a large mass of chain which is cost ineffective. Synthetic moorings have emerged as a promising technology to unlock FOWTs in the transitional depth [7]. Synthetic mooring systems provide a restoring force through the extensional properties of the fiber ropes [8]. The mechanics described above of a chain catenary mooring system and taut synthetic mooring system are illustrated in Figure 1.3. Although this technology has been used extensively in offshore oil and gas applications it has only recently gained traction in the floating offshore wind industry.

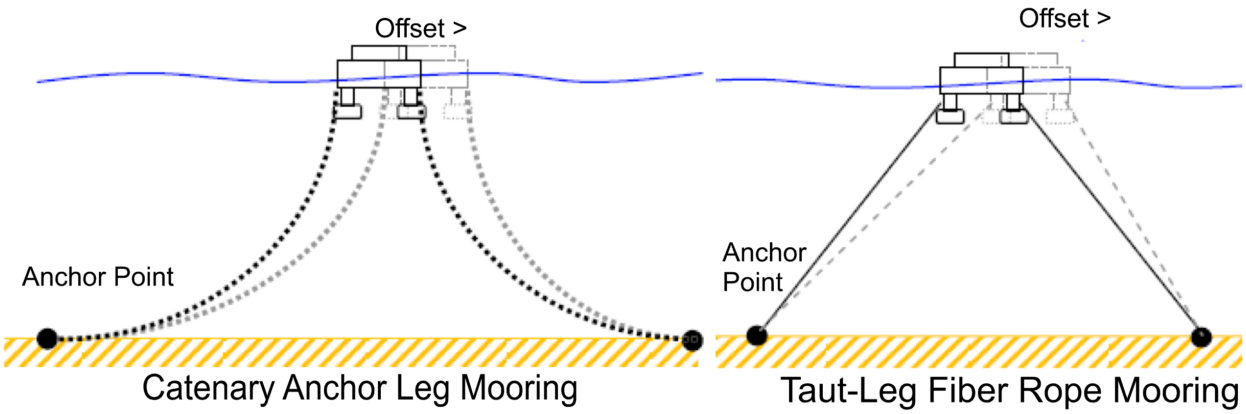

Figure 1.3. Comparison of a Chain Catenary System and Taut Synthetic System [8]

While synthetic ropes are a promising solution for deploying FOWT installations in the intermediate water depths there is still a lot of research necessary before the technology is ready for commercial use. One of the biggest challenges is modelling the behavior of synthetic ropes

which exhibit complex viscoelastic properties. Many of the building and classing agencies at this point recommend taking a simplified and conservative modelling approach but leave the door open to more complex solutions. The first part of this dissertation aims to begin addressing that problem by updating the numerical modelling software to accept mooring line inputs with general non-linear tension-strain responses.

The second issue is with the design of synthetic rope systems. At this point synthetic rope technologies have been used in offshore oil and gas, but the applications were very different. Those designs used polyester mooring lines in deep-water leading to design criteria and modelling techniques that are overly conservative. It is also unclear what constitutes an efficient synthetic design for shallow water applications. The third and fourth chapters of this dissertation set out to develop a methodology for screening the mooring system design space to identify initial candidate designs.

Specific deliverables from the work covered in this dissertation include:

- Modifying and expanding an open source FOWT design and analysis software, OpenFAST, specifically its MoorDyn module, to allow mooring materials with nonlinear tension-strain relationships to be modeled
- Validating and verifying the modified version of the OpenFAST MoorDyn module through 1:52-scale testing in the Advanced Structures and Composite Centers Harold Alfond Wind and Wave testing basin
- Developing a novel ‘tiered constraint’ method for evaluating computationally expensive constraints for a multi-objective genetic algorithm
- Verifying ways to expediate computationally expensive FOWT time-domain simulations in OpenFAST by extrapolating mooring line design values using a generalized extreme

value fit, pushing the limits of the MoorDyn and OpenFAST timesteps, and applying low-frequency loads on the system as a mean load

- Developing a novel method for optimizing mooring radius footprint and cost which applied to taut mooring system designs for a 6-MW FOWT
- Generalizing the mooring design optimization method to obtain the minimum cost mooring design over a range of footprints inclusive of additional realism in the mooring system geometry and cost estimates applied to semi-taut mooring system designs for a 15-MW FOWT

This dissertation is organized as follows: Chapter 2 which forms the basis of the publication titled "A Floating Wind Turbine Model Test to Verify a MoorDyn Modification for Nonlinear Elastic Materials" published in the Journal of Offshore Mechanics and Arctic Engineering. This Chapter gives an overview of the modifications that were done to MoorDyn. MoorDyn is a mooring modelling module within the popular opensource FOWT design and analysis tool OpenFAST. These modifications allow a user to input any arbitrary tension-strain relationship for a mooring material using a look up table. To validate and verify these changes a 1:52-scale 6-MW VolturnUS FOWT was tested in the Advanced Structures and Composites Center's (ASCC) Harold Alfond Wind and Wave (W^2) facility. The mooring system was a taut system based on a target nonlinear material that was approximated using a trilinear spring. The physical data developed in the basin was then compared to numerical models. A strong correlation between numerical models and physical tests were observed.

Chapter 3 which forms the basis of the publication titled "Development of a Multi-Objective Optimization Tool for Screening Designs of Taut Synthetic Mooring Systems to Minimize Mooring Component Cost and Footprint" published in the Journal *Modelling*. This

chapter outlines the development of a multi-objective genetic algorithm to screen the design space for feasible mooring designs. The novel aspect of this optimization routine is the 'tiered constraint' method developed to avoid running computationally expensive time-domain simulations of poor designs by screening out poor designs with more computationally efficient methods. This work also makes original contributions by exploring ways to predict the design load in the mooring system via extrapolation using a generalized extreme value fit and a smaller portion of time series data. To further save on computational time an extensive convergence problem was done to determine the relationship between the mooring line discretization, MoorDyn timestep, and OpenFAST timestep. This work was then used to develop taut synthetic mooring systems for a 6-MW FOWT. The results from this work showed that lower costed designs may be developed at the cost of larger turbine footprints.

Chapter 4 of this dissertation presents work on the development of a mapped objective method for use in a multi-objective optimization framework to determine the minimum-cost FOWT synthetic mooring system over a range of mooring radii. This work aims to implement many of the contributions from Chapter 3 while including more realistic mooring geometries that are practical to install, and updated mooring cost data by accounting for the sizing of the anchor. The entire process for determining the relationship between the mooring system cost and radius has been reformulated to use a mapped objective method. This method generalizes the method and ensures that the relationship between mooring cost and radius can be found when those two quantities are not necessarily competing, which can occur for certain configurations of interest. The chapter concludes by applying the techniques developed in both Chapters 3 and 4 to a next-generation 15-MW FOWT to determine the most cost-effective mooring setups over a range of

different radii. The results from this work showed across a suite of mooring radii the cost of the mooring systems would remain relatively constant.

The dissertation concludes by providing a summary of the key findings from each of the chapters. In addition, the summary outlines some recommendations for future work.

1.1. References

[1] IEA Wind TCP Annual Report 2020

[2] NREL. *2019 Offshore Wind Technology Data Update*; National Renewable Energy Laboratory: Golden, CO, USA, 2020.

[3] Draxl, C., B.M. Hodge, A. Clifton, and J. McCaa. 2015. *Overview and Meteorological Validation of the Wind Integration National Dataset Toolkit* (Technical Report, NREL/TP-5000-61740). Golden, CO: National Renewable Energy Laboratory.

[4] Draxl, C., B.M. Hodge, A. Clifton, and J. McCaa. 2015. "The Wind Integration National Dataset (WIND) Toolkit." *Applied Energy* 151: 355366.

[5] West, W. Design and Modelling of Synthetic Mooring Systems for Floating Offshore Wind Turbines. Master's Thesis, University of Maine, Orono, ME, USA, 2019.

[6] Musial, W., Parker, Z., Fields, M., Scott, G., Elliott, D., and Draxl, C. *Assessment of Offshore Wind Energy Leasing Areas for the BOEM Massachusetts Wind Energy Area*. United States: N. p., 2013. Web. doi:10.2172/1118096.

[7] Weller, S. D., Johanning, L., Davies, P., & Banfield, S. J. (2015). Synthetic mooring ropes for marine renewable energy applications. *Renewable Energy*, *83*, 1268–1278. https://doi.org/10.1016/j.renene.2015.03.058

[8] Flory, J. F., Banfield, S. J., Ridge, I. M. L., Yeats, B., Mackay, T., Wang, P., Hunter, T., Johanning, L., Herduin, M., & Foxton, P. (2016). Mooring systems for marine energy converters. In J. Zande, & B. Kirkwood (Eds.), *OCEANS 2016 MTS/IEEE Monterey, OCE 2016* [7761007] IEEE, Institute of Electrical and Electronics Engineers. https://doi.org/10.1109/OCEANS.2016.7761007

CHAPTER 2

A FLOATING WIND TURBINE MODEL TEST TO VERIFY A MOORDYN MODIFICATION FOR NONLINEAR ELASTIC MATERIALS

2.1. Overview and Comments

This chapter forms the basis of the paper titled "A Floating Wind Turbine Model Test to Verify a MoorDyn Modification for Nonlinear Elastic Materials" authored by William M. West, Andrew J. Goupee, Christopher K. Allen and Anthony M. Viselli. This paper was submitted to the Journal of Offshore Mechanics and Arctic Engineering on April 20th, 2021 and was accepted for publication on November 5th 2021. The modified OpenFAST executable file outlined and verified in this paper were used to generate the results presented in Chapter 3. The design of the experiment, data analysis and numerical modelling was done by William M. West. Design of the trilinear spring, experimental setup, calibration and data acquisition was conducted by Advanced Structures and Composites Center Staff in the W^2 facility.

2.2. Abstract

As the floating offshore wind industry matures it has become increasingly important for researchers to determine the next generation materials and processes that will allow platforms to be deployed in intermediate (50-85 m) water depths which challenge the efficiency of traditional catenary chain mooring systems and fixed-bottom jacket structures. One such technology, synthetic ropes, has in recent years come to the forefront of this effort. A significant challenge of designing synthetic rope moorings is capturing the complex physics of the materials which exhibit viscoelastic and nonlinear elastic properties. Currently numerical tools for modeling the dynamic behavior of FOWTs are limited to mooring materials that lack these strain-rate dependent properties and have a linear tension-strain response. In this paper a mooring modeling

module, MoorDyn, which operates within the popular FOWT design and analysis program, OpenFAST, was modified to allow for nonlinear elastic mooring materials to address one of these shortcomings in the numerical tools. Simulations from the modified OpenFAST tool were then compared with 1:52-scale test data for a 6-MW FOWT Semi-submersible platform in 55m of water subjected to representative design load cases. A strong correlation between the simulations and test data was observed.

2.3. Introduction

When designing floating offshore structures, access to numerical models for design and analysis is of paramount importance. To verify these models' accuracy they are often validated using experimental data with accurate and scaled wind and wave environments [1][2]. One such model that sees extensive use in research and industry is the National Renewable Energy Laboratory's (NREL's) OpenFAST [3]. OpenFAST is a comprehensive open-source software for modeling the coupled dynamic response of floating offshore wind turbines (FOWTs) subject to wind and wave loads that is designed to be interfaced with other modules, and easily modified and expanded to fit researchers' needs. In this paper, an existing module within OpenFAST, MoorDyn, has been modified in a way that allows mooring materials with a non-linear tension-strain response to be simulated, and lays a groundwork for more complex modification to be made later.

The offshore wind industry has often taken cues from the offshore oil and gas industry for advancing technology such as the advent of floating platforms [4]. Another example is for the platform mooring systems. Initially, chain catenary systems dominated, but as the offshore oil and gas industry pursued deeper waters chain became both prohibitively expensive and heavy [5]. Researchers at this time began to investigate if synthetic ropes made of materials such as

nylon and polyester could potentially be used to lower the cost and allow drilling in deeper waters.

Currently this trend is repeating itself within the floating offshore wind industry in an effort to cut capital costs [6]. However, this is not the only potential benefit as synthetic mooring systems could allow platforms to be deployed in shallower water and reduce the footprint of the mooring system. Synthetic systems do not come without their challenges, namely the nonlinear tension-strain relationship and viscoelastic response associated with synthetic ropes. Various classing agencies such as Det Norske Veritas (DNV), the American Petroleum Institute (API) and ABS have all suggested ways to simplify modeling these materials, which at this point is accomplished through multiple simulations with line stiffness based on the loads in the line or a bilinear static-dynamic model fit [7]. The DNV has also suggested that a more complex model using various springs and dashpots arranged in parallel and series may be used to directly simulate the viscoelastic response of the rope instead of estimating an appropriate stiffness [8]. Although OpenFAST can currently be configured with three distinct mooring modules, they all require mooring materials with a linear tension-strain relationship. This work is a first step towards enabling more complex spring-dashpot style systems by addressing one piece of the synthetic rope modelling challenge, the nonlinear elastic tension-strain relationships. In addition, these modifications will also allow methods requiring nonlinear elastic tension-strain relationships, such as the ABS static-dynamic model, to be implemented.

In this work one of the mooring modules compatible with OpenFAST, MoorDyn, is modified to allow modeling with nonlinear materials, such as synthetic ropes, by allowing the user to input nonlinear tension-strain data in the form of a lookup table. Second, a 1:52-scale model of the University of Maine's VolturnUS FOWT with a synthetic mooring system designed

to be deployed in a 55m water depth was tested in the Harold Alfond Wind and Wave (W^2) Basin. Lastly, data generated from this test campaign was used to verify the modifications made to MoorDyn.

This paper is organized as follows: First, the modifications made to MoorDyn to allow for nonlinear tension-strain material relationships will be outlined. Second, a description of the test setup including properties of the physical model and a description of the wind and wave environments will be presented. Next, standard test cases will be performed to verify that the physics of the physical model are being represented correctly in the numerical model, then a key design load case will be presented to assess the changes made to MoorDyn.

2.4. Modifications to MoorDyn

MoorDyn was selected as the mooring module within OpenFAST to be modified and enhanced for two main reasons. First, MoorDyn is one of the modules that models the inertia of the line and hydrodynamic loading on the line, and second, MoorDyn uses the lumped-mass method which is formulated independent of the line stiffness and lends itself to this enhancement. For the lumped-mass approach a mooring line is discretized into a number of "lumped masses" which are connected by massless springs and dampers to model the stiffness and internal damping in the line material [9]. With this approach there is not any assumption about the tension-strain response of the line being linear and the relationship between strain and stress can be specified in a more general way. In addition to the internal line forces represented by springs and dampers, external line forces such as buoyancy, gravity and both inertial and viscous fluid forces are included in the formulation. Using the applied internal and external forces the lumped mass equations of motion can be numerically integrated through time to obtain

the velocity and position of each mass. Then, using the position of the lumped masses the fairlead and anchor tensions in the line can be computed.

To modify MoorDyn the Fortran version of Microsoft Visual Studio was used. This software allowed the MoorDyn Fortran source code to be opened, modified, and then recompiled into an executable file. In the original MoorDyn formulation a line stiffness is specified in the input file. The position of each lumped mass is then used to find the strain in the segment, and the strain is multiplied by the line stiffness to obtain the tension in the segment. Staying consistent with other modules in OpenFAST, MoorDyn was modified to accept a line properties file which contains a table of strains and tensions that represent the tension-strain relationship for the synthetic line material. As OpenFAST is initialized these tables of strain and tension are read into MoorDyn and can be linearly interpolated to determine the line tension for any strain. This generic relationship also opens the possibility for designers to model other nonlinear elastic synthetic rope mooring line models, such as the bilinear static-dynamic model described by ABS in *The Application of Fiber Rope in Offshore Mooring*. While the MoorDyn modifications presented in this work can model a synthetic rope with this ABS recommended approach, a more generic nonlinear mooring line is used in this testing campaign.

In MoorDyn the forces applied to a lumped mass are represented by a vector. Originally, the line axial strain vector for a line segment would be directly mapped onto the internal line tension vector by multiplying the axial strain vector by the line stiffness. Mathematically this is represented in Equations (2.1.) and (2.2.):

$$\boldsymbol{T} = EA\boldsymbol{\varepsilon} \tag{2.1.}$$

$$\boldsymbol{\varepsilon} = \left(\frac{1}{l} - \frac{1}{|\boldsymbol{r}_{i+1} - \boldsymbol{r}_i|}\right)(\boldsymbol{r}_{i+1} - \boldsymbol{r}_i) \tag{2.2.}$$

Where: $\boldsymbol{T}$ is the tension vector in the line segment
EA is the line stiffness
$\boldsymbol{\varepsilon}$ is the axial strain vector in the line segment
l is the unstretched length of the line segment
$\boldsymbol{r}$ is the position of the i^{th} lumped mass

This approach however will not work for a generic nonlinear tension-strain relationship. Instead, the magnitude of the line axial strain vector is resolved by taking the Euclidean norm to determine the strain in a segment of line. The magnitude of the tension in a line segment is determined from the line segment strain via interpolation of the tension-strain relationship specified by the user. Finally, the segment tension magnitude is multiplied by the normalized axial strain vector to obtain the internal line tension components as shown in Equation (2.3.) and Equation (2.4.) where summation is implied over repeated indices:

$$\boldsymbol{T} = T_i e_i \tag{2.3.}$$

Where: e_i is the basis vector for the 1, 2 or 3 direction
T_i is the line tension component in the 1, 2 or 3 direction

$$T_i = \frac{\varepsilon_i}{\sqrt{\varepsilon_j \varepsilon_j}} \hat{T} \tag{2.4.}$$

Where: ε_i is the axial strain in the 1, 2 or 3 direction
$\hat{T}$ is the internal line tension in a segment interpolated from the tension strain relationship using the magnitude of strain $\sqrt{\varepsilon_j \varepsilon_j}$ in the line segment

2.5. Description of the Experiment

1:52-scale model testing was performed at the Harold Alfond W^2 Ocean Engineering Laboratory, housed at the University of Maine's Advanced Structures and Composites Center. This lab houses a 30 meter by 9 meter wave basin equipped with a 16 paddle wave maker

designed for doing scale model testing of offshore structures. In addition to the wave basin the W^2 also houses a 6 meter by 5 meter open jet wind tunnel which makes this facility well equipped for handling scale model testing of FOWTs. This section will serve as a description of the experimental setup including environmental loading, FOWT gross properties, and mooring system properties. All properties presented in this section and all results, unless otherwise noted, are specified at full scale.

2.5.1. Coordinate System

To capture the rigid body kinematics of the FOWT a Qualysis Oqus [10] optical tracking system with three infrared cameras was used. These cameras are used in conjunction with reflective markers on both the platform and nacelle to track the six rigid-body degrees of freedom of the FOWT platform.

Both the coordinate system used by the Qualisys system and the coordinate system used in OpenFAST have been made the same for convenience. All quantities in OpenFAST are referenced about the still water line (SWL) with positive heave defined as above the SWL. The surge axis is defined as positive in the direction of wind and wave propagation, meaning environmental loading applied at a heading corresponding to the positive surge direction will lead to both a positive surge and pitch displacement. All other coordinates are defined according to the right-hand rule. A schematic of this coordinate system is presented in Figure 2.1.

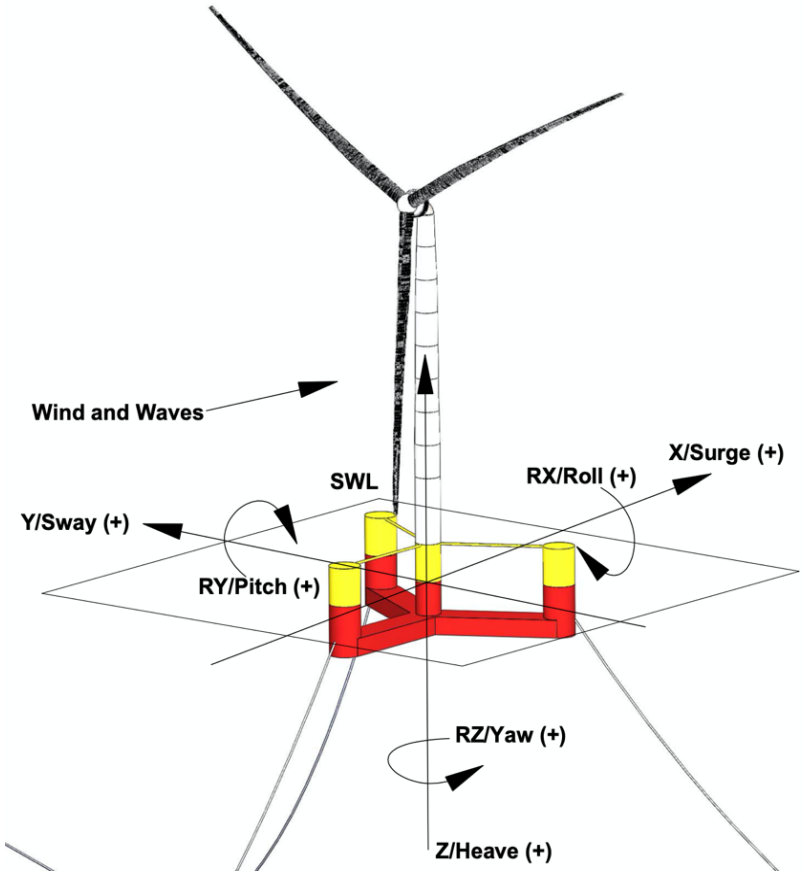

Figure 2.1. Experiment and OpenFAST Coordinate System

2.5.2. Environmental Loading

There were two load cases applied to the turbine for testing. The first a white noise wave, and the second a design load case (DLC) 1.6. DLCs for FOWTs are described within the ABS *Guide for Building and Classing Floating Offshore Wind Turbine Installations* [11] and IEC 6400-1-3 [12] classifications. White noise is a broadband wave in which a constant power is applied across a suite of different wave frequencies. This type of loading is important to apply during a scale model test as it is generally used to compute the response amplitude operator (RAO) of the physical model which is useful for understanding the physics of the tested system and performing model correlation studies. The RAOs of a floating platform represent the magnitude of a platform's response due to linear waves at a given frequency. The JONSWAP

wave spectrum for DLC 1.6 as well as the significant wave height of the white noise wave, and the rated wind speed for the turbine are presented in Table 2.1. The sea state power spectral density (PSD) for the white noise wave and DLC 1.6 are presented in Figure 2.2. and Figure 2.3. respectively.

Table 2.1. Environmental Loading

Wave Case	Significant Wave Height (Hs)	Period (s)	Shape Factor	Wind Speed (m/s)	Reference Height (m)
White Noise	8.5	5-25	N/A	-	-
DLC 1.6	8.5	13.1	2.75	11.5	100

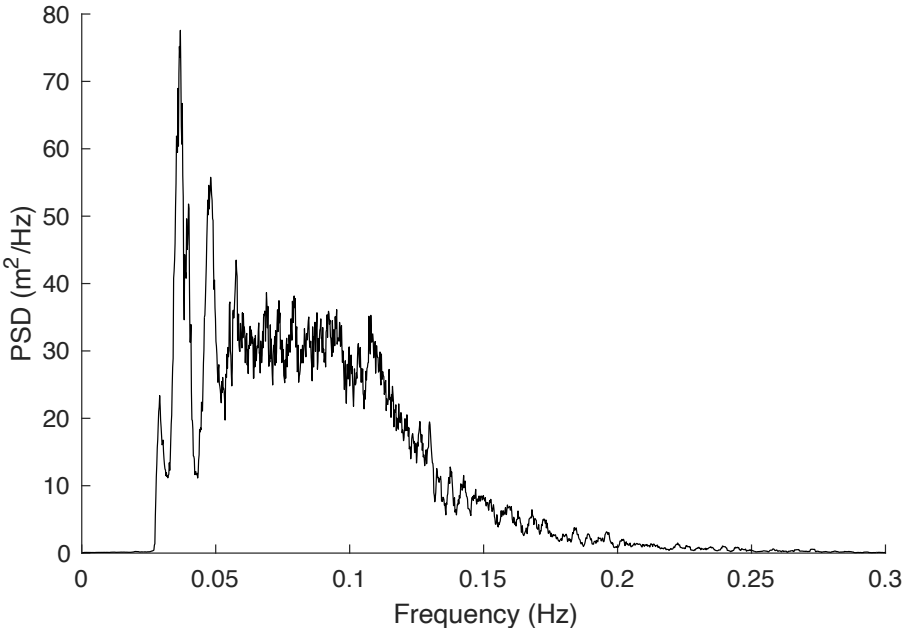

Figure 2.2. White Noise Wave PSD

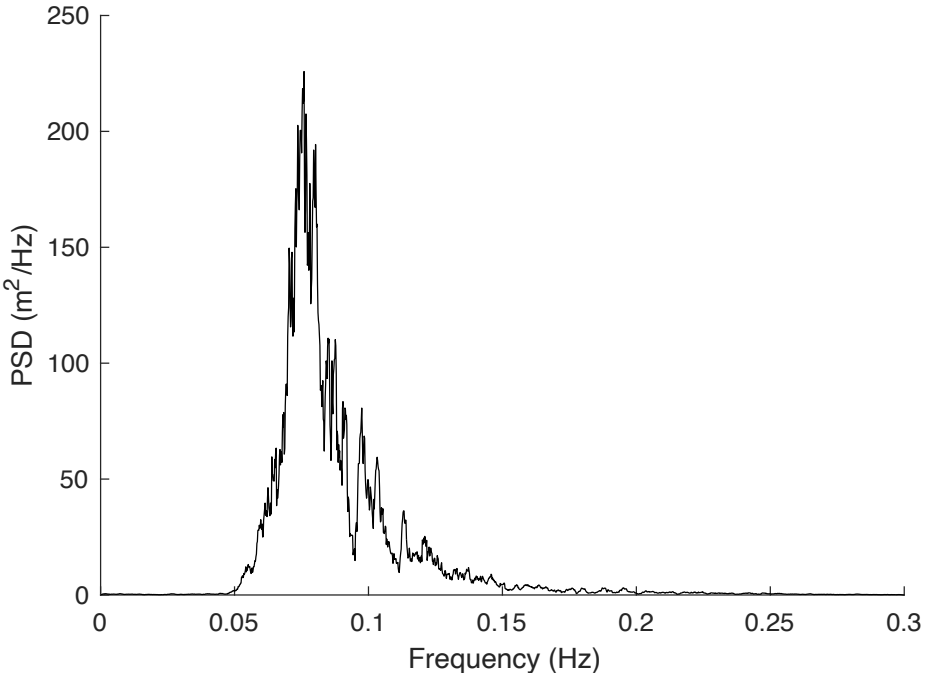

Figure 2.3. DLC 1.6 Wave PSD

The ABS/IEC design case chosen for this experiment was based on environmental wind and wave loading data gathered from the University of Maine's test site at Monhegan Island in the Gulf of Maine [13]. The design load case chosen for this test was DLC 1.6, power production at the turbine rated wind speed of 12 m/s in 50-year return period sea conditions associated with the rated wind speed. The steady wind loading is applied by the open jet wind wall at the W^2, and the wind turbine is operated at a constant rotor speed of 11.46 RPM, this being equivalent to the rated rotor speed. For this DLC the turbine produces the largest mean turbine thrust loads and platform offsets. This can lead to some of the largest extreme loads on the systems and can control elements of the design. There will also be large platform motions due to the extreme nature of the sea state making this an ideal test case for illustrating the enhancements to MoorDyn. Current was not included in this testing campaign as the W^2 does not have that capability.

2.5.3. Description of the Turbine

The physical model to be tested in the W^2 is a 1:52-scale model of a 6-MW turbine supported on the University of Maine VolturnUS concrete semi-submersible floating platform technology as shown in Figure 2.4. Froude scaling was applied to the test effort which is used extensively when testing model offshore structures [14]. In the following sections the hub and nacelle properties, blade properties, tower properties, platform properties and geometry, and the mooring system properties will be presented. It should be noted that these properties are measured from the physical model and are used as inputs in OpenFAST.

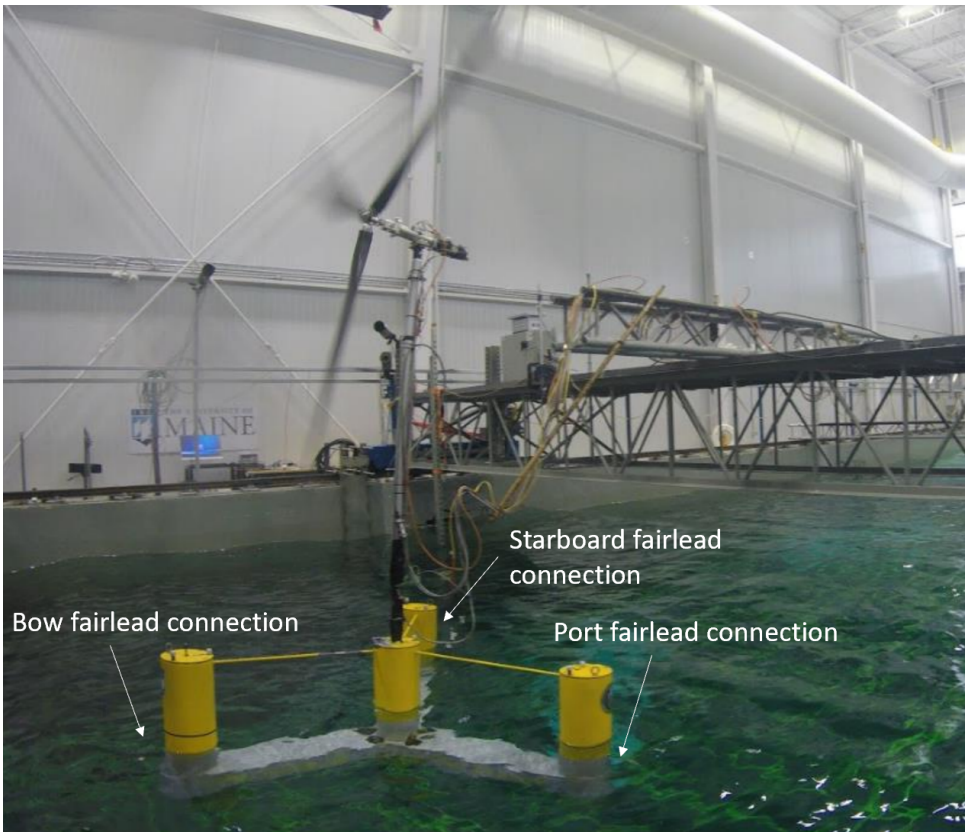

Figure 2.4. Image of VolturnUS FOWT with a Taut Synthetic Mooring System being Tested in the W^2 Basin

2.5.3.1 Turbine Gross Properties

The turbine used in this test campaign is a representative 6-MW turbine. Presented here will be a brief overview of the properties of the turbine focused on the information needed to

correctly model the FOWT dynamics in a situation where wind loading is applied. For more information on the design of the turbine including distributed blade properties and blade aerodynamics, refer to Ward et al. [15]. It is these blade aerodynamic properties that OpenFAST uses to determine the forces on the turbine using Blade Element Momentum theory (BEM) along with various corrections such as dynamic wake and unsteady airfoil aerodynamics.

The model turbine represents a 6-MW turbine with a hub height of 100 m and a rotor diameter of 150 m. Gross properties of the 6-MW turbine physical model are provided in Table 2.2. To model this turbine component masses are necessary. The total rotor nacelle assembly (RNA) mass includes the mass of the nacelle, hub, and blades and is provided in Table 2.3. The gross properties of the blades are provided in Table 2.4. For more information on the turbine including the design and manufacturing as well as the distributed properties of the blades refer to [15].

Table 2.2. Wind Turbine Gross Properties

Rotor Orientation, Configuration	Upwind, 3 blades
Rotor, Hub Radius	78.2 m, 4.26 m
Hub Height Above SWL	100 m
Overhang (Up Wind), Shaft Tilt, Precone	12.5m, 6°,4°
Vertical Distance Along Tower Centerline Between Tower top and Shaft	2.0 m
Height of Tower-Top Flange Above SWL	96.7m
Total Tower Top Mass	557,00 kg

Table 2.3. Hub and Nacelle Gross Properties (UMaine stock 6-MW turbine)

Nacelle Mass	275,00 kg
Nacelle Center of Mass (Above Tower)	2.0 m
Nacelle Center of Mass (Down Wind)	6.0 m
Rotor Mass	282,000 kg
Rotor Inertia	111,500,000 kg-m2
Hub Mass	217,000 kg
Hub Inertia about Rotor Axis	Negligible (0)

Table 2.4. Blade Gross Properties

Blade Length	73.9 m
Blade Mass	21,600 kg
Location of Blade Center of Mass (Measured from Blade Root)	32.0 m
Blade First Mass Moment of Inertia	691,000 kg-m
Blade Second Mass Moment of Inertia	30,100,000 kg-m^2

2.5.3.2. Tower Properties

The turbine described by this paper was designed to fit various different towers allowing for the flexibility to match important full scale tower natural frequencies [15]. For this setup, an aluminum tube with a circular cross section was used for the physical model of the tower. The properties of this tower are presented in Table 2.5. The distributed mass of the aluminum tube is not constant along the length to account for the mass of a bundle of cables coming from the nacelle of the turbine.

Table 2.5. Tower Gross Properties

Tower Gross Properties			
Tower Height		83.2 m	
Tower Base Elevation above SWL		13.5 m	
Tower Top Elevation above SWL		96.7 m	
Total Mass		246,000 kg	
Center of Mass above SWL		72.9 m	
Tower Distributed Properties			
Elevation (m)	Mass (kg/m)	Fore-aft Stiffness (Nm^2)	Side-Side Stiffness (Nm^2)
13.5-80.0	1370	8.24×10^{11}	8.24×10^{11}
80.0-96.7	9240	8.24×10^{11}	8.24×10^{11}

2.5.4. Description of the Floating Platform

The platform used to support this turbine is the University of Maine VolturnUS hull. This platform is a semi-submersible design with a concrete construction. The platform has four columns, three of which provide stability in pitch and roll. The concrete hull is designed to be

towed to the test site and then ballasted to the operational draft with water. Table 2.6. contains the gross properties of the 6-MW VolturnUS floating platform without mooring lines installed, and Figure 2.5. illustrates the submerged geometry of the platform.

Table 2.6. Floating Platform Gross Properties

Total Draft	20.0 m
Elevation to Platform Top (Tower Base) Above SWL	13.5 m
Platform Mass, Including Ballast	1.09×10^7 kg
Displacement	1.17×10^4 m^3
Center of Mass (CM) Location Below SWL Along Platform Centerline	11.85 m
Platform Roll Inertia About CM	5.23×10^9 kg-m^2
Platform Pitch Inertia About CM	5.23×10^9 kg-m^2
Platform Yaw Inertia About CM	8.33×10^9 kg-m^2

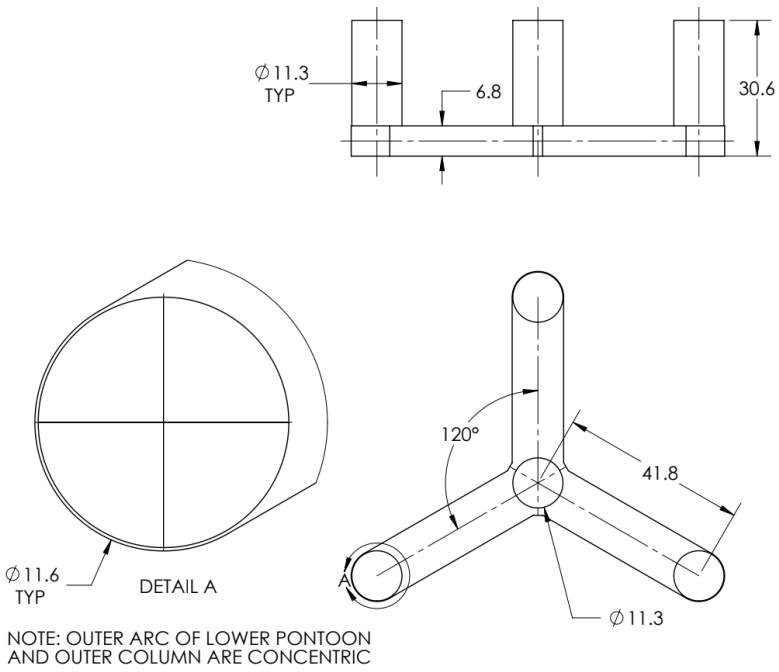

Figure 2.5. VolturnUS Submerged Platform Geometry

The hydrodynamics of the structure are determined using OpenFAST's module HydroDyn. The coefficients needed for this analysis are handled through the use of the commercially available code WAMIT [16], a software developed by the Massachusetts Institute of Technology for calculating the hydrodynamic forces on offshore structures. WAMIT uses a

potential flow-based panel method with the appropriate boundary conditions to solve for platform forces in the frequency domain. In this case WAMIT solves the radiation and diffraction problems for both the linear and second-order forces on the platform. The second-order forces are modeled by using the full second-order difference-frequency quadratic transfer function (QTF) as obtained from the second-order potential flow theory and then by enabling OpenFAST to calculate the second-order wave forces. It is important to note that the viscous excitation forces are not captured with this method.

Solving the potential flow problem provides the applied forces and moments on the structure and the phase shift (represented as a complex number X_i) relative to the incident wave. The forcing on the platform is a function of the incident wave frequency. The magnitude of the wave forces and moments, as well as the phase shift are provided for an incident wave propagating in the positive surge direction in Figure 2.6. The solution of the potential flow problem also provides the structure added mass and damping matrices which also vary based on the incident wave frequency. The translational, rotational, and coupled translation-rotational non-zero entries of the damping matrix are provided in Figure 2.7. Lastly, OpenFAST uses the hydrodynamic coefficients determined through the WAMIT potential flow analysis to transform the responses using superposition and convolution to determine the platform response in the time domain. In order for OpenFAST to perform these operations the infinite frequency added mass matrix [17][18] is required. The infinite frequency added mass matrix for the VolturnUS 6-MW platform is:

$$A(\infty) = \rho \begin{bmatrix} 8050\mathrm{m}^3 & 0 & 0 & 0 & -88900\mathrm{m}^4 & 0 \\ 0 & 8050\mathrm{m}^3 & 0 & 88900\mathrm{m}^4 & 0 & 0 \\ 0 & 0 & 11900\mathrm{m}^3 & 0 & 0 & 0 \\ 0 & 88900\mathrm{m}^4 & 0 & 4320000\mathrm{m}^5 & 0 & 0 \\ -88900\mathrm{m}^4 & 0 & 0 & 0 & 4320000\mathrm{m}^5 & 0 \\ 0 & 0 & 0 & 0 & 0 & 9690000\mathrm{m}^5 \end{bmatrix}$$

where ρ represents seawater density (1025 kg/m^3).

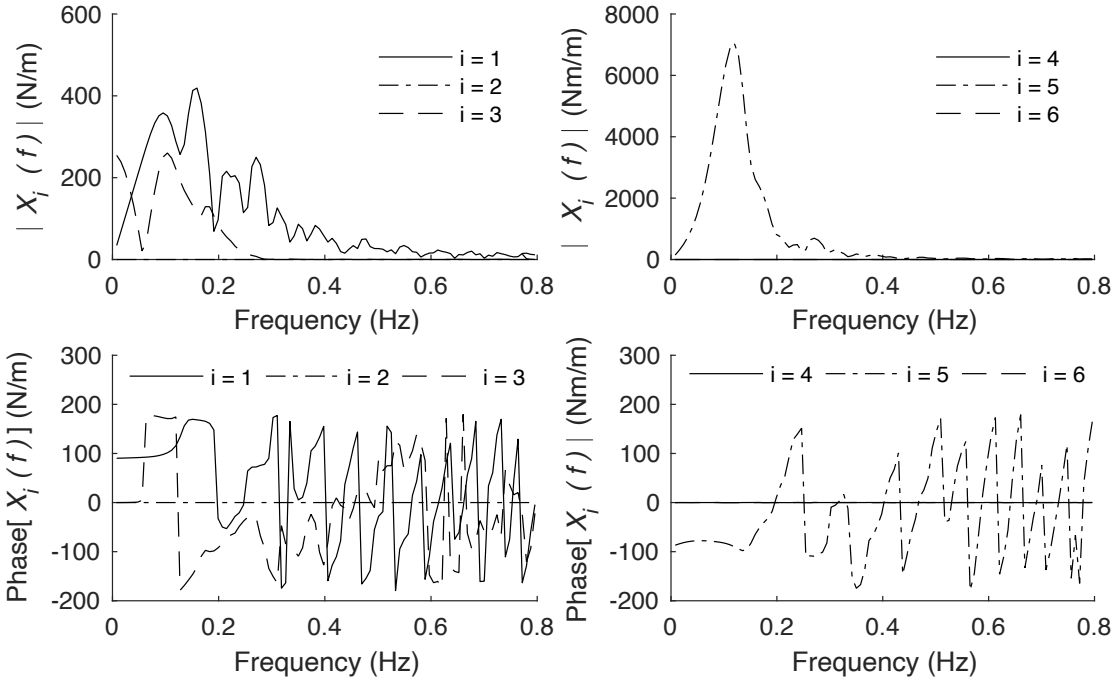

Figure 2.6. Transfer Function for Forces and Moments on the Platform (top) with Phase Shifts (bottom) due to a Linear Wave Propagating in the Positive Surge Direction

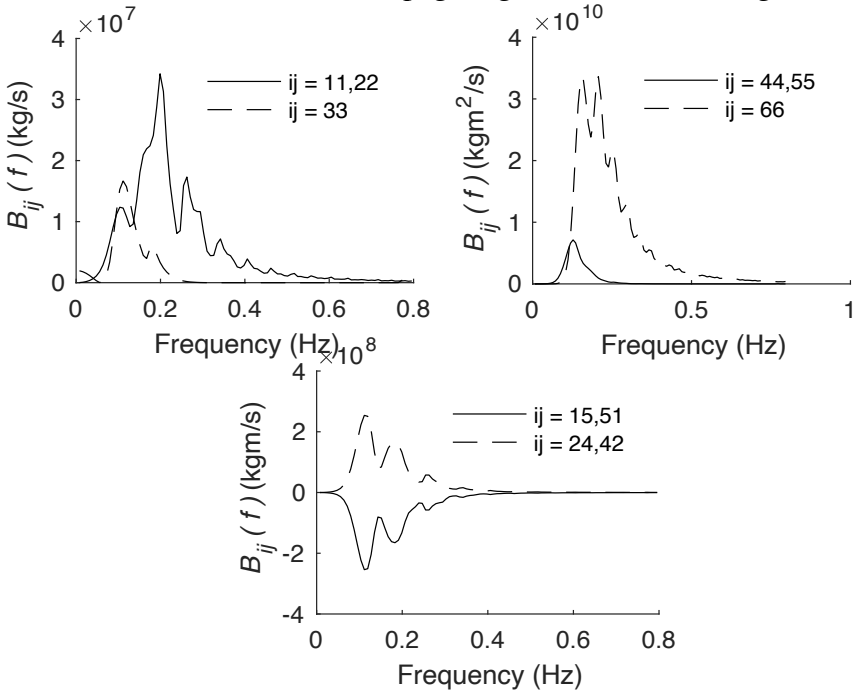

Figure 2.7. Damping Matrix Entries as a Function of Frequency for Translational (top left), Rotational (top right), and Coupled Translation-rotational (bottom) Non-zero Entries in the Matrix

In addition to solving the diffraction and radiation problem outlined above WAMIT also solves for the hydrostatic stiffness. WAMIT only solves for the stiffness contributions due to the center of buoyancy and the waterplane area of the platform. The stiffness contribution due to the FOWT's weight and its center of gravity is calculated separately based on the component masses and locations specified in the ElastoDyn input file and are then added back into the solution. The hydrostatic stiffness calculated by WAMIT for the 6-MW VolturnUS floating platform is:

$$C_H = \rho g \begin{bmatrix} 0 & 0 & 0 & 0 & 0 & 0 \\ 0 & 0 & 0 & 0 & 0 & 0 \\ 0 & 0 & 260.3\text{m}^2 & 0 & 0 & 0 \\ 0 & 0 & 0 & 6230\text{m}^4 & 0 & 0 \\ 0 & 0 & 0 & 0 & 6230\text{m}^4 & 0 \\ 0 & 0 & 0 & 0 & 0 & 0 \end{bmatrix}$$

where g represents gravity (9.81 m/s^2).

2.5.5. Mooring System Properties

The mooring system for this test is a semi-taut synthetic system designed to be deployed in a water depth of 55m with an anchor radius of 205m. For this configuration 20 meters of chain was deployed at the anchor side of the system to ensure that the synthetic rope is kept off the seabed. The synthetic rope is deployed with a stretched length 8% larger than the reference length which was chosen during the design process to ensure that the synthetic lines would stay taut during extreme loading. The gross properties for the mooring system are provided in Table 2. In addition to the mooring line properties the locations of both the anchors and fairlead connections are presented in Table 2.7. These coordinates are given with respect to the coordinate system defined in Figure 2.1.

Table 2.7. Mooring System Properties

Number of mooring lines	3
Angle of mooring lines (0° aligned with positive surge axis)	60°, 180°, 300°
Depth to anchors below SWL (water depth)	55 m
Depth to fairleads below SWL	5.4 m
Radius to anchors from platform centerline	205 m
Radius to fairleads from platform centerline	45.7 m
Unstretched chain length	20 m
Unstretched synthetic length	138.2 m
Synthetic line diameter	155 mm
Chain diameter	157 mm
Synthetic line mass density	14.6 kg/m
Chain mass density	493 kg/m
Bow Fairlead Location	[-45.7m, 0m, -5.4m]
Bow Anchor Location	[-205m, 0m, -55m]
Port Fairlead Location	[22.9m, -39.6m, -5.4m]
Port Anchor Location	[102.5m, -177.5m, -55m]
Starboard Fairlead Location	[22.9m, 39.6m, -5.4m]
Starboard Anchor Location	[102.5m, 177.5m, -55m]

2.5.5.1 Line Properties

To adequately emulate the properties of a nonlinear synthetic rope a spring mechanism was used to approximate the tension-strain relationship. The nonlinear target is a second order polynomial fit to a nylon rope quasi-static tension-strain response. To match this target a compliant element consisting of a steel spring along with two physical stops within the spring was used. These stops were placed so that when the spring was stretched to a certain length the stop would engage reducing the effective length of the spring. Two physical stops ensured that the physical tension-strain response would be piece-wise trilinear. The trilinear region was designed to be in the estimated working region of the rope. The working region of the rope was estimated based on simulations run during the initial design process. The nonlinear target tension-strain response and the spring element tension-strain response used in the experiment are

shown in Figure 2.8. The trilinear fit presented in Figure 2.8. fits well with the data. The biggest difference between the nonlinear target and data occurs at a strain of about 2.5%.

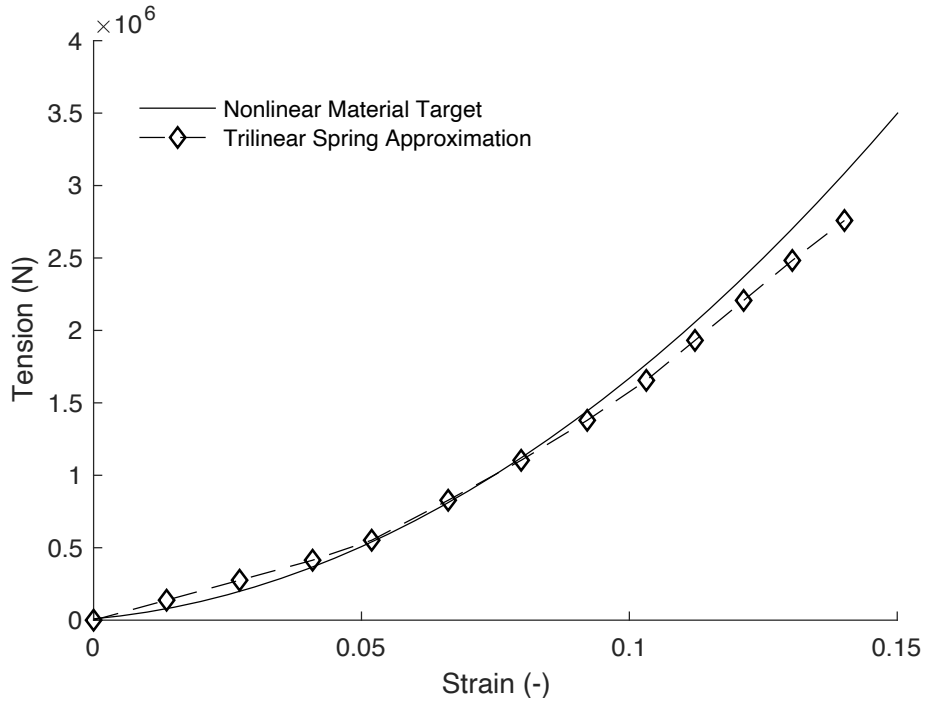

Figure 2.8. As Built Mooring

Although the stiffness characteristics of the spring closely matched the stiffness of the synthetic rope, the length did not match the full-scale length. To remedy this an axially-stiff cable leader was connected from the spring to the fairlead to match the length of the synthetic material. At the anchor, as with the full-size system, was 20m of chain joining the synthetic segment to the anchor. Simulations predicted that for some extreme cases the chain leader at the anchor could potentially contact the seafloor near the anchor. To avoid manufacturing a seafloor over the whole length of the basin 3 small plywood platforms were installed to represent the seabed. These platforms are small and located far away from the platform, so it is reasonable to neglect them in the hydrodynamic calculations. It should be noted that the WAMIT hydrodynamic analysis was performed for the basin depth of 234m for consistency between the

numerical model and experimental data. The experimental line setup described above is illustrated in Figure 2.9.

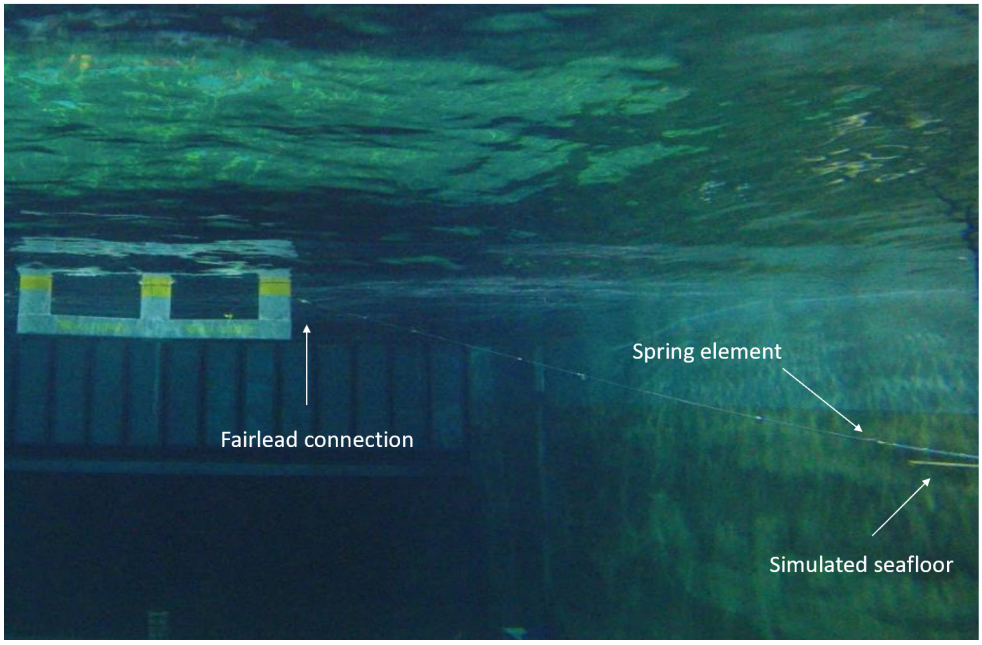

Figure 2.9. Model Synthetic Mooring Setup

For this experiment, the environmental loading was applied as to affect the largest loads in a single line, in this case the lead leg. The lead-line anchor and fairlead attachments were both equipped with Futek LSB210 load cells for measuring tension in the line. For the back two lines, port and starboard, only the fairleads were equipped with the same Futek load cells.

2.5.5.2. Mooring System Static Offsets

Static offset tests were performed by slowly moving the platform through a specific degree of freedom, typically surge and sway while recording line tensions and system positions. The test ensures that the physical models mooring system produces the correct tensions as predicted by OpenFAST in the absence of drag and inertial forces on the mooring line.

The results for the surge and sway static offset tests are presented in Figure 2.10. and Figure 2.11. respectively. Overall, the agreement between the experimental data and OpenFAST

matches well. Two areas where there are small discrepancies in the lead line tension occur for surge offsets of less than approximately -2.5m. With a surge offset of -8m the discrepancy between OpenFAST and the physical model is 123.6 kN. Fortunately, the environmental loading is applied to induce positive surge offsets, a region where OpenFAST predicts the tension within 3% of the physical model.

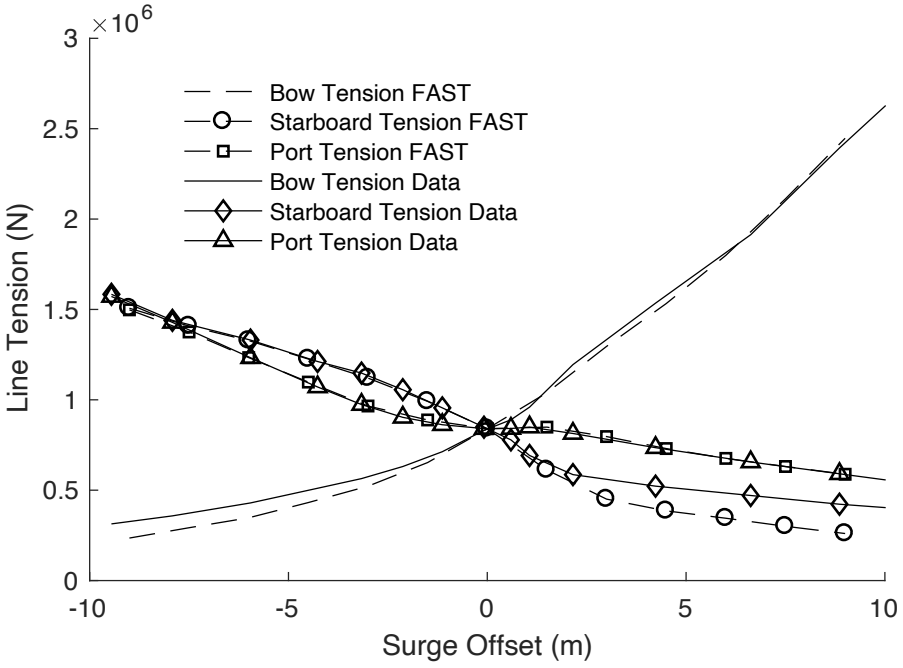

Figure 2.10. Surge Static Offset OpenFAST and Physical Model Comparison

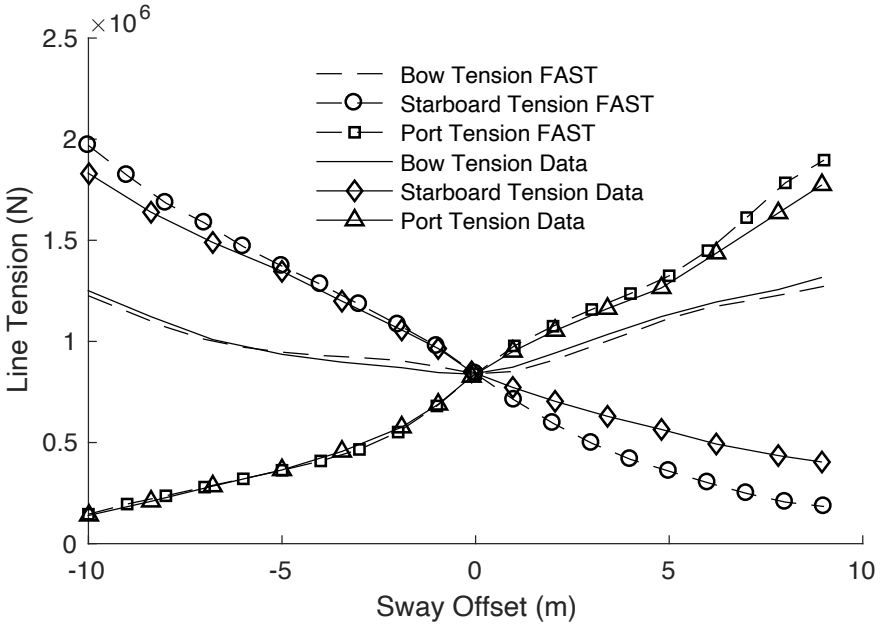

Figure 2.11. Sway Static Offset OpenFAST and Physical Model Comparison

The second minor discrepancy is the starboard line tension for surge displacements larger than about 2.5m. With a surge displacement of 9m the starboard line tension is off by 162.2 kN. The port tension in OpenFAST matches the physical model extremely well. As the goal of the experiment is to induce the largest possible tensions in the lead line the port line tension is less of a concern. The minor deviations between the as-built and as modeled response occur below tensions of 630 kN in both of the rear lines.

Many of the trends observed in Figure 2.10. for the surge static offset test can also be observed in the sway static offset test. Once again, the port line is the most accurate line, but there are some small inconsistencies for sway offsets larger than 8m. At this location however, OpenFAST only overpredicts the model by 7%. The OpenFAST predictions for the bow line tension overpredicts the tension by 3% at a sway displacement of -2m. The starboard line tension is predicted well for negative sway displacements but again when the tension falls below

600 kN OpenFAST begins to underestimate the tension in the line. With a sway displacement of 8m OpenFAST underpredicts the tension in the line by 228 kN.

2.6. Model Correlation

In this section various comparisons between the experimental data and data generated from the OpenFAST model will be presented. The first of these comparison cases that will be examined is the free-decay tests. These tests will provide confidence that the basic dynamics of the structure are being captured properly and will be used to calibrate the quadratic damping coefficients in OpenFAST. Subsequently, the white noise wave case will be examined for generating RAOs for quantities of interest. Comparisons of the RAOs aid in further verifying the rigid-body and mooring dynamics of the structure computed by the modified OpenFAST tool. Lastly, a comparison between the physical model and OpenFAST will be made with an operational turbine in a realistic loading condition to further verify the mooring module enhancements.

2.6.1 Free-Decay Testing

Free-decay tests are one of the most important aspects of a model test campaign as they help to ensure that the FOWT natural periods and damping ratios agree between the physical and numerical model. As the natural periods are a function of the physical and added masses and inertias of the system as well as the hydrostatic and mooring system stiffnesses these checks help ensure that the physics have been modeled correctly. For this test campaign the in-plane rigid body degrees of freedom surge, heave and pitch will be of particular interest, however, yaw will also be investigated as the mooring system provides all the restoring force in this degree of freedom. Table 2.8. contains a comparison between the damped natural periods in OpenFAST to the experimental data calculated from free-decay tests. The OpenFAST results for surge, heave

and pitch all compare within 2.5% of the experimental results indicating that both the mooring system restoring forces, and platform hydrodynamics have been captured well by OpenFAST. The yaw degree of freedom is approximately 7% higher in the experimental data than in OpenFAST. Higher period motion associated with very low restoring stiffnesses, such as yaw, can be more difficult to predict. This arises because small differences between the experimental yaw stiffness and the yaw stiffness in OpenFAST can lead to large differences for soft systems.

Table 2.8. Floating Platform Natural Periods

DOF	Data T_d (s)	FAST T_d (s)	Percent Difference (%)
Surge	65.7	64.2	2.3
Heave	19.1	18.8	1.6
Pitch	26.7	26.3	1.8
Yaw	74.9	69.7	6.9

2.6.1.1 Quadratic Damping Coefficient Calibration

The free-decay tests conducted are also useful for determining the quadratic damping coefficients of the structure. The potential flow theory used by WAMIT to predict the added mass, linear damping and forcing on the structure assumes that the fluid is irrotational and inviscid. As a result of the inviscid fluid assumption, the quadratic damping coefficients cannot be directly obtained from the potential flow analysis. Although these quadratic drag coefficients can be estimated based on drag coefficients and platform geometry, traditionally for physical model validation the free-decay tests are used to directly calibrate the quadratic drag coefficients.

This calibration was done manually by varying the quadratic damping coefficients and trying to match the simulated time series to the experimental data as best as possible. The time series comparisons between simulation and data for surge, heave and pitch free decays are presented in Figure 2.12., Figure 2.11. and Figure 2.12. respectively. The surge periods match closely as indicated in Table 2.8., but the response of the experimental platform is slightly larger

for large amplitudes and slightly smaller for small amplitudes. The heave free-decay experimental data is in good agreement with the simulated data. The pitch experimental data when compared to the OpenFAST results has a slightly shorter period as noted in Table 2.8., but the motion is more damped. This can possibly be attributed to the cable bundle which attaches to the tower of the physical model adding additional stiffness and damping to the system.

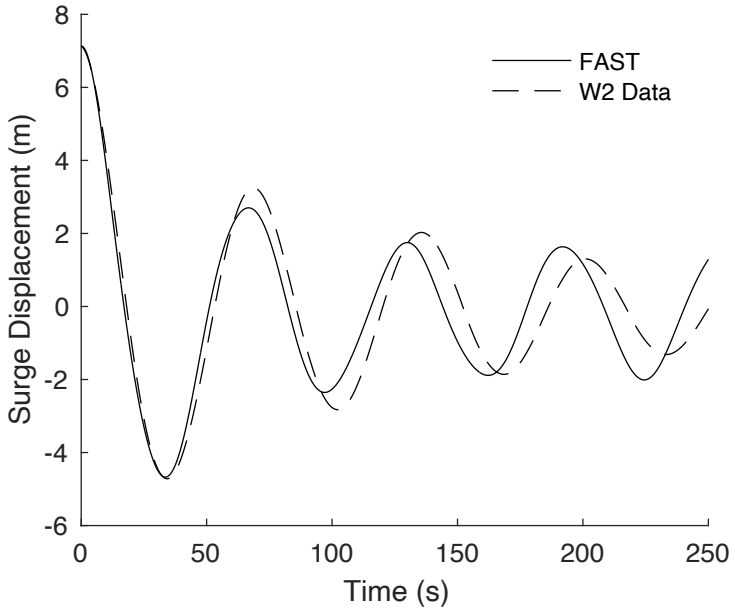

Figure 2.12. Platform Surge Free-decay Time-series Comparison between OpenFAST and Physical Model

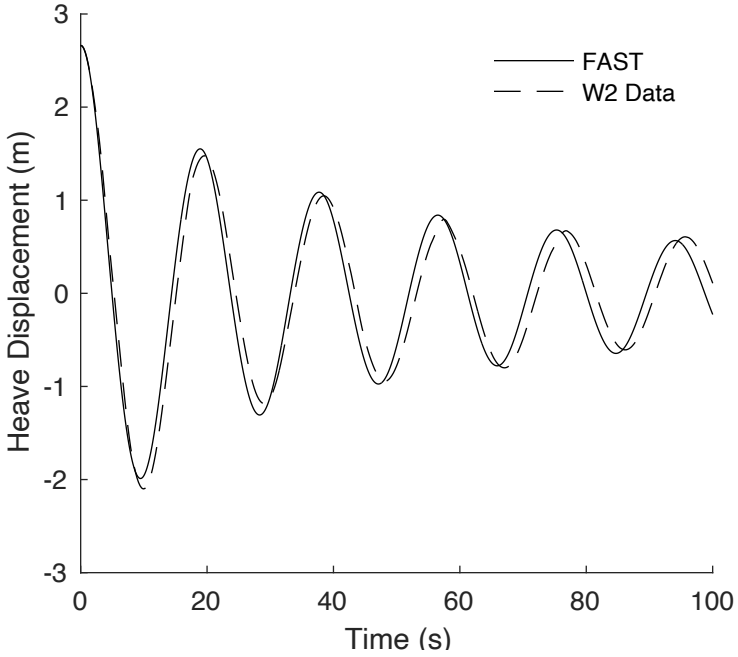

Figure 2.13. Platform Heave Free-decay Time-series Comparison between OpenFAST and Physical Model

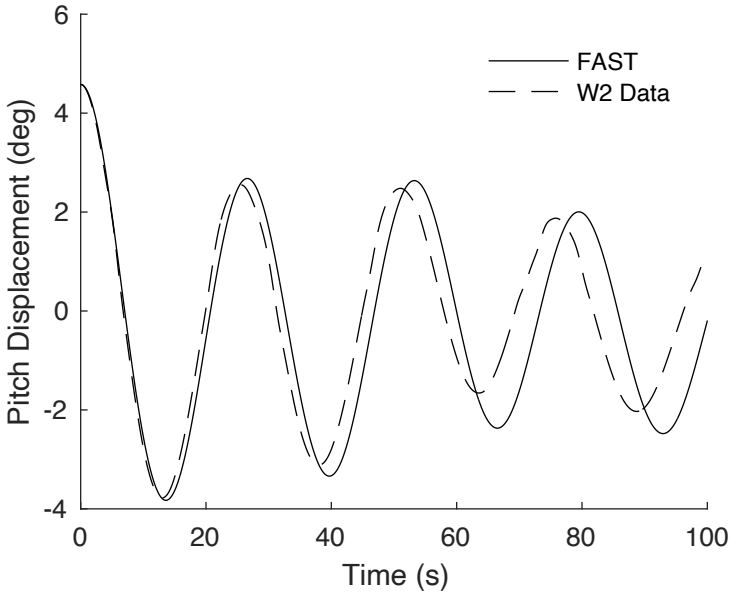

Figure 2.14. Platform Pitch Free-decay Time-series Comparison between OpenFAST and Physical Model

The calibrated damping ratios used in these free-decay comparisons are presented in Table 2.9. The calibrated values for surge and pitch were also used for sway and roll

respectively, as the platform is symmetric and the out of plane motions are small compared to the in-plane motions. Overall, the OpenFAST model overestimates damping for large amplitude motions and underestimates damping for small amplitude motions when compared to the physical model. This implies that the linear damping predicted by WAMIT is less than the linear damping observed in the physical model, and the quadratic damping being used in OpenFAST is likely higher than compared to the physical model.

Table 2.9. OpenFAST Tuned Quadratic Damping Coefficients

DOF	Quadratic Damping Coefficient
Surge	1.55e6 Ns^2/m^2
Sway	1.55e6 Ns^2/m^2
Heave	2.65e6 Ns^2/m^2
Pitch	4.70e10 Nms^2/rad^2
Roll	4.70e10 Nms^2/rad^2
Yaw	3.94e10 Nms^2/rad^2

2.6.2. White Noise Wave

In these white noise wave tests, the platform is subjected to a wave spectrum which has its energy distributed evenly across a range of frequencies in the wave energy range. The platform response to this wave environment can then be used to generate the RAOs. To generate these results the same wave time history as was used in the basin was utilized in OpenFAST.

The rigid-body degree of freedom RAOs of interest, surge, heave and pitch, are presented in Figure 2.15., Figure 2.16., and Figure 2.17. respectively. The surge OpenFAST RAO magnitude follows the same trend as the experimental RAO magnitude but is in general slightly larger. Within typical ocean wave periods of 10s to 15s the OpenFAST surge RAO overpredicts the experimental RAO around 10% to 15%. The heave OpenFAST RAO magnitude and experimentally-generated RAO magnitudes again follow the same trend with the values

matching well for wave forcing periods up to 13 seconds. At this point the RAO magnitudes deviate somewhat with the largest discrepancy occurring near 17 seconds. This is due to a well-documented phenomenon in the numerical model where the potential flow-derived heave forcing cancels out [19][20] which is not observed experimentally in the basin due to viscous wave loading. It is also observed that the experimental results are larger than the predicted OpenFAST response for 18s to 20s. One plausible explanation for this is the lack of interaction between the wave particles and the platform in the quadratic drag model. For damping calculations in OpenFAST, the absolute velocity of the platform is used to compute the quadratic drag forces whereas in the experiment, these damping forces depend on the relative motion between the water wave particles and the platform motion. For large sea states the heave motion of a semi-sub of this size tends to be fairly in phase with the waves which would result in less relative motion and less damping in the experimental data than predicted in the OpenFAST simulations. The last of the rigid-body RAO magnitude, the pitch degree of freedom, exhibits a strong correlation between the simulation and physical model. Overall, the rigid body RAOs agree well for wave periods of 5 to 15 seconds.

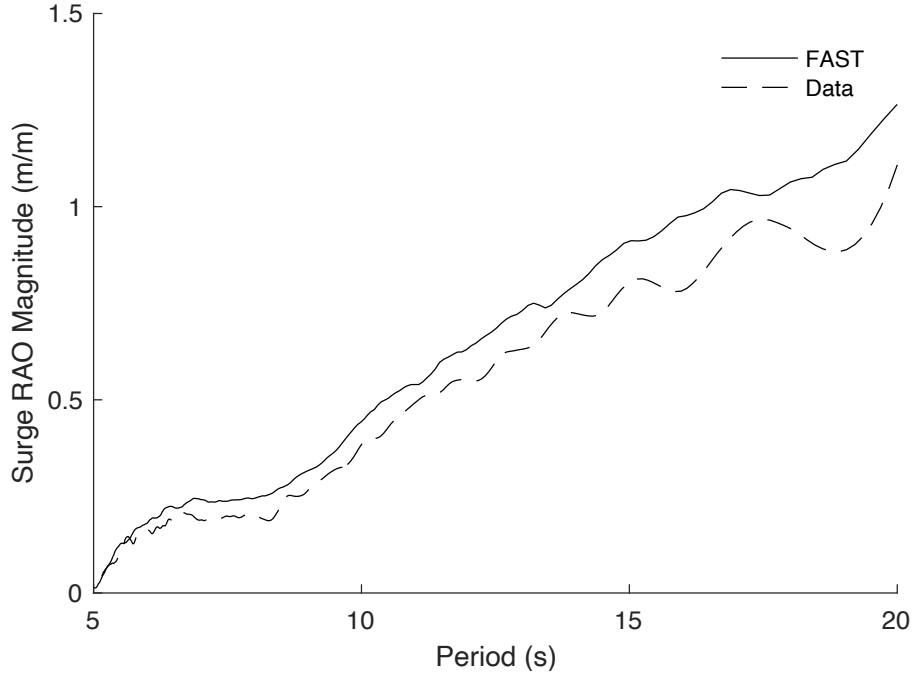

Figure 2.15. Surge RAO Magnitude OpenFAST and Physical Model Comparison

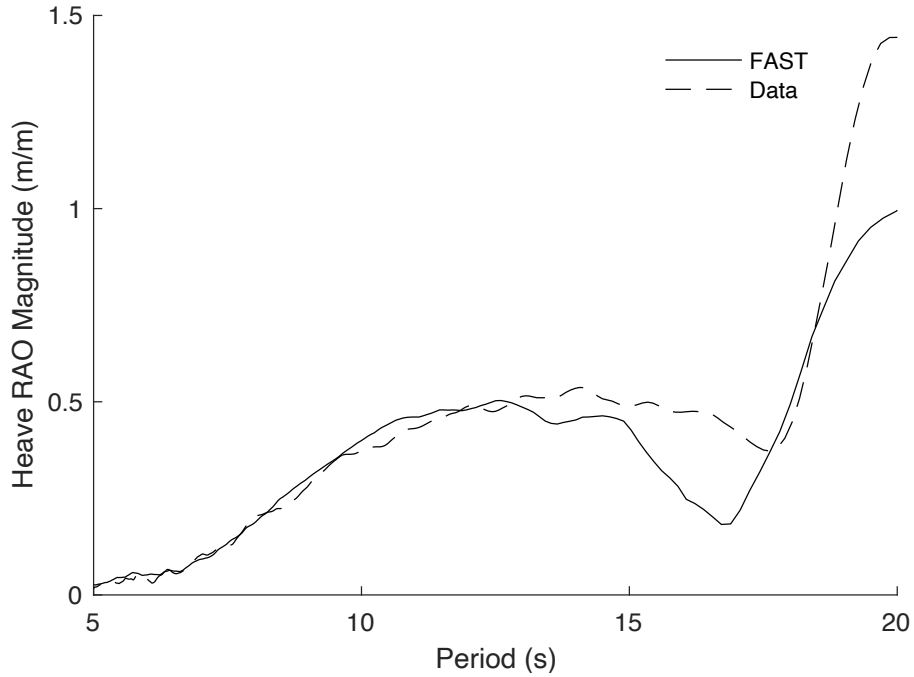

Figure 2.16. Heave RAO Magnitude OpenFAST and Physical Model Comparison

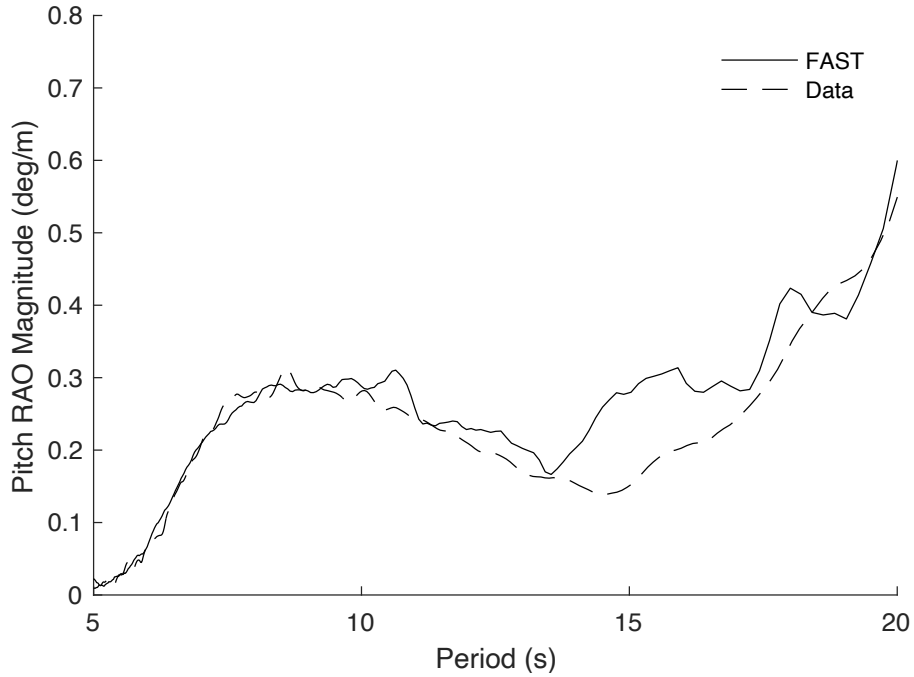

Figure 2.17. Pitch RAO Magnitude OpenFAST and Physical Model Comparison

As the focus of this paper is the validation of the nonlinear mooring system enhancements made to MoorDyn, the bow fairlead and anchor tension RAO magnitude comparisons are also included in Figure 2.18. and Figure 2.19. Both the anchor and fairlead RAO magnitudes generated from the data and from the OpenFAST model closely mimic the trends observed in the surge RAO magnitudes. The one difference in the RAOs occur at 19 seconds, as was also the case with the surge results. Similar to the surge results the OpenFAST generated RAO magnitudes overpredict the tension RAO magnitudes generated from the basin data. This is to be expected as the fairlead tension is most strongly a function of surge, and the surge response is larger in OpenFAST than it is in the experimental data. This is supported by the surge and tension OpenFAST response being 15% and 20% larger than the experimental results, respectively at a wave period of 10s. Again, it should be noted that the largest

discrepancies fall outside of typical ocean wave periods and overall, the trends correlate very well.

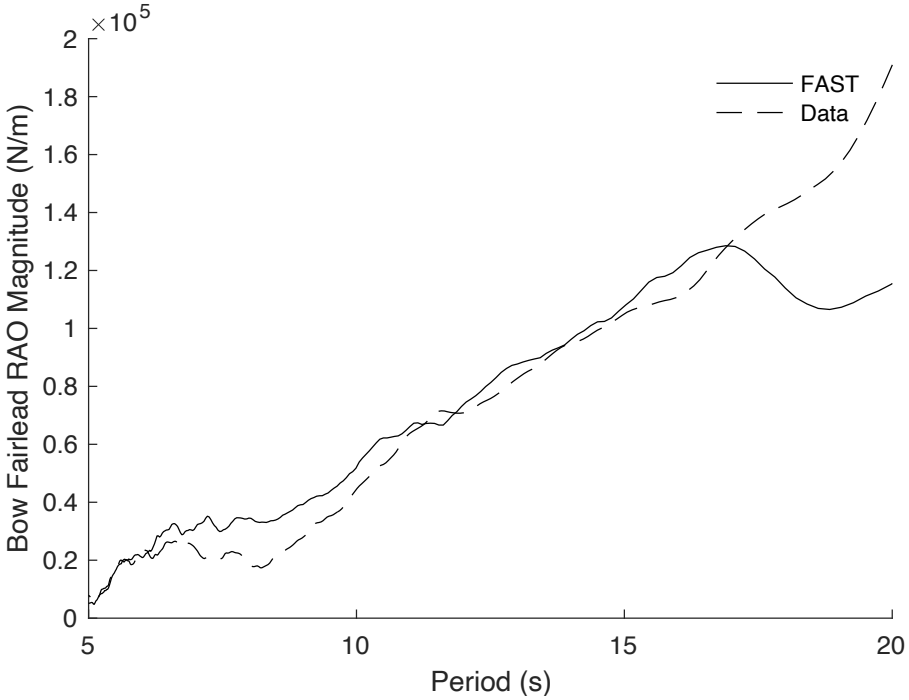

Figure 2.18. Bow Fairlead Tension RAO Magnitude OpenFAST and Physical Model Comparison

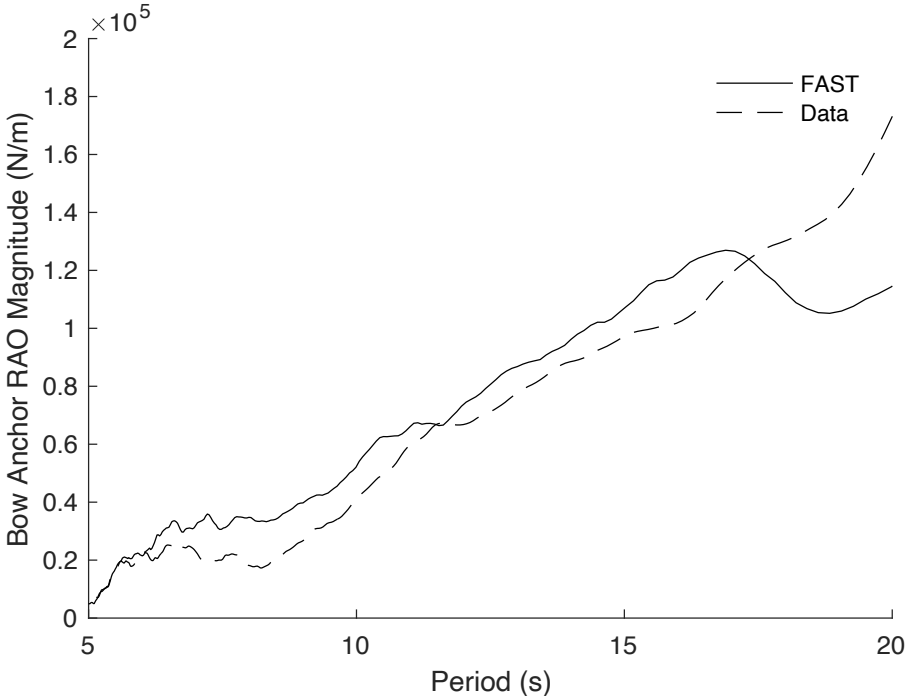

Figure 2.19. Bow Anchor Tension RAO Magnitude OpenFAST and Physical Model Comparison

2.6.3. DLC 1.6

DLC 1.6 at rated wind speed is an important design case since the turbine is operating at its peak thrust load in a large sea state. A comparison between the platform responses simulated in OpenFAST and experimental values is provided in Table 2.10. The results presented in the table are generally consistent with the white noise tests as the differences reflected in the standard deviation comparison shows simulated values to be only slightly larger in OpenFAST for surge, pitch and fairlead tension when compared to the physical model results. Overall, the responses measured from the physical model match what is predicted by OpenFAST well, and while the variance is slightly larger in OpenFAST for surge and pitch it is close to the experimental data. In addition to the standard deviations agreeing well between the OpenFAST and experimental data, the range of the data is also close indicating that OpenFAST is accurately predicting the dynamics of the structure. One discrepancy between the OpenFAST simulated results and the experimental data is the mean surge response, which for the basin test was approximately 1.5m larger. This 1.5m difference is also evident in the maximum and minimum values of surge as they are approximately 2m larger in the experimental data than simulated in OpenFAST, but overall, this consistent overprediction indicates that the dynamics are being captured properly but suggests there is a mean load not captured in OpenFAST that is observed in experimental data. The fairlead tension simulated by OpenFAST displays the same trends as the surge response as the mean fairlead tension measured from the experimental data is about 20kN higher than the tension predicted by OpenFAST. Again, this is reflected in the measured maximum and minimum values in the experimental line tension as they are approximately 40kN larger than what has been predicted by OpenFAST which again reaffirms that a mean load found in experimental data is not captured adequately in the simulations.

Table 2.10. DLC 1.6 Statistics

DOF	Source	Mean	Percent Difference (%)	Std/ Dev.	Maximum	Minimum	Range
Surge (m)	FAST	4.65	23.1	1.49	9.88	-0.74	10.6
	Data	6.05	-	1.36	12.05	1.57	10.4
Heave (m)	FAST	-0.14	173	0.92	2.85	-3.16	6.01
	Data	0.19	-	0.99	4.44	-3.51	7.95
Pitch (deg)	FAST	5.49	1.08	0.70	8.20	2.24	5.96
	Data	5.55	-	0.64	7.73	2.35	5.38
Fairlead Tension (N)	FAST	1.73e6	7.49	2.93e5	2.71e6	8.76e5	1.83e6
	Data	1.87e6	-	2.85e5	3.26e6	1.13e6	2.13e6
Anchor Tension (N)	FAST	1.68e06	3.07	2.92e5	2.67e6	8.24e5	1.85e6
	Data	1.63e06	-	2.65e5	2.94e6	9.50e5	1.99e6

The PSDs associated with platform surge, pitch and heave motions are presented in Figure 2.20., Figure 2.21. and Figure 2.22. respectively. The spectral responses of the platform were generated based on 10,800 s of time-series data. Both the OpenFAST surge and pitch responses are slightly larger in the wave energy region associated with periods of 5 to 15 s then measured in the basin which is again consistent with the RAOs generated by the white noise waves. The heave response PSD of the OpenFAST model matches the experimental data extremely well except for frequencies of about 0.4 Hz to 0.7 Hz which corresponds to a period of about 15-20 seconds. This likely correlates to the dip seen in the heave RAO magnitude of Figure 2.16. corresponding to the heave forcing cancellation.

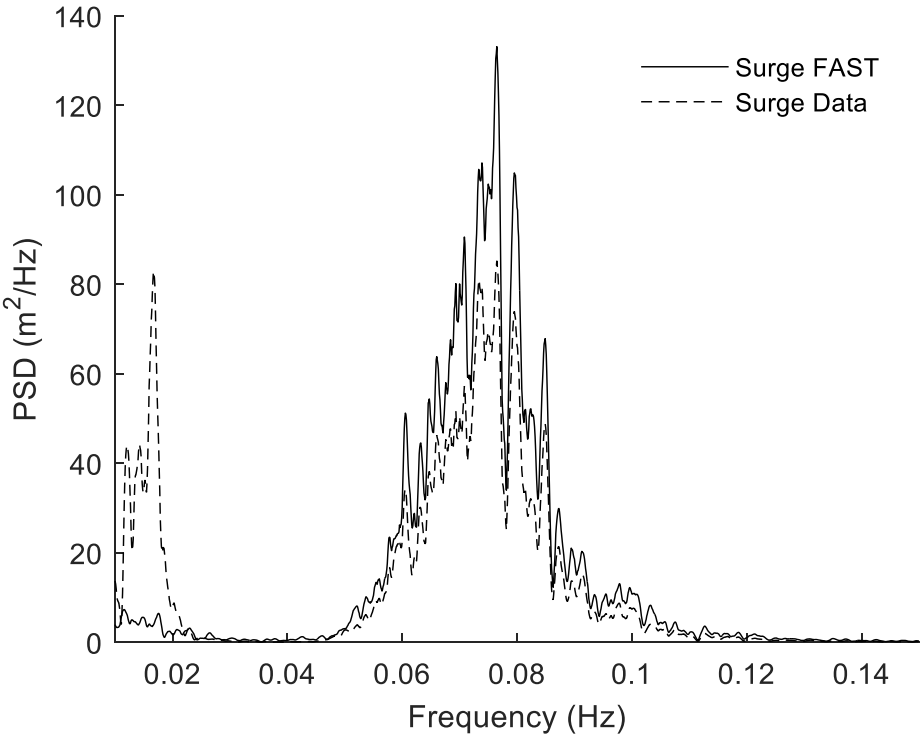

Figure 2.20. DLC 1.6 Surge OpenFAST and Physical Model Comparison PSD

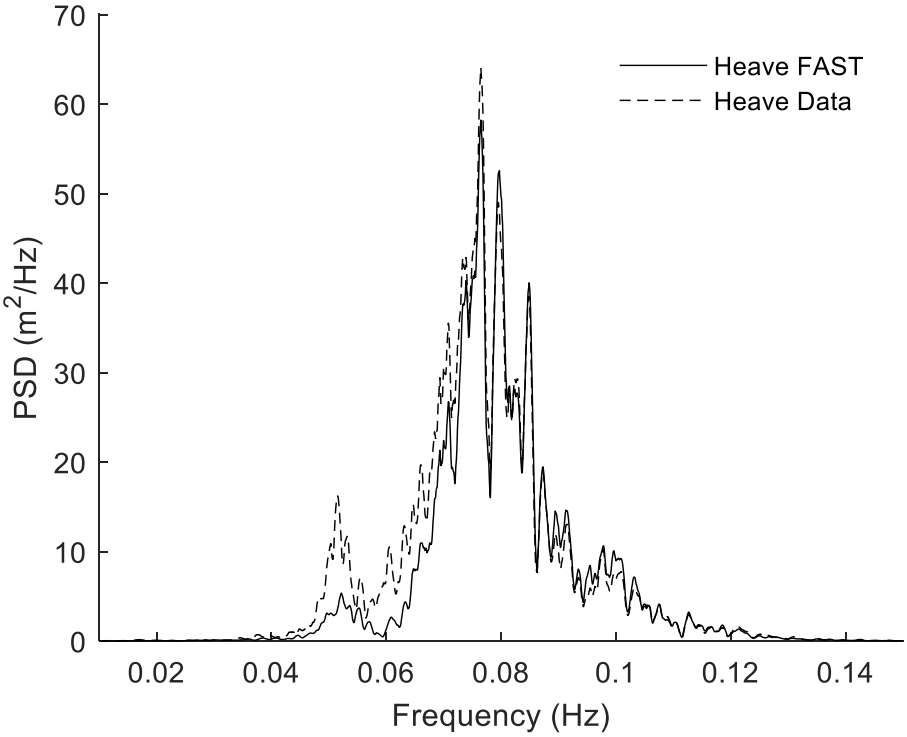

Figure 2.21. DLC 1.6 Heave OpenFAST and Physical Model Comparison PSD

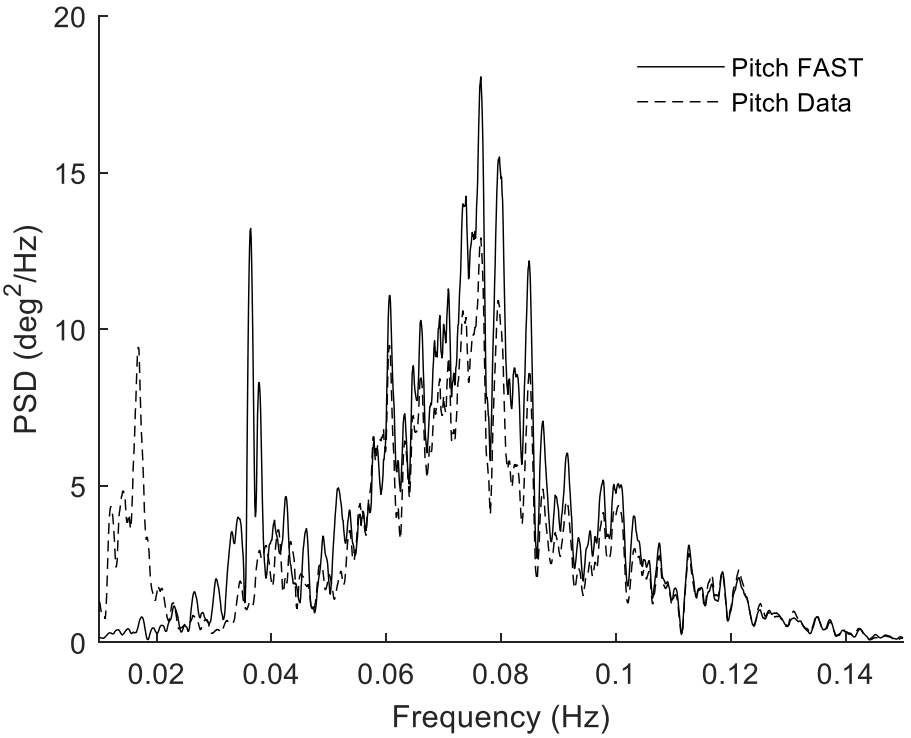

Figure 2.22. DLC 1.6 Pitch OpenFAST and Physical Model Comparison PSD

One difference between the simulation and experiment is the low frequency response, which is very strong in the experimental data, but almost nonexistent in the OpenFAST data. This is likely due to the second-order difference frequency forcing not being predicted well in the model. The second-order wave forcing is traditionally more difficult to capture than the response due to the linear waves but are necessary for predicting vessel response particularly in large sea states [21], [22]. In addition, it has been found that for semi-submersible platforms of this size and for systems with relatively stiff mooring systems the second-order responses are likely to be underpredicted [23]. It is very likely that the deficiencies in the numerical modeling of the second-order low-frequency surge response is then transmitted to the line tension response as line tension depends heavily on the surge motion of the floating platform. The second-order wave loading that is not captured adequately by OpenFAST for this model is also likely the

reason that the average surge displacement and line tension are low as there is an additional slow drift force exhibited in the physical model.

Lastly, the bow fairlead and anchor tension PSD plots are presented in Figure 2.23., and Figure 2.24. These plots share a lot of similar characteristics with their surge PSD as they follow the same trends where the OpenFAST response overpredicts the experimental response. In addition, the OpenFAST results lack the low-frequency response observed in the experimental data, but this is also consistent with the simulated surge results.

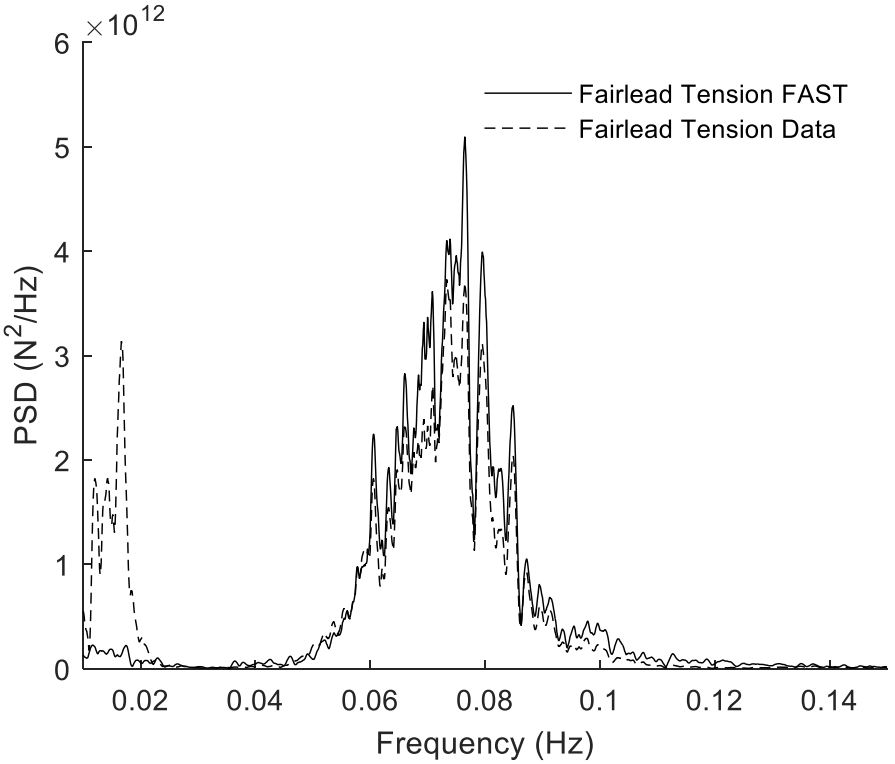

Figure 2.23. DLC 1.6 Bow Fairlead Tension OpenFAST and Physical Model Comparison PSD

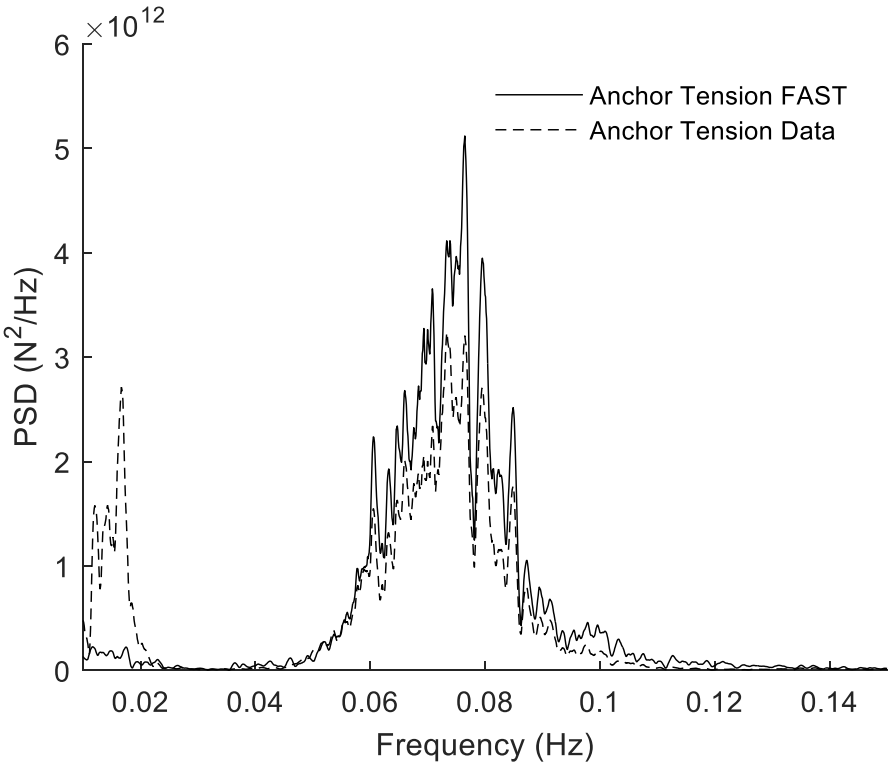

Figure 2.24. DLC 1.6 Bow Anchor Tension OpenFAST and Physical Model Comparison PSD

2.7. Conclusions

This chapter highlights key results of a scale model test campaign in which a 6-MW FOWT was outfitted with a synthetic mooring system. Previously none of the mooring modules compatible within OpenFAST were capable of modeling materials such as a synthetic fiber ropes which can have highly nonlinear tension-strain responses and viscoelastic responses. One such mooring module, MoorDyn, was modified to allow nonlinear elastic mooring line tension-strain responses to be input via a lookup table. This modification also allows for simplified synthetic mooring line material modeling approaches, such as the ABS static-dynamic model to be implemented. Simulations utilizing OpenFAST with the modified MoorDyn module were then compared with experimental data generated in the Harold Alfond W^2 Wind Wave Lab at the

University of Maine Advanced Structures and Composites Center. The simulation and experimental results were found to correlate well with one another.

The results generated show that the mooring module modifications are working as expected. The tensions in the line match very closely with experimental data for both the surge and sway static offset tests which ensures that OpenFAST is determining the tension in the mooring line properly. The damped natural periods determined from the experimental data and OpenFAST also agree well which provide confidence that the MoorDyn enhancements have been implemented properly as for these degrees of freedom the restoring force is strictly due to the mooring system.

There are however some minor differences in the line tension for dynamic loading, as illustrated by the white noise wave case and the DLC 1.6 loading. This is very likely due to the surge motion of the platform being slightly over-predicted as line tension and surge offset are strongly correlated. In the case of both surge RAO and the surge PSD plots the OpenFAST model over-predicts the experimental data in the linear wave region, but this is consistently observed across the results. As line tension and platform surge response are strongly correlated the over-prediction of the surge response leads to an over-prediction of line tension. One other difference between line tension in the OpenFAST model compared to the experiment is the lack of the low-frequency tension response in OpenFAST. It is more difficult to accurately model the second-order wave forces than it is to determine the platform responses due to linear waves. Unfortunately, in this case the forcing due to the second-order wave loading has not been captured adequately by OpenFAST, which in turn causes the low-frequency surge response to be under-predicted. The mean load caused by second-order wave forcing is likely under-predicted

as well leading to the mean surge offset and mean line tension in OpenFAST to be lower than what was measured in the basin.

Although some of the simulated mean platform responses are smaller than the experimental data the dynamic response of the platform and line tensions are captured very well. The tensions calculated in OpenFAST due to the modifications made to MoorDyn only differ slightly from the experimental data with respect to the mean platform surge response and line tension. These results tend to indicate that this difference is due to the simulated platform motion in OpenFAST underpredicting the response the physical model. Overall, the tension simulated by OpenFAST tends to match the experimental data well, and the smaller simulated mean line tension is consistent with the simulated surge offset which indicates the MoorDyn enhancements are working as expected.

2.8. Acknowledgment

The authors would like to express gratitude to the Harold Alfond Foundation for providing the funding to support this research.

2.9. References

[1] B. J. Koo, A. J. Goupee, R. W. Kimball, and K. F. Lambrakos, "Model Tests for a Floating Wind Turbine on Three Different Floaters," *J. Offshore Mech. Arct. Eng.*, vol. 136, no. 2, p. 020907, 2014.

[2] H. R. Martin, R. W. Kimball, A. M. Viselli, and A. J. Goupee, "Methodology for Wind/Wave Basin Testing of Floating Offshore Wind Turbines," 2014.

[3] "OpenFAST Documentation Release v2.3.0 National Renewable Energy Laboratory," 2020.

[4] A. Arapogianni *et al.*, "Deep Water: The Next Step for Offshore Wind Energy," 2013.

[5] C. Del Vecchio, "Lightweight Materials for Deep Water Moorings," University of Reading, 1992.

[6] S. D. Weller, L. Johanning, P. Davies, and S. J. Banfield, “Synthetic mooring ropes for marine renewable energy applications,” *Renew. Energy*, vol. 83, pp. 1268–1278, 2015.

[7] W. M. West, A. J. Goupee, A. M. Viselli, and H. J. Dagher, “The Influence of Synthetic Mooring Line Stiffness Model Type on Global Floating Offshore Wind Turbine Performance The Influence of Synthetic Mooring Line Stiffness Model Type on Global Floating Offshore Wind Turbine Performance,” *J. Phys. Conf. Ser.*, 2020.

[8] E. Falkenberg, L. Yang, and V. Ahjem, “SPRING-DASHPOT SIMULATIONS OF POLYESTER ROPES : VALIDATION OF THE SYROPE MODEL,” *Proc. ASME 2019 38th Int. Conf. Ocean. Offshore Arct. Eng.*, pp. 1–8, 2019.

[9] M. Hall and A. Goupee, “Validation of a lumped-mass mooring line model with DeepCwind semisubmersible model test data,” *Ocean Eng.*, vol. 104, pp. 590–603, 2015.

[10] Qualysis, “QTM Version: 2.15,” 2017.

[11] ABS, “Guide for Building and Classing Floating Offshore Wind Turbine Installations,” *Standardization*, no. October, 2015.

[12] IEC, “IEC 61400-3 Design requirements for offshore wind turbines.” 2019.

[13] A. M. Viselli, G. Z. Forristall, B. R. Pearce, and H. J. Dagher, “Estimation of extreme wave and wind design parameters for offshore wind turbines in the Gulf of Maine using a POT method,” *Ocean Eng.*, vol. 104, pp. 649–658, 2015.

[14] A. J. Coulling, A. J. Goupee, A. N. Robertson, J. M. Jonkman, and H. J. Dagher, “Validation of a FAST semi-submersible floating wind turbine numerical model with DeepCwind test data,” *J. Renew. Sustain. Energy*, vol. 5, no. 2, 2013.

[15] J. C. Ward, M. J. Fowler, A. M. Viselli, A. J. Goupee, and H. J. Dagher, “Design and Validation of a Multi-Scale Model Floating Offshore Test Wind Turbine.” Nov-2018.

[16] “WAMIT R USER MANUAL.”

[17] W. E. Cummins, “The Impulse Response Function and Ship Motions,” in *Symposium on Ship Theory*, 1962, p. 6.

[18] J. Wichers, “Slowly Oscillating Mooring Forces in Single Point Mooring Systems,” in *Second International Conference on Behaviour of Off-Shore Structures*, 1979.

[19] M. G. Gaeta, G. Segurini, A. M. Moreno, and R. Archetti, “Implementation and validation of a potential model for a moored floating cylinder under waves,” *J. Mar. Sci. Eng.*, vol. 8, no. 2, 2020.

[20] H. A. Haslum, “Simplified methods applied to nonlinear motion of spar platforms,” Norwegian Univeristy of Science and Technology, Trondheim, 2000.

[21] A. J. Coulling, A. J. Goupee, A. N. Robertson, and J. M. Jonkman, “Importance of second-Order difference-Frequency wave-Diffraction forces in the validation of a fast semi-Submersible floating wind turbine model,” *Proc. Int. Conf. Offshore Mech. Arct. Eng. - OMAE*, vol. 8, no. June, 2013.

[22] J. R. Browning, J. Jonkman, and A. Robertson, “The effects of second-order hydrodynamics on a semisubmersible floating offshore wind turbine ,” *J. Phys. Conf. Ser*, vol. 524, p. 12094, 2014.

[23] C. Lopez-pavon, R. A. Watai, F. Ruggeri, A. N. Simos, and A. Souto-iglesias, “Influence of Wave Induced Second-Order Forces in Semisubmersible FOWT Mooring Design,” vol. 137, no. June, pp. 1–10, 2015.

CHAPTER 3

DEVELOPMENT OF A MULTI-OBJECTIVE OPTIMIZATION TOOL FOR SCREENING DESIGNS OF TAUT SYNTHETIC MOORING SYSTEMS TO MINIMIZE COST AND RADIUS

3.1. Overview and Comments

This chapter forms the basis of the paper titled "Development of a Multi-Objective Optimization Tool for Screening Designs of Taut Synthetic Mooring Systems to Minimize Mooring Component Cost and Footprint" authored by William M. West, Andrew J. Goupee, Spencer T. Hallowell and Anthony M. Viselli. This paper was submitted to the Journal *Modelling* on October 1st 2021 and was accepted for publication on November 29th 2021. The process outlined to screen for optimized mooring systems was modified and applied to the IEA 15-MW system presented in Chapter 4.

3.2. Abstract

As the offshore wind industry develops, more lease sites in the intermediate water depth (50–85 m) are being released to developers. In these water depths floating wind turbines with chain catenary systems and fixed-bottom turbines with jacketed structures become cost prohibitive. As such, industry and researchers have shifted focus to floating turbines with taut or semi-taut synthetic rope mooring systems. In addition to reducing the cost of the mooring systems, synthetic systems can also reduce the footprint compared to a chain catenary system which frees areas around the turbine for other maritime uses such as commercial fishing. Both the mooring systems component cost and footprint are pertinent design criteria that lend themselves naturally to a multi-objective optimization routine. In this paper a new approach for efficiently screening the design space for plausible mooring systems that balance component cost

and footprint using a multi-objective genetic algorithm is presented. This method uses a tiered-constraint method to avoid performing computationally expensive time domain simulations of mooring system designs that are infeasible. Performance metrics for assessing the constraints of candidate designs are performed using open-source software such as Mooring Analysis Program (MAP++), OpenFAST and MoorDyn. A case study is presented providing a Pareto-optimal design front for a taut synthetic mooring system of a 6-MW floating offshore wind turbine.

3.3. Introduction

The global pipeline for floating offshore wind more than tripled in 2020 and as a result new floating technologies are needed as the industry looks to lease sites in deeper waters [1]. Currently fixed bottom jacket structures or monopiles are used in shallow waters (less than 40 m) and floating offshore wind turbines (FOWTs) with chain catenary mooring systems are used as the water gets deeper (greater than 100 m). In the intermediate water depths of roughly 55–80 m there has not been a clear solution, as fixed bottom structures and floating systems with chain catenary systems both become prohibitively expensive [2]. As researchers have worked to tackle this problem one potential solution, taut synthetic mooring systems have come to the forefront.

Taut-synthetic systems provide restoring force to the platform by the elastic properties of the rope [3]. By comparison, a chain catenary system provides restoring force through the geometry of the mooring system and the weight of the chain [4]. For a chain catenary system to be functional in the intermediate depths a large amount of chain needs to be used to provide the necessary restoring force for the platform. For a taut synthetic system, it is somewhat less clear what makes a good design. Larger diameter ropes are stiffer and attract more load, but a larger diameter rope can also handle larger loads. It is also unclear what level of pretension should be used to ensure that the line can handle the loads while also not becoming slack.

Researchers have begun to develop optimization techniques to determine the best mooring systems specific to the floating platform and environmental conditions. Generally optimizing the mooring system to minimize the cost is a priority but determining if a mooring configuration is feasible is challenging. Some researchers have linearized the FOWT system and used a frequency-domain analysis [5] to estimate the response of the system or used simplified models to determine the maximum vessel responses [6], but this neglects some of the important physics such as the hull hydrodynamic load nonlinearities and fluid loading on the line. Depending on the type of mooring system, for example a chain catenary system, neglecting these nonlinear loadings can greatly under-predict the tension in the mooring lines [7].

Another approach that has been attempted is to train a surrogate-model using many time domain simulations [8] [9] [10]. With this approach potential mooring systems throughout the design space are simulated in the time-domain. These results are then used to build a meta-model or surrogate model where the responses of other designs in the space can be estimated by interpolating between the originally analyzed designs. With this method computational resources need to be set aside at the beginning of the optimization to generate the surrogate model, but after the model is generated, the need
for computational resources decreases. Although the appropriate physics are used to generate the meta-model, there is no guarantee that the designs will behave as the meta-model predicts until a physics-based simulation is performed.

Lastly, time-domain simulations can be used for evaluating the performance of the mooring system within the optimization process [11]. Although this is the most computationally expensive of the approaches, it will lead to the most accurate results. Researchers have also

experimented with screening the designs which time-domain simulations are run on to avoid wasting computational time on poor designs [10] [11].

In this study a new approach is presented which continues to make the time-domain approach more computationally feasible. For this approach a tiered method for evaluating constraints is used to prevent running time domain simulations on undesirable designs. In this process progressively more restrictive constraints are evaluated to determine the effectiveness of a mooring system based on criteria like the platform natural periods which are computationally trivial compared to time-domain simulations used for determining peak mooring line tensions. Only when a design has a fair chance of success is a time domain simulation run to determine the maximum and minimum tensions in the lines. This prevents wasting unnecessary computational time on designs that were destined to fail from the beginning. The tiered constraint approach is applied in this work to optimize a taut synthetic mooring system for a 6-MW FOWT.

3.4. Implementation of the MOGA

The optimization technique used for this study is a multi-objective genetic algorithm (MOGA) coined the NSGA II which was developed by Deb et al. [12]. The version used here is identical to that implemented by Goupee et al. [13]. Genetic algorithms use the biological concept of survival of the fittest to find optimal solutions. In the case of multi-objective optimization there is not one optimal design, but instead a front of Pareto-optimal designs where one objective value cannot be made better without worsening another. The role of the NSGA II algorithm is to find many solutions on this Pareto front.

The algorithm starts by initializing a random population of individuals which represent potential solutions. These individuals have several genes which represent the various design variables. The random population is then evaluated to determine values for the multiple

objectives, and if there are any constraint violations. First, designs are evaluated based on the constraint violation. A member of the population has violated a constraint if the constraint value is greater than zero. The optimizer at first aims to find designs which are not constraint dominated which encourages the optimizer to select parents that have small or zero constraint values. Next, the optimizer will prioritize designs that are non-dominated meaning the other solutions only have one objective value that is better than it while being worse in the other values. Finally, the NSGA II algorithm aims to encourage formation of the Pareto front by first favoring the non-dominated individuals and secondly favoring individuals which have a larger distance between the solutions.

After the individuals have been ranked and sorted, they are placed into a mating pool. Members of the population that have zero constraint values, are non-dominated and possess larger crowding distances are more likely to make it into the mating pool. From this pool individuals will be selected, and reproduction will occur to create new solutions called children. Reproduction consists of crossover between the parents to create offspring. The NSGA II algorithm uses simulated binary crossover where a randomly generated number is used to calculate a number, beta. This beta value is then used to determine the children via a weighted average of the two parents. At this point random mutations may also occur. Each individual gene has a probability of mutating where its value can be changed to any value between the upper and lower bound values for the variable associated with a particular gene. The children created then have their objective values determined, and the constraints are evaluated. This process is repeated for a set number of generations specified by the user until a Pareto-optimal front is reached. An overview of the NSGA II is shown in Figure 3.1.

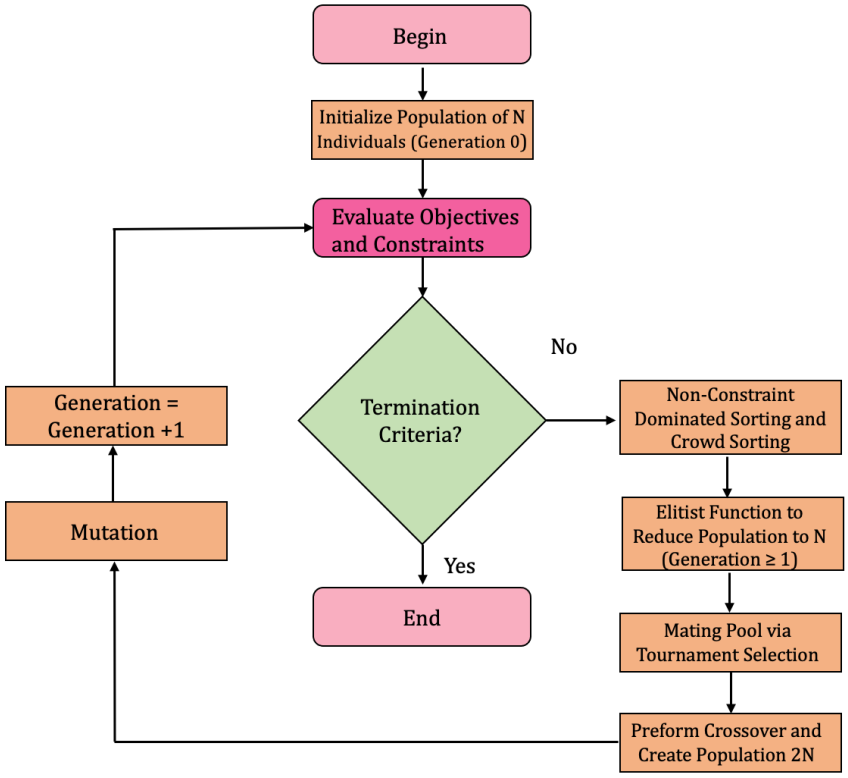

Figure 3.1. NSGA II Flowchart

In general, an optimization problem is expressed as finding a solution which will minimize various objective functions, while simultaneously passing constraints. Mathematically this is represented in Equation (3.1.):

$$\text{Find } x_i \text{ , } i = 1, 2, \dots, V \tag{3.1.}$$

$$\text{Minimize } [f_n(\boldsymbol{x})]\,; n = 1, 2, \dots, N$$
$$\text{Subject to } g_p(\boldsymbol{x}) \geq 0; p = 1, 2, \dots, P$$

Where: $\boldsymbol{x}$ is the vector of design variables
V is the number of design variables
$f_n(\boldsymbol{x})$ are the objective functions to be minimized
N is the number of objective functions
$g_p(\boldsymbol{x})$ are the constraint violations
P is the number of inequality constraints the optimization problem is subject to

For this problem the solution vector of design variables will include important characteristics of a mooring system for a FOWT from which other properties will be derived. The vector of design variables of interest for this problem is provided in Equation (3.2.):

$$\boldsymbol{x} = [R, L_{syn}, d_{syn}, d_{chain}] \tag{3.2.}$$

Where: R is the mooring system radius as measured from the platform centerline
L_{syn} is the length of the synthetic line (expressed as a fraction of *R)*
d_{syn} is the diameter of the synthetic line
d_{chain} is the chain diameter

This optimization problem will feature two objective functions that are of importance for a FOWT mooring system, cost and mooring radius. Reducing cost for any renewable energy application is of utmost importance to ensure that the technology is economically feasible. In addition, it is crucial to try and minimize the radius, and by extension footprint, of the FOWT to minimize environmental impacts and impacts on other ocean uses such as fishing. For a multi-objective optimization routine to successfully find a Pareto-optimal front it is necessary that the objectives are competing. At first glance it would seem as though these objectives are not competing as smaller mooring radii have smaller corresponding line lengths which will be less expensive. However, there are two trends that cause larger mooring radii to ultimately be cheaper for taut systems based on initial designs that were generated [14]. First, for a taut mooring system as the mooring radius increases the line length will also increase effectively reducing the stiffness of the mooring system for the same line stiffness (EA). This softer system will lead to the mooring system attracting less loads which will ultimately require a smaller diameter line. Second, as the mooring system radius increases the line becomes more horizontal which makes it better able to resist platform motions. Mathematically, the multi-objective minimization problem is stated in Equation (3.3.):

$$\text{Minimize } [f_1(\boldsymbol{x}), f_2(\boldsymbol{x})] \tag{3.3.}$$
$$\text{Subject to: } g_i(\boldsymbol{x}) \geq 0, i = 1,2,\dots,6$$
$$210 \text{ m} \leq R \leq 290 \text{ m}$$
$$0.68 \leq L_{syn} \leq 0.80$$
$$100 \text{ mm} \leq d_{syn} \leq 192 \text{ mm}$$
$$100 \text{ mm} \leq d_{chain} \leq 177 \text{ mm}$$

Where: $f_1(\boldsymbol{x})$ is the mooring system radius
$f_2(\boldsymbol{x})$ is the mooring system component cost
$g_1(\boldsymbol{x})$ is the mooring system geometric constraint violation
$g_2(\boldsymbol{x})$ is the platform heave natural period constraint
$g_3(\boldsymbol{x})$ is the platform pitch natural period constraint
$g_4(\boldsymbol{x})$ is the maximum chain tension constraint
$g_5(\boldsymbol{x})$ is the maximum synthetic tension constraint
$g_6(\boldsymbol{x})$ is the minimum synthetic tension constraint

The constraints for this optimization problem ensure that the mooring system being analyzed is a valid solution. Many of these constraints are based on the ABS/IEC guidelines for designing and simulating floating offshore wind turbines, but time-domain simulations are very computationally expensive. To avoid running time-domain simulations, if possible, a tiered constraint system has been implemented where simpler and more computationally efficient constraints are used to screen potential designs. If the simple constraints are not met this indicates that the design would not be worth analyzing in the time domain. At a high level the constraints and their order from simple to complex are as follows:

1) A geometric feasibility constraint is implemented to avoid analyzing designs where the line lengths for a certain mooring radius yield nonsensical designs (i.e., $g_1(\boldsymbol{x})$).

2) Next, the FOWT platform periods are estimated so that designs which do meet minimum natural period requirements and would likely have resonance issues due to the wave loading are not analyzed (i.e., $g_2(\boldsymbol{x})$ *and* $g_3(\boldsymbol{x})$).

3) Designs which pass the aforementioned constraints are subjected to DLC 6.1 simulations to determine the maximum and minimum loads in the mooring system and assess constraints requiring these values (i.e., $g_4(\boldsymbol{x}) - g_6(\boldsymbol{x})$).

The various constraints are posed in such a way that failing earlier on in the screening process leads to larger constraint violations, thus encouraging the optimizer to favor designs that make it further into the screening process. A design that makes it further into the screening process is more likely to have design characteristics that are desirable. A flow chart illustrating how the objective functions and constraints are calculated is provided in Figure 3.2. The mathematical specifics of the constraints are discussed in the subsequent text.

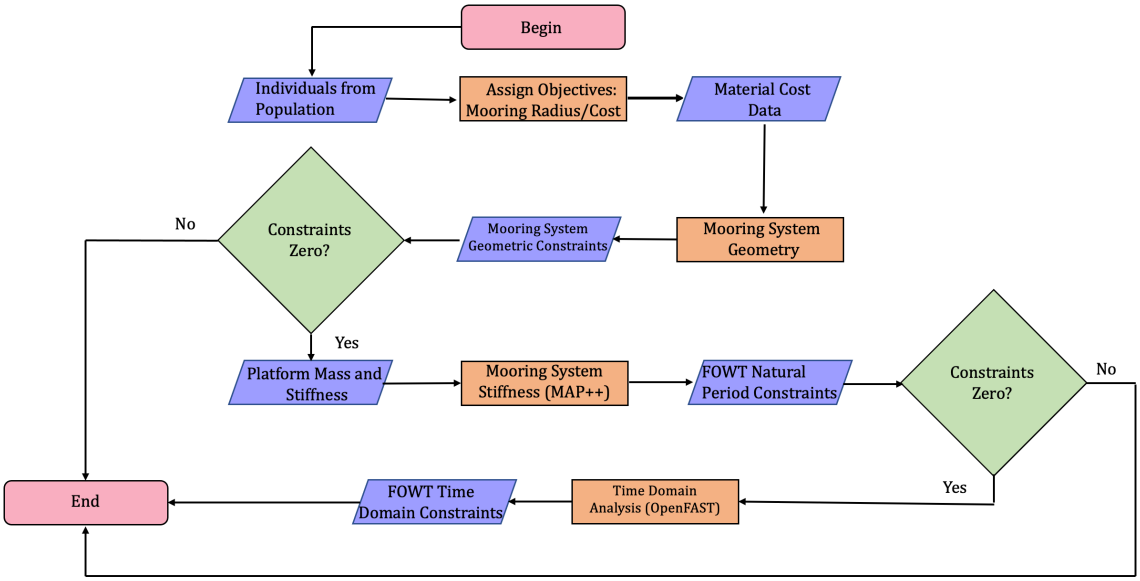

Figure 3.2. Constraint and Objective Calculation Flow Chart.

The first constraint considered in Figure 3.2. is whether the mooring system is geometrically feasible. There are two obvious scenarios where the mooring system would be geometrically infeasible and lead to constraint violations. The first is the situation where there is no horizontal component to the reaction in the line. A line that goes directly from the fairlead

connection point vertically to the seafloor will not provide a restoring force so any line length that is greater than the sum of the distance from the fairlead depth to the seafloor and the fairlead radius to the anchor radius will be considered an invalid solution and penalized accordingly. Similarly, there is a maximum level of prestrain in a synthetic line for which the dynamics of the turbine will not be handled. Generally, it would not be feasible to have a line which has a prestrain more than roughly 10%. As such, line length less than approximately 90% of the straight-line distance between the fairlead and anchor connections are also subject to a large constraint violation. Depending on the synthetic materials used for analysis this percentage could change. For example, an extremely stiff synthetic material such as Dyneema would only be feasible for a much lower prestrain. The mooring system schematic illustrating the mooring system and platform geometry needed to determine if a design meets this geometric feasibility constraint is illustrated in Figure 3.3.

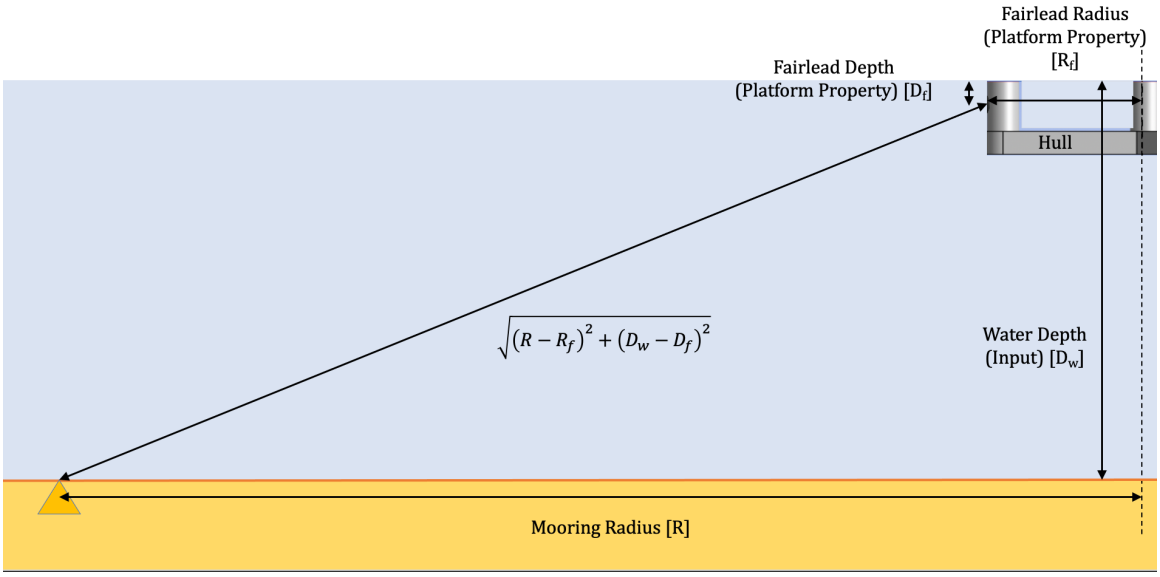

Figure 3.3. Geometric Feasibility Design Constraint.

For the constraints to guide the optimizer towards feasible solutions they must be carefully constructed. The minimum line length geometric constraint is provided in Equations (3.4.) and (3.5.). The constraint violation is crafted in such a way that a line that is just barely infeasible, such as a line prestrain of 11%, will have a smaller constraint violation than more egregious designs which will yield larger constraint violations. In this way the design variable vector will be guided towards feasible solutions. The maximum line length geometric constraint is constructed in a very similar way to ensure that the optimizer is guided towards good designs. If the mooring system fails these initial constraints, it will not be worth evaluating the more computationally expensive constraints, and these poor designs will be screened out immediately.

$$\text{If:} \quad L_T \leq 0.9\sqrt{\left(R - R_f\right)^2 + \left(D_w - D_f\right)^2} \tag{3.4.}$$

$$\text{Then:} \quad g_1 = 100\frac{0.9\sqrt{\left(R - R_f\right)^2 + \left(D_w - D_f\right)^2} - L_T}{0.9\sqrt{\left(R - R_f\right)^2 + \left(D_w - D_f\right)^2}} + 100$$

$$\text{Else:} \quad g_1 = 0$$

$$\text{If:} \quad \left(R - R_f\right) + \left(D_w - D_f\right) \leq L_T \tag{3.5.}$$

$$\text{Then:} \quad g_1 = 100\frac{L_T - [\left(R - R_f\right) + \left(D_w - D_f\right)]}{[\left(R - R_f\right) + \left(D_w - D_f\right)]} + 100$$

$$\text{Else:} \quad g_1 = 0$$

Where:
R_f is the distance from the center of the platform to the fairlead connection point
D_w is water depth
D_f is the depth from the mean water line (MWL) to the fairlead connection point
L_T is the total line length

The next constraints to check are the rigid-body natural periods of the platform. If the heave and pitch natural periods of the platform are too close to typical periods of ocean waves it is more likely that the platform motion will experience resonance increasing loads throughout the

FOWT, and thus, the mooring system design would be unsatisfactory. To calculate the natural periods for heave and pitch as shown in Equations (3.6.) and (3.7.), the stiffnesses due to the hydrostatic restoring force and mooring system stiffness as well as the mass/inertia and added mass/inertia properties of the platform are needed. All the quantities except the mooring system stiffness are from the turbine and tower masses and locations as well as the platform mass and dimensions. The mooring system stiffness is determined using Mooring Analysis Program (MAP++).

MAP++ [15] is a quasi-static catenary line solver which is more computationally efficient then a lumped mass model such as MoorDyn [16] which will be used for the time domain simulations. It can be used within OpenFAST [17] to model a mooring system or can be called on its own to determine properties like the 6 × 6 mooring system stiffness matrix. The one downside to MAP++ is that it only allows linear elastic materials in the mooring system. As a result, it is important to estimate the stiffness of the synthetic segment of the mooring line at the corresponding installed strain. This approach will lead to a mooring system that has the right stiffness characteristics about the undisplaced position of the FOWT which is sufficient for computing natural frequencies.

As with the geometric constraints the constraint values have been carefully crafted to return smaller values for natural periods that are closer to the specified values to drive the vector of design variables towards a feasible solution. The total constraint violation for the natural periods will be the sum of the constraint violations calculated in Equations (3.6.) and (3.7.). For this method of estimating the natural periods the hydrodynamic quantities are calculated about the waterline. For a semi-submersible hull where the center of gravity is close to the water line this method will yield reasonable estimates of the natural periods.

$$T_{n\_\text{heave}} = \frac{2\pi}{\sqrt{\frac{k_{33} + k_{33\text{Mooring}}}{m_{\text{platform}} + a_{33}}}} \tag{3.6.}$$

If: $T_{n\_\text{heave}} \leq 18$

Then: $g_2 = 30\frac{18 - T_{n\_\text{heave}}}{18} + 50$

Else: $g_2 = 0$

Where: k_{33} is the platform heave stiffness
$k_{33\text{Mooring}}$ is the mooring system heave stiffness
m_{platform} is the mass of the platform
a_{33} is the infinite period added mass of the platform in heave
T_{n_heave} is the platform heave natural period

$$T_{n\_\text{pitch}} = \frac{2\pi}{\sqrt{\frac{k_{55} + k_{55\text{Mooring}}}{I_{\text{platform}} + a_{55}}}} \tag{3.7.}$$

If: $T_{n\_\text{pitch}} \leq 25$

Then: $g_3 = 30\frac{25 - T_{n\_\text{pitch}}}{25} + 50$

Else: $g_3 = 0$

Where: k_{55} is the platform pitch stiffness
$k_{55\text{Mooring}}$ is the mooring system pitch stiffness
I_{platform} is the platform pitch inertia
a_{55} is the infinite period added inertia of the platform in pitch
T_{n_pitch} is the platform pitch natural period

If the previous constraints are not violated by the mooring system a time-domain simulation is run in OpenFAST to check the tensions in the lines due to ultimate loading. This includes checking the tension both at the chain fairlead and in the synthetic section to ensure that the line tension is below the line MBS with the appropriate ABS/IEC factors of safety, as well as ensuring that the tension in the synthetic section does not go slack. The constraint violations for the tension in the chain leader are given by Equation (3.8.) and the constraint violation for the

maximum tension in the synthetic segment is given by Equation (3.9.). The last of the constraints to be checked is the minimum synthetic tension requirement given in Equation (3.10.). Chain sizes are typically driven by fatigue, so a fatigue factor is used to ensure the chain diameter is large enough. A minimum tension in the synthetic segment is also included to ensure that the line does not go slack. The values for the factors of safety and how they are chosen is outlined in the optimization inputs section.

$$\text{If:} \quad F_{f\_\text{chain}}\, \mathrm{T}_{\text{fairlead\_max}} \geq \mathrm{MBS}_{\text{chain}} \tag{3.8.}$$
$$\text{Then:} \quad g_4 = \frac{F_{f\_\text{chain}}\, \mathrm{T}_{\text{fairlead\_max}} - \mathrm{MBS}_{\text{chain}}}{\mathrm{MBS}_{\text{chain}}}$$
$$\text{Else:} \quad g_4 = 0$$

Where: $\mathrm{T}_{\text{fairlead\_max}}$ is the maximum tension at the fairlead
F_{f_chain} is chain fatigue factor
$\mathrm{MBS}_{\text{chain}}$ is the minimum breaking strength of the chain

$$\text{If:} \quad F_{s\_\text{syn}}\mathrm{T}_{\text{syn\_max}} \geq \mathrm{MBS}_{\text{syn}} \tag{3.9.}$$
$$\text{Then:} \quad g_5 = \frac{F_{s\_\text{syn}}\mathrm{T}_{\text{syn\_max}} - \mathrm{MBS}_{\text{syn}}}{\mathrm{MBS}_{\text{syn}}}$$
$$\text{Else:} \quad g_5 = 0$$

Where: $\mathrm{T}_{\text{syn\_max}}$ is the maximum tension at the fairlead
F_{s_syn} is the ABS synthetic factor of safety for a synthetic rope
$\mathrm{MBS}_{\text{syn}}$ is the minimum breaking strength of the synthetic rope

$$\text{If:} \quad \mathrm{T}_{\text{syn\_min}} \leq F_{\text{min\_syn}} \cdot \mathrm{MBS}_{\text{syn}} \tag{3.10.}$$
$$\text{Then:} \quad g_6 = \frac{F_{\text{min\_syn}}\, \mathrm{MBS}_{\text{syn}} - \mathrm{T}_{\text{syn\_min}}}{F_{\text{min\_syn}} \cdot \mathrm{MBS}_{\text{syn}}}$$
$$\text{Else:} \quad g_6 = 0$$

Where: $\mathrm{T}_{\text{syn\_min}}$ is the minimum tension at the fairlead
$F_{\text{min\_syn}}$ is the minimum allowable line tension to avoid slack lines as a percentage of MBS

The last part of the constraint violations that is worth discussing is the constant added to the geometric and natural period constraint violations. These are crafted to guide the optimizer toward more suitable solutions. In this case a design which fails the geometric constraint will automatically be larger than any designs that fail the natural period constraint or the time-domain constraints. Because designs that fail the geometric constraints will be especially poor designs, this will guide the optimizer towards solutions that are at least evaluated for the natural periods and/or in the time domain. Similarly, a design which fails one of the natural period constraints will always have a larger constraint value than a design which makes it through to the time domain simulations. This ensured that the optimizer always favors designs that made it further in the process which helps the optimizer find feasible solutions while also avoiding computationally taxing time domain simulations of poor designs.

3.5. Optimization Inputs

To perform an optimization for a FOWT mooring system a few key inputs are necessary. First, mooring line property and cost data for both the chain and the synthetic materials are provided. In the case of synthetics, the nonlinear tension-strain response of the line are key inputs and crucial to obtaining the correct mooring line responses. The second key input is the FOWT properties including the location of the center of gravity and mass of various components such as the tower, turbine, and platform. In addition, the hydrodynamic properties of the floater are needed. Lastly, the design criteria such as factors of safety, and the environmental loading on the turbine including the wind, wave, and current loading necessary for performing the optimization are provided.

For this case study a taut synthetic mooring system for a 6-MW turbine based on the University of Maine's VolturnUS floating platform will be optimized to minimize the mooring

footprint and component cost. This turbine will be subject to the ABS/IEC DLC 6.1 conditions associated with the University of Maine Monhegan test site.

3.5.1. Mooring System

The mooring system to be optimized is a taut synthetic system. This system includes a chain leader at the fairlead as well as chain at the anchor as required by ABS to mitigate Ultra-Violet (UV) and sediment damage respectively. A design schematic for the mooring configuration described is provided in Figure 3.4.

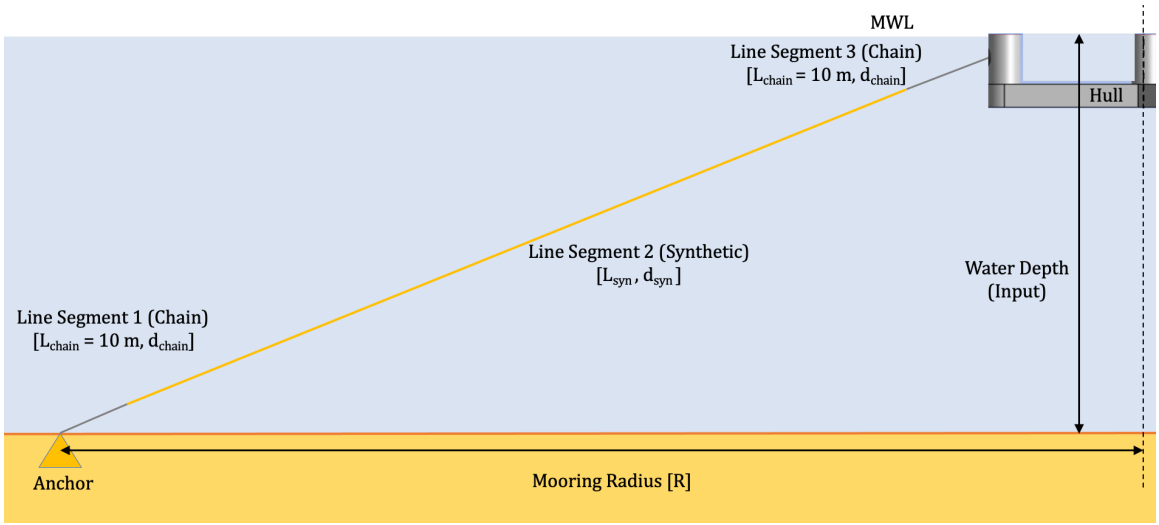

Figure 3.4. Mooring System Schematic for Optimization

For this optimization case study, the chain leaders at the top and bottom of the mooring line were fixed at 10 m each and both were required to have the same chain diameter which could range from 100 mm to 177 mm. The synthetic diameter could range from 100 mm to 192 mm as long as the design constraints were met. The mooring system properties for this configuration including the fairlead connection points on the platform and orientation of the mooring lines are provided in Table 3.1.

Table 3.1. Mooring System Properties.

Number of mooring lines	3
Angle of mooring lines (0° aligned with positive surge axis; positive defined as counter-clockwise)	60°, 180°, 300°
Depth to anchors below SWL (water depth)	55 m
Depth to fairleads below SWL	5.4 m
Radius to anchors from platform centerline	Design Variable
Radius to fairleads from platform centerline	45.7 m
Unstretched chain length (Leader)	10 m
Unstretched chain length (Anchor)	10 m
Unstretched synthetic length	Design Variable
Synthetic line diameter	Design Variable
Chain diameter	Design Variable

Synthetic lines exhibit a nonlinear tension-strain response that is important to account for when designing a system. A modified version of OpenFAST that has been validated against experimental data is used to incorporate the nonlinear behavior [18]. In this modified version of OpenFAST a general line tension strain response can be input into the model via a lookup table. For this problem the synthetic and chain tension-strain curves are provided in Figure 3.5. Note that both the synthetic and chain tension-strain responses provided are non-dimensionalized based on the line MBS.

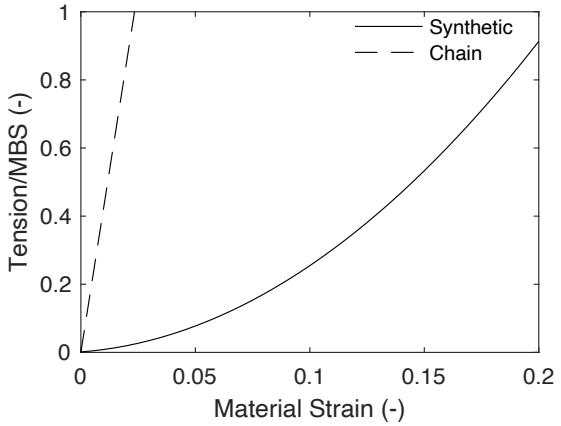

Figure 3.5. Material Tension-Strain Relationships.

The chain and synthetic load capacity and mass properties are provided in Figure 3.6. The mass properties provided are the line dry mass per unit length. The specific gravity of the synthetic mooring lines is 1.15.

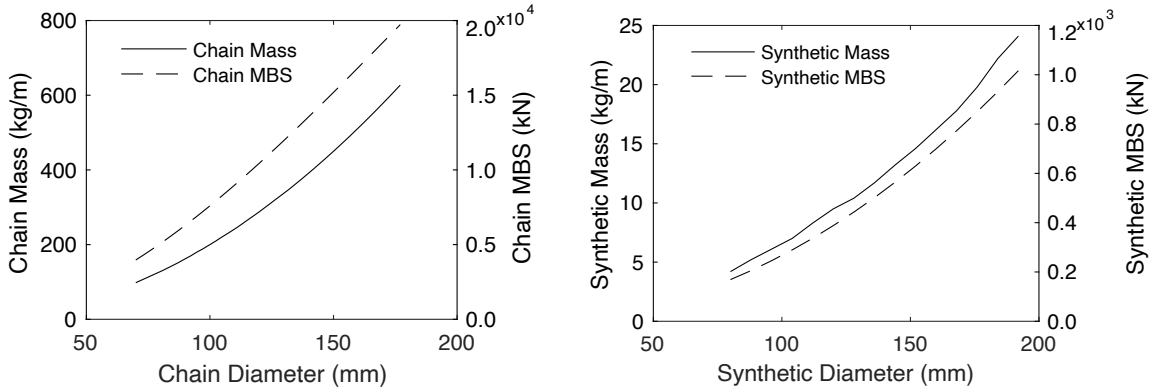

Figure 3.6. Dry Chain Mass and Chain Load Capacity (left) and Dry Synthetic Mass and Synthetic Load Capacity (right)

The last piece of data needed to optimize the mooring system is the cost data for each of the line components which is provided in Table 3.2. For this optimization only the mooring line component cost will be minimized so connections, installation and anchor costs will not be included. In future work the optimizer will be expanded to account for these other costs, but where the designs are similar it will be assumed that these costs not accounted for will be similar across the various designs.

Table 3.2. Mooring System Material Costs.

Material	Cost (USD/kg)
Steel	1.50
Synthetic	17.00

3.5.2. Description of the Turbine

For this study a 6-MW turbine based on the University of Maine VolturnUS technology is used. The VolturnUS platform is a concrete semi-submersible design with three radial columns providing stability and a center column which the turbine is mounted to. Three pontoons connecting the columns also serve as ballast tanks which can be filled with seawater to ensure that the draft of the platform is 20 m. The dimensions of the VolturnUS 6-MW floating platform are provided in Figure 3.7.

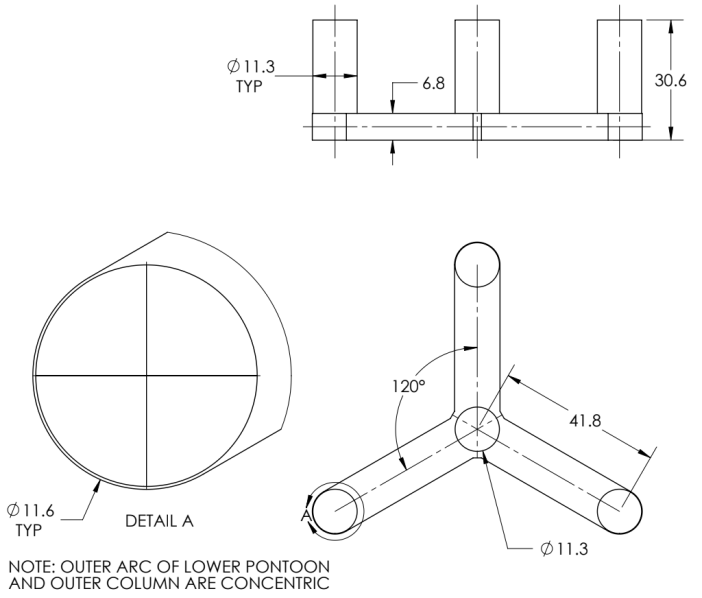

Figure 3.7. VolturnUS 6-MW Platform Dimensions in Meters.

OpenFAST uses hydrodynamic information from a potential flow solver, WAMIT [19], to solve for the forcing on the hull as well as the frequency-dependent added mass and damping coefficients. WAMIT solves the frequency-domain potential flow wave-structure interaction problem using a panel-based method with the appropriate boundary conditions. The hydrostatic stiffness matrix as well as the infinite-period added mass matrix are needed to estimate the

natural periods of the structure and are obtained from the potential flow analysis using the submerged geometry of the 6-MW VolturnUS platform. WAMIT provides the stiffness contribution due to both the waterplane area and the center of buoyancy, but the center of gravity contribution is handled separately in OpenFAST by finding the component masses and locations, some of which are deformable, and using those to compute the FOWT weight and center of gravity at any instant in time. The FOWT mass properties are provided in Table 3.3.

Table 3.3. FOWT Component Mass and Locations.

Total Draft	20.0 m
Platform Mass, Including Ballast	1.09×10^7 kg
Displacement	1.17×10^4 m^3
Center of Mass (CM) Location Below SWL Along Platform Centerline	11.85 m
Platform Roll Inertia About CM	5.23×10^9 kg-m^2
Platform Pitch Inertia About CM	5.23×10^9 kg-m^2
Platform Yaw Inertia About CM	8.33×10^9 kg-m^2
Hub Height Above SWL	100 m
Total Tower Top Mass	557,000 kg
Tower Mass	246,000 kg
Tower CM above SWL	72.9 m

3.5.3. Design Criteria

The design criteria for FOWT installations are provided by the American Bureau of Shipping (ABS) classing agency and International Electrotechnical Commission (IEC) standards organization. Certain extreme design load cases (DLCs), such as DLC 6.1 the 50-year extreme storm environment, are commonly found to dictate the size of the mooring system [20][21]. For this DLC, ABS/IEC require that six simulations of at least
one-hour duration be analyzed with different random conditions representing the turbulent wind field and irregular wave field, and the mooring line design value is based on mean of the maximum mooring line response from these six simulations.

In addition to the DLCs of importance, the classing agencies also give guidance on the material factors of safety to be used and other requirements of the mooring system. For a taut synthetic mooring system with non-redundant mooring lines the material factor of safety is 2.184. This value is derived from a synthetic material factor of safety of 1.82 which is increased by 20% for a non-redundant mooring system [21][22][23]. Fatigue damage for synthetic ropes is not a concern because the steel connections are far more susceptible to fatigue failure. The guidelines also require that the synthetic section be submerged to mitigate UV damage [24] and kept off the seafloor to prevent coarse sand and dirt from becoming embedded in the rope and damaging it. This requires chain leaders to be installed at both the anchor side and fairlead side of the mooring system.

In addition to the maximum tension requirements, the classing agencies also prohibit slack line events for certain synthetic materials. With this requirement there is some flexibility, and it is not explicitly stated what that would entail for synthetics such as nylon and polyester. Guidance, however, is given for aramid fiber ropes which have failed on oil and gas platforms due to the phenomenon of axial compressive fatigue [22][25]. To prevent that from occurring in those types of synthetic fiber ropes it is required that the minimum load in the line stay above 2% of the minimum breaking strength (MBS) of the line. Although this value is likely conservative for materials such as nylon and polyester which do not risk failure due to the axial fatigue phenomenon, it is applied here to ensure a robust design. The design requirements in this work are summarized in Table 3.4.

Table 3.4. Mooring System Design Requirements.

Synthetic Minimum Breaking Factor of Safety	2.18
Chain Minimum Breaking Factor of Safety	6.78
Partial safety factor for DLC 6.1 Loads	1.35
Minimum Line Tension	2% of Synthetic MBS
Minimum Platform Surge Period	40s
Minimum Platform Heave Period	18s
Minimum Platform Pitch Period	25s

The second value from Table 3.4., the minimum chain factor of safety used, does not follow directly from design standards. This value was derived from a fully designed and ABS-approved [26] chain catenary mooring system for the same platform and environmental conditions. To obtain this value the 100% ABS approved catenary system was simulated according to DLCs 1.2 (operational wind turbine with associated wave conditions), which makes up most of the fatigue damage conditions for the mooring system, and DLC 6.1 which is assumed to control ultimate limit state design. The minimum breaking strength required for a given chain size to satisfy the DLC 1.2 conditions was divided by the minimum breaking strength required to satisfy the DLC 6.1 conditions, resulting in a fatigue factor. Such a factor is used to estimate chain sizes that would satisfy fatigue requirements after only running DLC 6.1.

The last values presented in the table are the minimum platform periods. If the mooring system has a surge period less than 40 s it is extremely likely that the mooring system will be overly stiff and attract large loads to the mooring system requiring larger mooring components. The minimum heave and pitch periods are dictated by the wave loading on the platform. If the mooring system adds too much stiffness to heave and pitch responses the platform responses could get too close to wave energy periods leading to resonance issues with the FOWT and excessive wind turbine loads and accelerations.

3.5.4. Environmental Loading

The environmental loading applied to the model is due to wind, wave, and current loading for the ABS DLC 6.1 50-year event. The wave loading applied to the structure is based on the University of Maine Monhegan test site [27]. For the VolturnUS system at this location the ABS/IEC DLC 6.1 is the driving load case for ultimate loads. Although the Survival Load Case (SLC) has a larger associated significant wave height of 12.0 m vs. 10.2 m [28] the partial safety factors for normal and abnormal loading are specified by ABS/IEC by 1.35 and 1.1, respectively. This leads to the DLC 6.1 factored loads being larger than the SLC loads [29].

The environmental loading is applied at both 0 degrees and 180 degrees to produce the largest and smallest loads in the front line parallel to the environmental loading directions, respectively. The DLC 6.1 environment including the parameters that describe the JONSWAP wave spectrum (significant wave height, peak period and a shape parameter) as well as the mean loads due to wind, second order wave and current is provided in Table 3.5.

Table 3.5. FOWT Environmental Loading.

Wave Loading			
JONSWAP Spectrum	H_s (m)	T_p (s)	γ
	10.7	14.2	2.75
Mean Load due to Second-order Wave Effects	Mean Load (kN)		
	19.9		
Current Loading			
Mean Load due to Current	Current Velocity (m/s)	Mean Load (kN)	
	0.28	49	
Wind Loading			
Mean Load due to Wind	Wind Velocity (m/s)	Mean load (kN)	
	23.8	290	

Generally, DLC 6.1 requires applying a turbulent wind field to the FOWT which requires that the simulations use small timesteps (~10 ms) to resolve high frequency responses in the

structure. To avoid unnecessary computational expense, tower and blade degree of freedoms in OpenFAST were disabled, and the aerodynamic loading was applied as a mean load. These responses likely will only marginally influence mooring line tensions, which ultimately dictate the design of the mooring system components. The mooring system tensions are driven largely by the motion of the platform, which has low rigid-body natural frequencies and whose motions are well predicted even with large timesteps.

Similarly, the low-frequency and second order wave response is approximated by applying a mean load onto the FOWT. It is possible to model these responses in OpenFAST using second-order sum and difference frequency quadratic-transfer functions (QTFs) but during initialization it takes OpenFAST ~40 s to read in the QTFs which will quickly make the problem computationally infeasible on the average desktop computer with four cores. Ideally, with sufficient computational resources the time domain simulations would be performed with both a turbulent wind field and the full second-order QTFs, but for computational efficiency the mean load due to the second order-wave effects was determined by using only the diagonal terms of the difference QTF and the wave heights from the JONSWAP spectrum as outlined in DNV's Global Performance of Deepwater Floating Structures [30].

3.6. Acceleration the Simulation Process for Obtaining Design Constraint Values

With enough computational resources designs generated with the optimization process outlined in this paper could follow the guidance provided by the ABS/IEC including running all the required DLCs. Unfortunately, this is computationally infeasible with the computational resources used in this study and instead one of the design-driving load conditions, DLC 6.1 the 50-year wind and wave loading, is chosen as the controlling design scenario. Even running only one DLC requires many seeds and wind/wave headings and for this design that would include six

one-hour simulations as required by ABS. To induce both the maximum and minimum responses in the lead line this would require two DLC 6.1 runs, 0 and 180 degrees, and would bring the total number of one-hour simulations to 12. Unfortunately, even with the simplifications made to the environmental loading by modeling the current, second-order wave loading and wind loading as a mean load the problem is still too computationally expensive with normal computational resources. To make the problem posed more computationally tractable on an average desktop computer with four cores, several approaches were applied that reduced computational time during the optimization process.

3.6.1. Extrapolating the Maximum DLC 6.1 Line Response Based on a Shorter Simulation Time

Ideally all six one-hour simulations would be run for the 0- and 180-degree loading scenarios, and this could be done given the right computational resources. The maximum and minimum tension response in the line is estimated based on a generalized extreme value (GEV) fit of a shortened simulation, and second a seed is carefully selected such that the maximum tension response in the line closely matches the DLC 6.1 maximum design load obtained from the full complement of full-length simulations. In order to select this seed, the maximum line tension design load is found using the ABS/IEC design guidelines for a representative design that involves taking the mean of the maximum tensions from six one-hour simulations using randomly generated seeds to generate the JONSWAP wave spectra. The DLC 6.1 simulations were run on a representative design for a taut nylon moorings system deployed in a water depth of 55 m with a mooring radius of 205 m [20]. The results of these simulations including the randomly generated seeds and line tensions statistics used in this work are presented in Table 3.6.

Table 3.6. DLC 6.1 Results for VolturnUS 6-MW Moored with a Basin Tested 6-MW System (0 Degree Loading; Front Line).

HydroDyn SEED 1	HydroDyn SEED 2	Max Tension (N)	Min Tension (N)	Mean Tension (N)	STD Tension (N)
674802239	-228621085	2.36e6	2.78e5	1.13e6	3.44e5
-2090187775	1455391302	2.92e6	2.27e5	1.13e6	3.63e5
-1973081278	-629542915	2.59e6	2.59e5	1.13e6	3.67e5
301302578	-328425023	2.82e6	1.33e5	1.13e6	3.88e5
81611327	265255796	2.48e6	2.52e5	1.13e6	3.38e5
133186342	1154134095	3.31e6	1.75e5	1.13e6	3.82e5

The smallest and largest maximum line tension simulated by OpenFAST for the six one-hour simulations was 2362 kN and 3318 kN, respectively. The maximum line tension used for design is the average of these six runs or 2751 kN. The coefficient of variation of the mean load in the line is 0.2% which is expected since the mean environmental load is the same for all simulations. Lastly, the coefficient of variation for the line tension standard deviation is 5.4% which signals that each simulation contains a similar amount of energy from the environmental loads. This is also to be expected as a JONSWAP spectrum with different seeds should induce a similar statistical response to the platform with sufficient simulation time.

Before the simulation results could be fit to a statistical distribution the tension peaks from the mooring line tension time history had to be extracted. To ensure the selected data points are truly peaks the data was first smoothed using a Savitzky-Golay Filter by calling MATLABs built in function sgolay. This ensures that small numerical errors from OpenFAST are not selected as peaks and that peaks are not accounted for more than one time. It is also important

that the method for searching for peaks is repeatable across different mooring designs. For this problem it was found that searching for peaks where the minimum peak prominence was two times the standard deviation of the line tension signal would return good results. In this context, minimum peak prominence was found by comparing the local maximum to the local minimums on either side, and the smaller of the differences between the local maxima and minima is defined as the prominence. The peaks in the signal were determined using MATLABs built in function findpeaks.

Once the peaks of the mooring line tension response were determined a GEV distribution was fit to the peaks as illustrated in Figure 3.8. The empirical cumulative density function matches the GEV distribution well and stays within the 95% confidence intervals providing evidence that the GEV is a good statistical fit for this data.

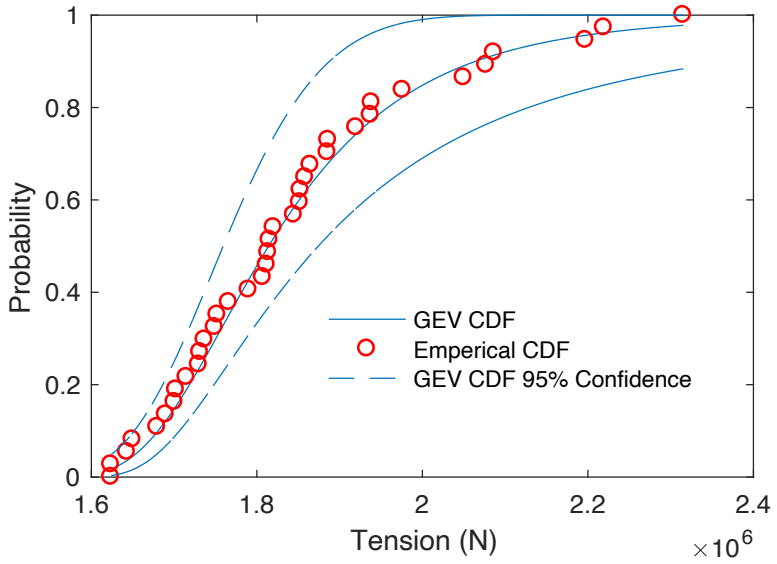

Figure 3.8. Example Fairlead Tension Cumulative Distribution Function.

The maximum tension response in the mooring line was extrapolated using 1000 s worth of data. To extrapolate the maximum tension in the mooring line all the peaks in the signal

during the 1000 s simulation were counted. The number of peaks were then used to estimate the number of peaks that would occur in a one-hour simulation, and the GEV distribution was fit to the tension peaks of 1000 s worth of data. Using the estimated peaks that would occur in the signal the probability of the maximum event was determined, and this probability was used with the GEV cumulative distribution function to estimate the maximum tension response in the line. The results of using this method of 1000 s used to estimate the tension response is presented in Table 3.7.

Table 3.7. Extrapolating the Maximum 1-Hour DLC 6.1. Line Tensions using 1000s of Simulation Data.

Run	Number of Peaks in 1000s	Number of Peaks Extrapolated to 3600s	Probability of Maximum Tension in 3600s	Predicted Tension (N)
A	46	165	99.39%	2.81e6
B	45	162	99.38%	3.97e6
C	46	165	99.39%	3.18e6
D	44	158	99.36%	3.67e6
E	45	162	99.38%	2.44e6
F	51	183	99.45%	2.17e6

The DLC 6.1 design value for tension in the mooring line was 2751 kN based on the mean of the maximum line responses for the six–one-hour simulations, and the value extrapolated from the first 1000 s of seed A, 2810 kN, is close to the design value. One thousand seconds of Seed A in tandem with extrapolating the maximum tension response in the line returned a tension that was 2% larger than the ABS derived DLC 6.1 design value. This particular seed and the proposed extrapolation approach were used to evaluate mooring system design constraints requiring peak (or minimum) tensions. It is once again worth noting that more

accurate peak values could be obtained by running the full suite of full-length simulations with the aerodynamics and second order wave forcing calculations enabled in OpenFAST. This approach for the optimization routine would be recommended if the computational resources were available.

3.6.2 Selection of OpenFAST and MoorDyn Timesteps

Another important and non-trivial simulation setting is the selection of OpenFAST and MoorDyn timesteps as well as the discretization of the mooring line. Smaller timesteps will provide more accuracy in the solution at the expense of more computational resources. It was also found through testing that the OpenFAST and MoorDyn timesteps have a dependency on each other. For a given OpenFAST timestep and a taut-synthetic mooring configuration with 10 m of chain at the anchor and fairlead there is a limit on how small the MoorDyn timestep can become, and if it is too small, the model loses numerical stability. This may be due to the loose coupling that is used within OpenFAST where the physics of the mooring line and the platform motions are solved separately of one another, and information is passed between each solver through the OpenFAST glue code. Another plausible explanation for this observation could be due to high-frequency axial models of vibration in the line that can only be resolved with a sufficiently small timestep.

To determine the right level of mooring line discretization in tandem with the appropriate OpenFAST and MoorDyn timesteps a convergence study was undertaken. In this convergence study the line was discretized into 10, 40 and 160 line segments. The largest and smallest MoorDyn and OpenFAST timesteps, respectively, were determined based on the highest estimated natural frequency of a lumped mass node. The OpenFAST and MoorDyn timesteps used in this study are provided in Table 3.8.

Table 3.8. OpenFAST and MoorDyn Convergence Study

10 Lumped Masses		40 Lumped Masses		160 Lumped Masses	
OpenFAST Timesteps (s)	MoorDyn Timesteps (ms)	OpenFAST Timesteps (s)	MoorDyn Timesteps (ms)	OpenFAST Timesteps (s)	MoorDyn Timesteps (ms)
0.25	2.5	0.25	2.5	0.1	1.0
0.175		0.175		0.075	
0.125	1.25	0.125	1.25	0.05	0.5
0.075		0.075		0.025	
0.025	0.25	0.025	0.25	0.01	0.1

With the discretization scheme provided a grid can be constructed in which quantities of interest such as line tension and platform displacements can be determined. For these convergence studies 1000 s of simulation with 250 s of dumped transients was used to determine the FOWT's maximum response. One way to visualize these results is through a heat map like the one for the line maximum tension presented in Figure 3.9.

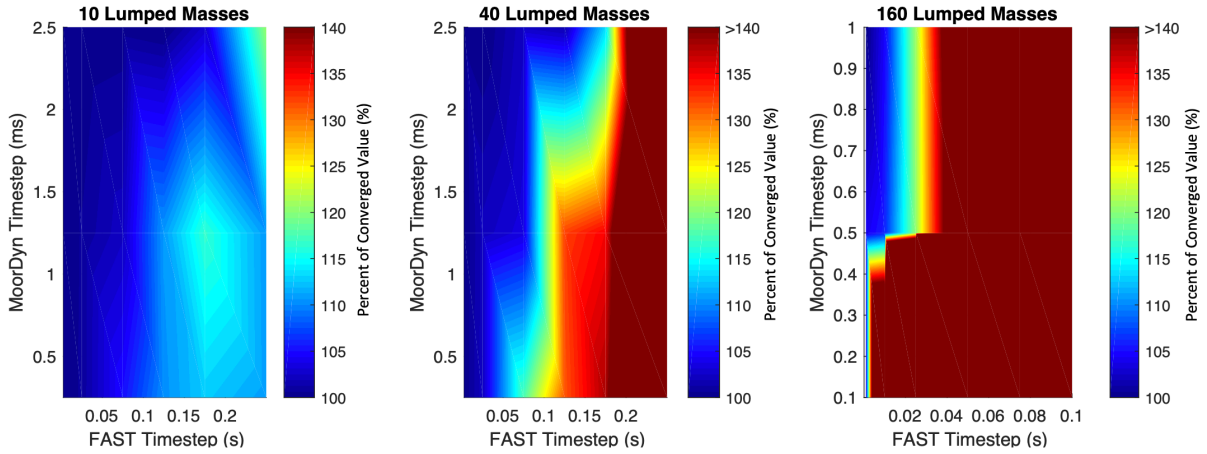

Figure 3.9. OpenFAST and MoorDyn Time Step Convergence Study

As can be seen from the three surfaces plotted in Figure 3.9. mooring systems with a coarser discretization can be simulated with more aggressive OpenFAST and MoorDyn timesteps with reasonable accuracy saving on computational efficiency. For the taut synthetic systems being modeled, the internal line tension will be much larger than the inertial force of the

line as well as the fluid loading on the line. This is due to the line having a small mass resulting from the use of synthetic materials and having relatively small motions relative to the fluid. If the system being optimized was a chain catenary system the mooring lines would likely need to be discretized more finely to capture the line inertia and the fluid loading, which are very substantial for that type of system. Table 3.9. compares the selected mooring discretization with 10 lumped masses and the selected OpenFAST and MoorDyn timesteps of 0.175 s and 2.5 ms respectively to the converged values for platform and mooring system properties of interest.

Table 3.9. OpenFAST and MoorDyn Convergence Study.

	Converged Value	Value for dtM = 2.5 ms ; dtF =0.175 s ; LM = 10	Percent difference (%)
Max Fair Tension	1273 kN	1308 kN	2.7
Max Syn Tension	1274 kN	1263 kN	-0.9
Min Syn Tension	353 kN	343 kN	-2.8
Max Anch Tension	1271 kN	1253 kN	-1.4
Max Surge Displacement	9.89 m	9.79 m	-1.0
Max Pitch Displacement (From Resting Position)*	0.52 deg	0.46 deg	-1.9

**Mean Pitch displacement is -2.54 degrees*

With the selected MoorDyn and OpenFAST settings it is possible to run the simulation quickly and still maintain a good amount of accuracy as all quantities investigated are within 5% of the converged values. The values that are most important to the design, the mooring line tensions, vary from 2.7% too large to 2.8% too low relative to the high node count, small timestep simulation which is very reasonable considering the coarse line discretization and the large OpenFAST timestep used.

3.7. MOGA Mooring Optimization Results

Using the optimization procedure outlined a mooring system was optimized for the VolturnUS 6-MW system provided. The aim of the optimization was to find feasible designs that passed the ABS 6.1 50-year wind and wave loading by using the constraint screening method and computational improvements outlined in this paper. The optimum designs in terms of mooring radius and mooring line component cost generated by the MOGA are shown in Figure 3.10. These designs were generated with a population of 180 individuals that were run for a total of 200 generations, and even with the performance enhancements implemented, the algorithm took ~7 days to run. The Pareto front shows that to have a FOWT with a smaller mooring radius a larger capital investment must be made in the mooring system. The cheapest design along this front has a component cost of approximately 86,000 USD and has a radius of about 265 m. As the radius of the mooring system is decreased the cost increases in a somewhat linear fashion to a design which has a cost of 108,000 USD and corresponding radius of about 252 m. At this point there is a jump in the Pareto front until a design which has a radius of 239 m and a cost of 113,000 dollars. After this jump in the Pareto front, mooring system radius can be reduced in radius slightly to about 235 m, but this 4 m reduction comes at a large increase in price.

The optimization performed started with 180 randomly generated individuals of which there were no restrictions on the initial seeding in the population. The constraint values were determined through the tiered-constraint method presented which was designed to both avoid running time domain simulations on infeasible designs, and to guide the optimizer towards feasible designs. This optimization was run several times with similar results observed including the jump in the Pareto front.

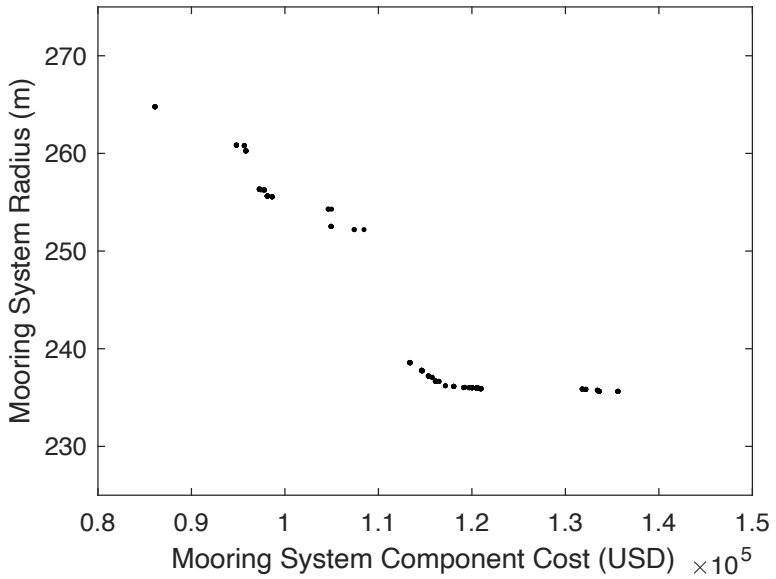

Figure 3.10. Designs along the Pareto-Optimal Front.

In this optimization problem one of the objectives, mooring system component cost, is a function of chain diameter, synthetic length and synthetic diameter. To gain a better understanding of the relationship between mooring system radius with respect to these variables, plots are provided for mooring system radius vs. synthetic line length, chain diameter and synthetic diameter in Figure 3.11., Figure 3.12. and Figure 3.13., respectively. The data for these plots are taken from the final generation of the genetic algorithm run.

Figure 3.11. shows that the synthetic segment length increases with the mooring radius in a nearly linear fashion. This makes sense as one of the constraints of the mooring system is to keep the line tensions below a certain maximum, but it is also important to keep the tensions above a certain threshold to prevent slack lines. To maintain this balance the optimizer will need to increase the synthetic line length as the mooring radius increases

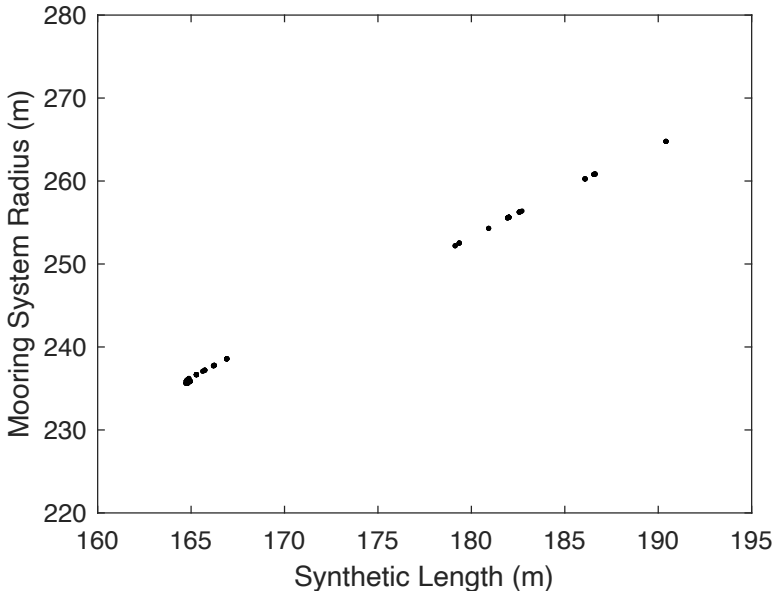

Figure 3.11. Mooring System Radius vs. Synthetic Line Length.

The second phenomenon illustrated in both Figure 3.12. and Figure 3.13. is the decrease in line diameter as mooring radius increases. This is likely due to two different effects acting in concert. First as mooring system radius increases so does mooring line length. As a result, the effective stiffness of each mooring line as well as the whole mooring system stiffness will decrease which will attract less loads, allowing smaller lines. In addition, as the radius increases the mooring line becomes more horizontal leading to a larger portion of the line tension vector counteracting the applied mean environmental load, in turn, resulting in smaller lines.

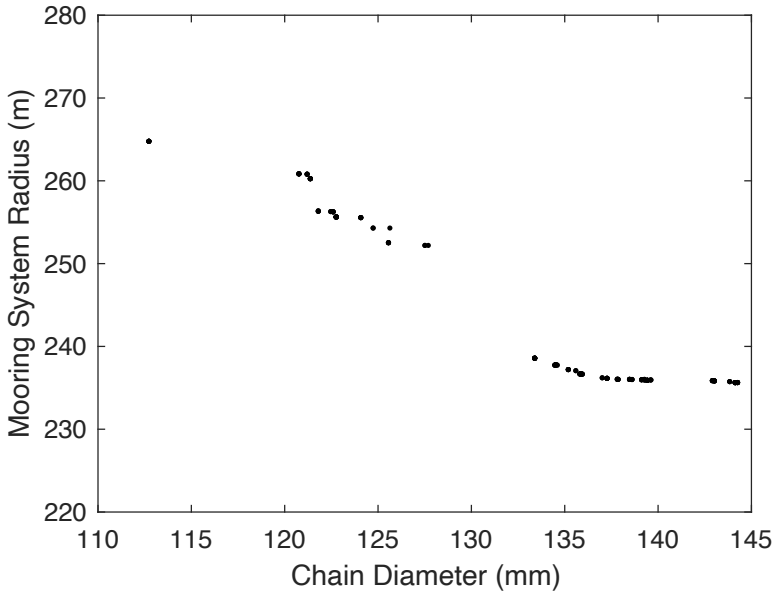

Figure 3.12. Mooring Radius vs. Chain Diameter for Designs on the Pareto-optimal Front.

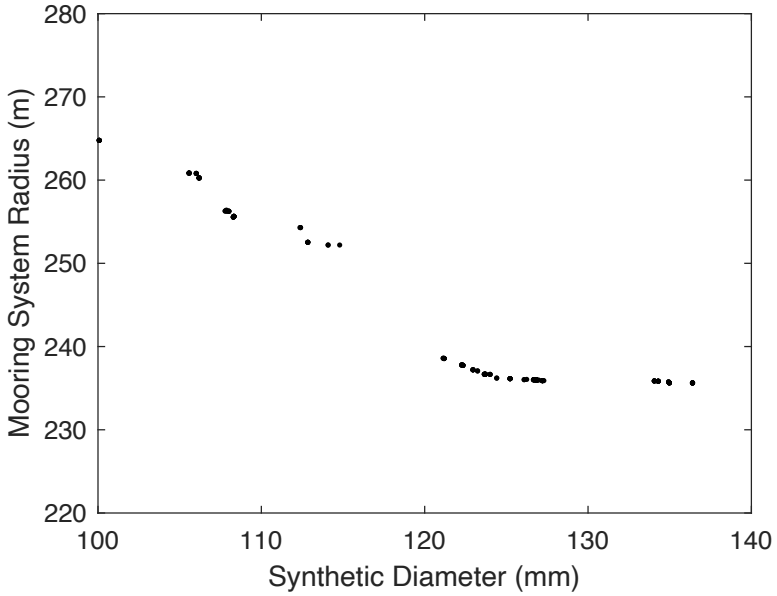

Figure 3.13. Mooring Radius vs. Synthetic Diameter for Designs along the Pareto-optimal Front.

The most interesting aspect of the Pareto-optimal front presented in Figure 3.10. is the gap in the front from designs jumping from a radius of 252 m to 239 m. To investigate the phenomenon the 252 m radius and 239 m radius designs were used to generate three interpolated designs

between them. These three designs where then evaluated for potential constraint violations, which all failed. This suggests that the region between these two feasible designs contains designs that if feasible are dominated by other designs along the Pareto front. The three failed interpolated designs are presented as red dots on the Pareto-optimal front in Figure 3.14.

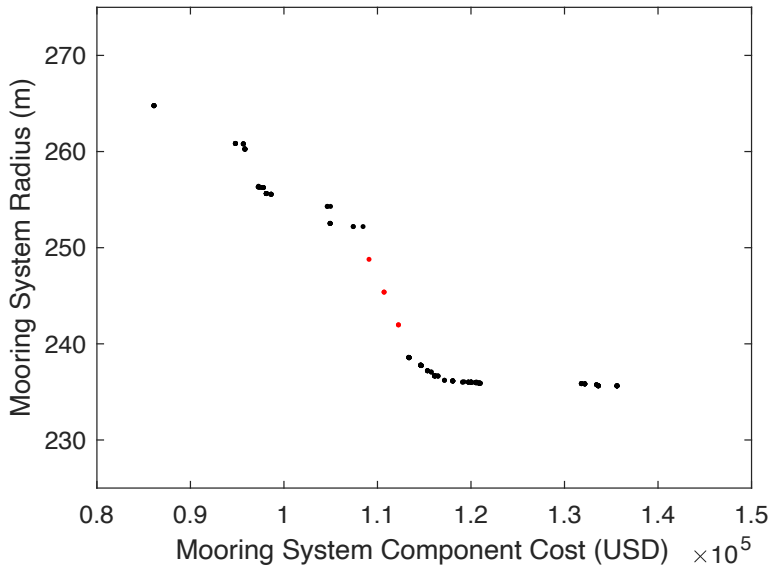

Figure 3.14. Designs along the Pareto-Optimal Front with a) interpolated designs with constraint violations (red) and b) a modified interpolated value with no constraint violation (black)

3.7.1. Verification of Candidate Design with Full Suite of DLC 6.1. Simulations

To make the optimization problem computationally feasible performance enhancements such as predicting the maximum design tension based on a shorter simulation time was used in addition to running fairly large timesteps for the simulations. In order to determine if this influenced the Pareto-optimal designs in any way, a full DLC 6.1 suite of simulations was run for one of the candidate designs and the tensions required for evaluating the constraints reexamined. The design picked to be analyzed was a design with a mooring radius of 239 m and a component cost of roughly 113,000 USD. This design was selected as it allowed for the smallest radius design before the mooring line costs begin to increase very drastically. This design has a

mooring radius that is 10% smaller than the least expensive design and accomplishes this at a price that is 30% more than the least expensive design. A schematic of the mooring system shown to scale is provided in Figure 3.15.

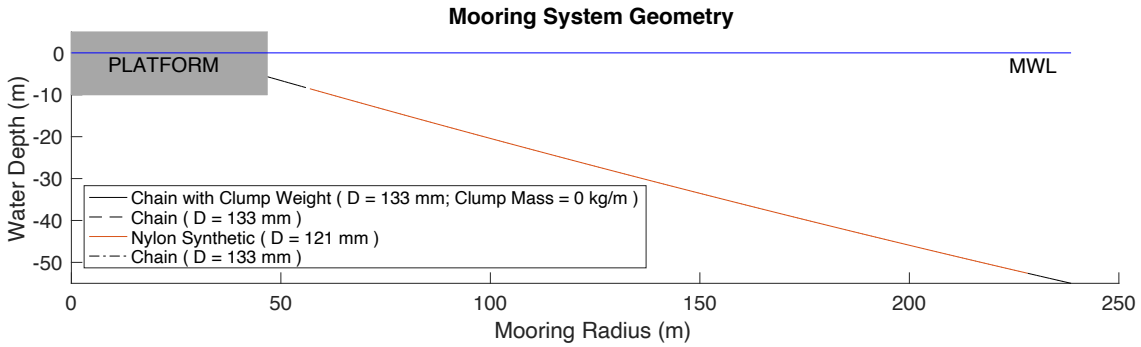

Figure 3.15. Illustration of the optimized Candidate Design for the VolturnUS 6-MW Turbine.

The candidate design mooring system is described in Table 3.10. As outlined in the optimization problem description, this mooring system has three mooring lines spaced equally with each line fairlead connected to one of the outer columns on the VolturnUS 6-MW hull. This mooring system has 10 m of 133 mm diameter chain at the fairlead and anchor with a 167 m long length of 121 mm diameter synthetic spanning between the two chain segments. The fairlead attachments are situated 5.4 m below the water connected to the radius of the outer columns 45.7 m away from the center of the platform.

Table 3.10. VolturnUS 6-MW Optimized Candidate Design.

Number of mooring lines	3
Angle of mooring lines (0° aligned with positive surge axis)	60°, 180°, 300°
Depth to anchors below SWL (water depth)	55m
Depth to fairleads below SWL	5.4 m
Radius to anchors from platform centerline	239 m
Radius to fairleads from platform centerline	45.7 m
Unstretched chain length (Leader)	10 m
Unstretched chain length (Anchor)	10 m
Unstretched synthetic length	167 m
Synthetic line diameter	121 mm
Chain diameter	133 mm
Component Cost	113,310 USD

The results for the DLC 6.1 runs are presented in Table 3.11. The same seeds were used as presented in Figure 3.9. for determining the GEV parameters. The initial run and the statistics are similar when compared to the initial run with the coefficients of variation for the mean tension and the standard deviation of the line being 0.2% and 6.1% respectively. This compares well with the statistics from the trial run of 0.2% and 5.4% for mean tension and standard deviation. The 1000 s extrapolated value for the candidate design using the GEV distribution was 1815 kN which is 1% lower than the ABS design value based on the mean of the maximum tension response value of 1835 kN. Again, this compares very well with the trial run where the GEV extrapolated value was 2% higher than the ABS design value. If proper care is taken to carefully choose a seed and an appropriate statistical fit a shorter simulation can be run to obtain maximum line responses that are close to the ABS design values. It should be noted that this was for one wave orientation, and it is possible that this approach will not work in all cases. However, the results for this one optimization scenario were deemed very acceptable.

Table 3.11. DLC 6.1 Results for VolturnUS 6-MW Moored with the Optimized Candidate Design

SEED 1	SEED 2	Max Tension (N)	Min Tension (N)	Mean Tension (N)	STD Tension (N)
674802239	-228621085	1.63e6	3.32e5	9.4605	1.86e5
-2090187775	1455391302	1.97e6	3.29e5	9.47e5	1.98e5
-1973081278	-629542915	1.74e6	3.50e5	9.45e5	2.01e5
301302578	-328425023	1.79e6	2.30e5	9.45e5	2.14e5
81611327	265255796	1.69e6	3.30e5	9.43e5	1.85e5
133186342	1154134095	2.16e6	2.80e5	9.47e5	2.11e5

3.8. Conclusions

This paper outlines the effort to implement a MOGA, NSGA II, for design optimization of synthetic mooring systems for FOWTs. The objective functions for this problem are fairly trivial, but a significant time investment was made ensuring the constraints implemented would lead to mooring designs that were realistic and adhered to the ABS/IEC design guidelines. To adequately capture the physics of a mooring system which can experience both geometric and material non-linearities it is imperative that time-domain simulations are run. Time-domain simulations are computationally expensive so the constraints are posed in such a way that inadequate designs can be screened out which prevents running time domain simulations unnecessarily. To make the problem computationally feasible on a normal desktop computer some concessions needed to be made such as reducing the number of simulations done, using fairly large timesteps and carefully selecting seeds which will produce line tensions representative of the true design value.

This method was then used to develop a set of Pareto-optimal designs which balance the footprint of the mooring system and the mooring system component cost. The Pareto-optimal

solutions found from this optimization contained a gap in the front which was found to be a result of the designs in that area having constraint violations due to the tensions in the line being slightly too large for the materials load capacity. The lines would handle the load in the lines if both the synthetic and chain segments were increased in diameter by 3% however the cost increase from this resulted in a design that would be dominated by designs having a smaller component cost and radius.

A design that resulted in a small footprint was analyzed more in depth to determine if the 1000 s of data used to extrapolate the maximum tension was adequate. The seed used was carefully chosen based on a DLC 6.1 run for another synthetic mooring system. The candidate design mooring system was then subjected to the same DLC 6.1 simulations with the same seed as the initial analysis of the synthetic mooring system. The value obtained from the 1000 s of extrapolated data was within 2% of the ABS design value found by taking the mean of the maximum values of the six one-hour simulations. Overall, this methodology provides designs that balance mooring line cost and mooring footprint and would be a good starting point for performing a full suite of ABS/IEC simulations.

Ideally, for future work this method would be used without the performance enhancements needed to make it computationally feasible on the hardware available. This would be fairly easy to implement given a computer with more cores available for parallel processing as the computer used in this study was an average desktop computer with four cores. With adequate computational resources the OpenFAST time domain simulations could be run with fully turbulent wind fields for the full 3600 s which at this point is not possible as it would require timesteps that are so small it would make the problem computationally infeasible.

Moving forward there are recommendations for improvements. Most importantly increasing the accuracy of the cost data for evaluating the cost objective function. Currently the only cost considered is the material cost for the chain and synthetic segments, but to deploy a FOWT there are many additional costs that need to be considered including engineering and project management, installation costs and connection costs. Lastly and most importantly from an engineering perspective is the anchoring costs which depend on both soil conditions and loads which would only be known after running the OpenFAST time domain simulations. Factoring in these additional costs would lead to much more realistic estimates moving forward.

It would be interesting to expand this approach to other types of mooring system configurations such as chain catenary or hybrid semi-taut systems. It is not clear if these configurations would be a good candidate for multi-objective optimization as it is unknown if cost and mooring footprint would be competing. These configurations could be good candidates for single objective optimization where the same tiered-constraint methodology proposed by the authors could be implemented to determine the feasibility by screening out designs and avoid running time-domain simulations on infeasible designs.

3.9. Acknowledgments

This research was funded by the New York State Energy Research and Development Authority (NYSERDA).

3.10. References

[1] US Department of Energy. *Offshore Wind Market Report: 2021 Edition*; US Department of Energy: Washington, DC, USA, 2021.

[2] Xu, K.; Larsen, K.; Shao, Y.; Zhang, M.; Gao, Z.; Moan, T. Design and comparative analysis of alternative mooring systems for floating wind turbines in shallow water with emphasis on ultimate limit state design. *Ocean Eng.* 2021, *219*, 108377.

[3] Davies, P.; Weller, S.D.; Johanning, L.; Banfield, S.J. A review of synthetic fiber moorings for marine energy applications. In Proceedings of the 5th International Conference on Ocean Energy, Halifax, NS, Canada, 4–6 November 2014; pp. 1–6.

[4] Flory, J.F.; Banfield, S.J.; Ridge, I.M.; Yeats, B.; Mackay, T.; Wang, P.; Hunter, T.; Johanning, L.; Herduin, M.; Foxton, P. Mooring systems for marine energy converters. In Proceedings of the OCEANS 2016 MTS/IEEE Monterey, Monterey, CA, USA, 19–23 September 2016; pp. 1–13.

[5] Brommundt, M.; Krause, L.; Merz, K.; Muskulus, M. Mooring System Optimization for Floating Wind Turbines using Frequency Domain Analysis. *Energy Procedia* 2012, *24*, 289–296.

[6] Benassai, G.; Campanile, A.; Piscopo, V.; Scamardella, A. Optimization of Mooring Systems for Floating Offshore Wind Turbines. *Coast. Eng. J.* 2015, *57*, 1550021.

[7] Hall, M.; Goupee, A. Validation of a lumped-mass mooring line model with DeepCwind semisubmersible model test data. *Ocean Eng.* 2015, *104*, 590–603.

[8] Thomsen, J.B.; Ferri, F.; Kofoed, J.P.; Black, K. Cost Optimization of Mooring Solutions for Large Floating Wave Energy Converters. *Energies* 2018, *11*, 159.

[9] Pillai, A.C.; Thies, P.R.; Johanning, L. Mooring system design optimization using a surrogate assisted multi-objective genetic algorithm. *Eng. Optim.* 2019, *51*, 1370–1392.

[10] Li, L.; Jiang, Z.; Ong, M.C.; Hu, W. Design optimization of mooring system: An application to a vessel-shaped offshore fish farm. *Eng. Struct.* 2019, *197*, 109363.

[11] Ferreira, F.M.; Lages, E.; Afonso, S.M.B.; Lyra, P.R. Dynamic design optimization of an equivalent truncated mooring system. *Ocean Eng.* 2016, *122*, 186–201.

[12] Deb, K.; Pratap, A.; Agarwal, S.; Meyarivan, T. A Fast and Elitist Multiobjective Genetic Algorithm. *IEEE Trans. Evol. Comput.* 2002, *6*, 182–197.

[13] Goupee, A.J.; Vel, S.S. Multi-objective optimization of functionally graded materials with temperature-dependent material properties. *Mater. Des.* 2007, *28*, 1861–1879.

[14] West, W. Design and Modelling of Synthetic Mooring Systems for Floating Offshore Wind Turbines. Master's Thesis, University of Maine, Orono, ME, USA, 2019.

[15] Masciola, M. MAP ++ Documentation. 2018. Available online: https://map-plus-plus.readthedocs.io/_/downloads/en/latest/pdf/ (accessed on 1 October 2021).

[16] Hall, M. *MoorDyn User's Guide*; University of Maine: Orono, ME, USA, 2015.

[17] NREL. *OpenFAST Documentation Release v2.3.0*; National Renewable Energy Laboratory: Golden, CO, USA, 2020.

[18] West, W.M.; Goupee, A.J.; Allen, C.; Viselli, A.M. Floating Wind Turbine Model Test to Verify a MoorDyn Modification for Nonlinear Elastic Materials. *J. Offshore Mech. Arct. Eng.* 2021, 1–41.

[19] WAMIT. WAMIT R User Manual. 2020. Available online: https://www.wamit.com/manualupdate/v74_manual.pdf (accessed on 1 October 2021).

[20] IEC. *IEC 61400-3 Design Requirements for Offshore Wind Turbines*; IEC: Geneve, Switzerland, 2019.

[21] ABS. *Guide for Building and Classing Floating Offshore Wind Turbine Installations*; ABS: Spring, TX, USA, 2015.

[22] ABS. *Guidance Notes on the Application of Fiber Rope for Offshore Mooring*; ABS:Spring, TX, USA, 2014.

[23] ABS. *Guide for Position Mooring Systems*; ABS: Spring, TX, USA, 2020.

[24] Weller, S.D.; Johanning, L.; Davies, P.; Banfield, S.J. Synthetic mooring ropes for marine renewable energy applications. *Renew. Energy* 2015, *83*, 1268–1278.

[25] API. *API RP 2SM: Recommended Practice for Design, Manufacture, Installation, and Maintenance of Synthetic Fiber Ropes for Offshore Mooring*; API: Washington, DC, USA, 2014.

[26] ABS. *ABS Review Advances University of Maine's Innovative Floating Offshore Wind Concept*; ABS: Spring, TX, USA, 2017.

[27] Viselli, A.M.; Forristall, G.Z.; Pearce, B.R.; Dagher, H.J. Estimation of extreme wave and wind design parameters for offshore wind turbines in the Gulf of Maine using a POT method. *Ocean Eng.* 2015, *104*, 649–658.

[28] Dagher, H.; Viselli, A.; Goupee, A.; Kimball, R.; Allen, C. *The VolturnUS 1:8 Floating Wind Turbine: Design, Construction, Deployment, Testing, Retrieval, and Inspection of the First Grid-Connected Offshore Wind Turbine in US*; University of Maine: Orono, ME, USA, 2017.

[29] Allen, C.; Viselli, A.; Dagher, H.; Goupee, A.; Gaertner, A.; Abbas, N.; Hall, M.; Barter, G. *Definition of the UMaine VolturnUS- S Reference Platform Developed for the IEA Wind 15-Megawatt Offshore Reference Wind Turbine*; NREL/TP-5000-76773; National Renewable Energy Laboratory: Golden, CO, USA, 2020. Available online: https://www.nrel.gov/docs/fy20osti/76773.pdf (accessed on 23 November 2021).

[30] DNV. *Global Perfomance Analysis of Deepwater Floating Structures*; DNV: Bærum, Norway, 2004.

CHAPTER 4

DETERMINATION OF MINIMUM-COST SYNTHETIC MOORING SYSTEMS FOR LARGE FLOATING WIND TURBINES DEPLOYED IN INTERMEDIATE WATER DEPTHS

4.1. Overview and Comments

This chapter presents the unpublished graduate research conducted for this dissertation which concluded in January 2022. This work is planned to be submitted for consideration in the *Journal of Renewable and Sustainable Energy*.

4.2. Abstract:

As the wind industry develops larger turbines for offshore deployment the problems with stationkeeping systems are exacerbated. As turbines increase in size, so do the loads on the turbine. Meanwhile, many offshore sites available for leasing occur in intermediate water depths (55-85m) which will appear ever smaller relative to the increasing platform size of floating offshore wind turbines (FOWTs). This complicates the process of designing mooring systems for these larger systems and emphasizes the importance of having a good methodology for automating this process. In this paper a routine is developed that will map objectives for a multi-objective genetic algorithm (MOGA) to obtain mooring radius-lowest cost designs over a range of radii simultaneously. This work will implement and expand on a tiered-constraint evaluation scheme that was developed in previous work by West et al. [1]. New components and constraints are added to the optimization problem to allow the optimizer to find realistically deployable designs with reasonably accurate cost estimates. These techniques will then be used to find the most economic mooring designs for a 15-MW floating offshore wind turbine with a hybrid mooring system.

4.3. Introduction

As the floating offshore wind industry matures both industry and research have begun to focus on larger turbines between 10 and 15-MW [2]. Although the size of the turbines is increasing the troubles finding mooring solutions for the transitional depth (50 – 85m) remain [3]. In addition, the loading on these turbines is substantially different than the first-generation floaters due to a much larger mean load from the larger turbine support structures and the smaller, relative to the size of the hull, sea states. These problems are further worsened by the limitations on mooring materials and installation techniques. Simply put, the FOWT units are becoming much larger while the mooring materials and components stay the same size.

These problems necessitate the need for automated procedures to develop initial feasible mooring systems. In the past researchers have used various techniques such as frequency domain analysis or linearized models to model the mooring systems of floating structures [4][5]. Although these types of models are quick to run, lending themselves for use in an optimization algorithm, there are some serious limitations. Most notably these simplified models can underpredict peak tensions in the mooring line by around 50% [6].

The other approaches that have been developed by researchers involve time domain simulations. The most computationally-efficient way this can be done is by using a meta-model [7][8][9]. With this approach many time domain simulations are run upfront to construct a surrogate model, and the designs selected by optimization schemes are ultimately based on these proxy models. This method ultimately allows for less time-domain simulations to be performed, but there is no guarantee that an optimal design will behave in the same manner as the meta-model predictions. The alternative method is to perform the time-domain analysis directly [10].

Although this will presumably lead to the best results it is also by far the most computationally expensive.

Previous work by West et al. aimed to improve of the direct time domain simulation method by using a tiered constraint screening method for a multi-objective genetic algorithm (MOGA) [1]. This method was developed to screen poor designs from the algorithm to avoid running computationally-expensive time-domain methods unnecessarily. This method was implemented to make the problem more computationally feasible when solving via direct time-domain simulation. This work aims to include and supplement the tiered constraint system developed by West et al. [1] and apply it to a next-generation large-scale 15-MW FOWT installation. To ensure that optimal designs are generated simultaneously over a suite of various mooring system radii, a mapping of objective values is used. In addition, new components such as anchors are added to the cost estimates of the mooring system to ensure that the total component costs are as more accurate. Additional constraints, ensuring that the synthetic portion of the mooring line does not contact the seabed are added to ensure that the mooring systems are realistic and deployable designs.

4.4. Overview of the Optimization Framework

The optimization framework used in this study is the multi objective genetic algorithm NSGA-II developed by Deb et al. [11] and implemented by Goupee and Vel [12]. This implementation is modified to use a mapped objective values approach to obtain the aforementioned minimum cost-mooring radii relationships. The NSGA-II algorithm uses concepts from Darwin's theory of evolution to find and generate Pareto-optimal designs. A design is Pareto-optimal when one of the mapped objective functions cannot be made better without worsening another. The general way a multi-objective routine works is as follows:

1) Calculate the (mapped) objective values and constraint values (usually simultaneously for simple problem)
2) Constraint-dominated sorting
3) Ranking and crowding of the non-constraint dominated values
4) Tournament selection, crossover, and mutation
5) Repeat until satisfactory solutions obtained

In cases of more complex problems, such as determining if a mooring configuration is valid, determining constraint values can be extremely computationally expensive. This paper aims to extend of the work done in West et al. [1] where a tiered constraint system was used to avoid running more computationally-expensive time-domain simulation. In this work one of the main goals was to improve on the cost estimates of the system by enforcing deployable geometries and adding important components to the mooring system such as the anchor. Unfortunately, the anchor can only be sized after a time domain simulation is run. In this case it is not possible to know the final cost of the system until the constraint violation of the system is calculated. The way this is handled is to first determine the initial cost of the components (minus the anchor). Then the value of the constraints is calculated and if a time domain simulation is run the cost of the anchor is calculated based on the tension at the anchor. Lastly the cost of the mooring system is adjusted to include the cost of the anchor.

The second major difference between the MOGA implemented in [1] and this work is the objective functions to be minimized. Two of the most important characteristics for a mooring system are the cost (adds to capital expenditures) and the radius (which influences turbine siting and causes competing use issues). In the previous work for a 6-MW turbine those two objectives where themselves competing. The main reason is because as the radius and line lengths increase

the overall stiffness of the system decreases leading to lower loads in the line. These lower loads ultimately mean that smaller lines can be used. Even though the line lengths increase with mooring radius the decrease in line diameter means there is a net decrease in cost which results in mooring cost and mooring radius competing.

4.4.1. Multi-objective Optimization Problem for Finding Minimum-cost Designs over a Range of Mooring Radii

For a more general system it is not known if the mooring system and cost compete but the relationship between the two is still important to understand. For a multi-objective approach to work and obtain this relationship between mooring radius lowest-cost with a single run competing objectives are needed. To ensure that relevant objectives were competing the mooring system radius and cost were mapped into competing objectives. A diagram illustrating how the modified NSGA II algorithm operates within this framework is presented in Figure 4.1.

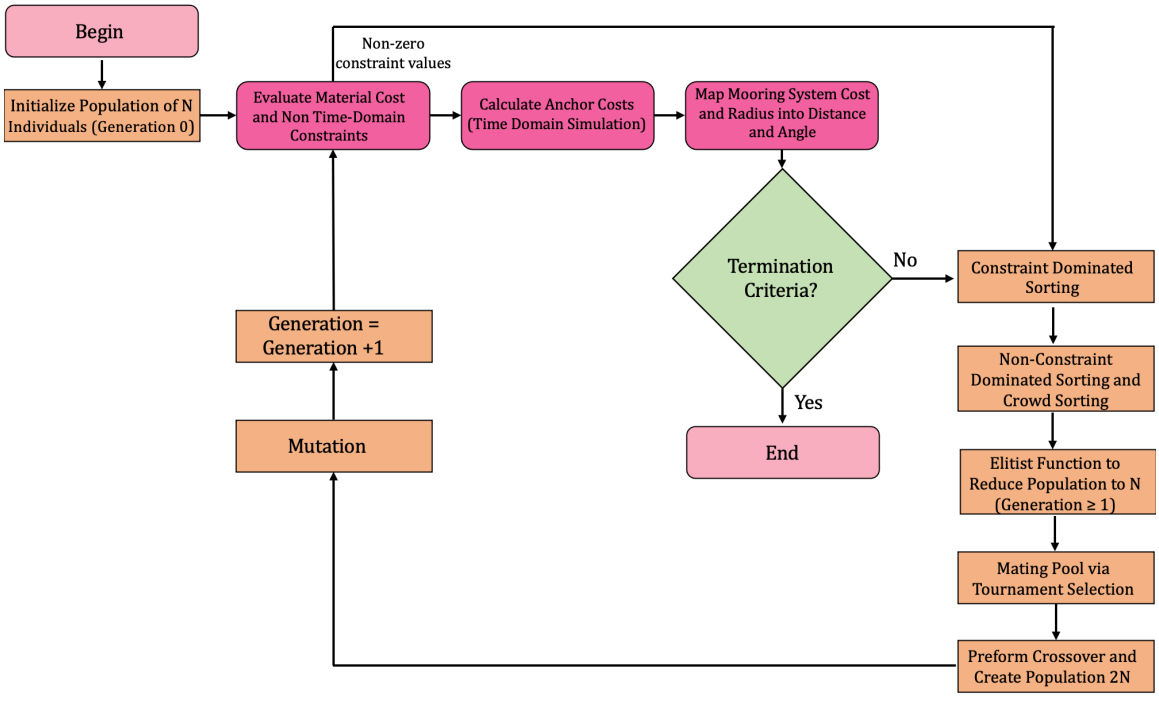

Figure 4.1. Overview of the Modified Objective Optimization within the NSGA II Framework

Before discussing how the mooring system radius and cost are mapped into the objective functions the optimization problem is defined mathematically. In general, a multi-objective optimization seeks to find a vector which maximizes some number of objective functions. In addition, this vector can be subject to several constraint violations. The optimization problem of interest subject to constraints is stated mathematically in Equation (4.1.).

$$\begin{gathered} \text{Maximize } [-L(\boldsymbol{x})] \text{ and } [\varphi(\boldsymbol{x})] \\ \text{Subject to: } g_i(\boldsymbol{x}) \geq 0, i = 1,2,\dots,7 \\ R_{\min} \leq R \leq R_{\max} \\ L_{syn\_\min} \leq L_{syn} \leq L_{syn\_\max} \\ d_{syn\_\min} \leq d_{syn} \leq d_{syn\_\max} \\ d_{chain\_\min} \leq d_{chain} \leq d_{chain\_\max} \\ V_{\min} \leq V \leq V_{\max} \end{gathered} \tag{4.1.}$$

Where:

$L(\boldsymbol{x})$ is the vector length describing a design in mooring radius – lowest cost space
$\varphi(\boldsymbol{x})$ is the vector angle defining a design in mooring radius – lowest cost space
$g_1(\boldsymbol{x})$ is the mooring system geometric constraint violation
$g_2(\boldsymbol{x})$ is the platform heave natural period constraint
$g_3(\boldsymbol{x})$ is the platform pitch natural period constraint
$g_4(\boldsymbol{x})$ is the platform surge natural period constraint
$g_5(\boldsymbol{x})$ is the synthetic touchdown constraint
$g_6(\boldsymbol{x})$ is the time-domain chain ultimate strength constraint
$g_7(\boldsymbol{x})$ is the time-domain synthetic ultimate strength constraint
R is the mooring system radius as measured from the platform centerline
L_{syn} is the length of the synthetic line (expressed as a fraction of R)
d_{syn} is the diameter of the synthetic line
d_{chain} is the diameter of the chain line
V is the displaced volume of the bouy
$R_{\min}$ is the minimum mooring radius
$R_{\max}$ is the maximum mooring radius
$L_{syn\_\min}$ is the minimum synthetic length (as a fraction of mooring radius)
$L_{syn\_\max}$ is the maximum synthetic length (as a fraction of mooring radius)
$d_{syn\_\min}$ is the minimum synthetic diameter
$d_{syn\_\max}$ is the maximum synthetic diameter
$d_{chain\_\min}$ is the minimum chain diameter
$d_{chain\_\max}$ is the maximum chain diameter
$V_{\min}$ is the minimum buoy displaced volume
$V_{\max}$ is the maximum buoy displaced volume

For this optimization problem there are five distinct variables that define the entire mooring system. The variables are the mooring radius, synthetic line length, synthetic line diameter, chain diameter and buoy displaced volume. All other qualities of the mooring system including the cost and performance can be determined from these quantities.

4.4.1.1. Mapping of the Objective Function

To ensure that there are two competing objectives, a mapping is performed on the mooring radius and mooring system cost. For each feasible design there is a vector defined from zero mooring cost, and the lower bound of the radii selectable from the optimizer. The goal is to minimize the length of this vector to pressure the optimizer to find designs that are lower in cost and maximize the angle of the vector to preserve a variety of the designs along the front. This process of mapping mooring radius and cost is illustrated in Figure 4.2.

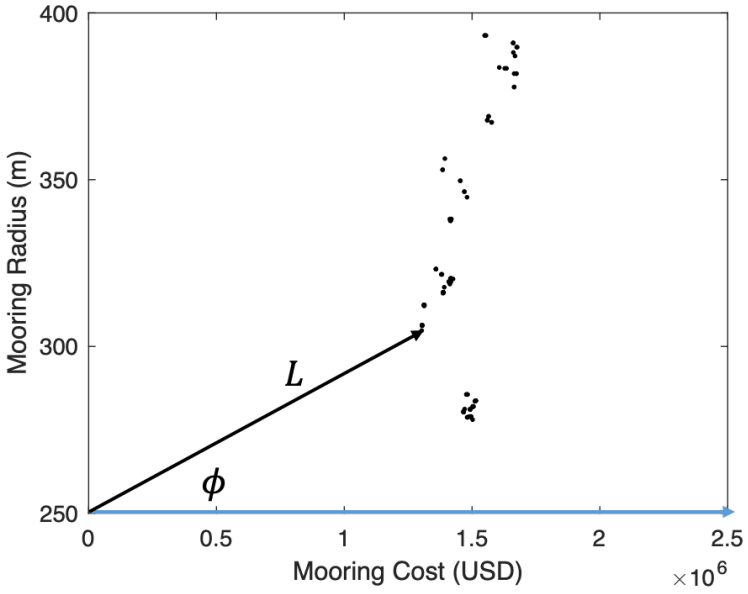

Figure 4.2. Mapping Mooring Radius and Cost into a Vector of Angle and Length

It is important to explicitly describe how the vector length and the vector angle are determined. To ensure that the vector length and angle change sufficiently the cost is normalized

to make it the same order magnitude as the radius. The equation for vector length and vector angle are defined in Equations (4.2.) and (4.3.) respectively. At the end of each generation the length and angle vector that describe the position of each design were used to map the designs back into the mooring radius-lowest cost space.

$$L(\boldsymbol{x}) = \sqrt{(C(\boldsymbol{x})/M_{\text{norm}})^2 + (R - R_{\text{min}})^2} \tag{4.2.}$$

$$\varphi(\boldsymbol{x}) = \tan^{-1}\frac{R - R_{\text{min}}}{C(\boldsymbol{x})/M_{\text{norm}}} \tag{4.3.}$$

Where: $C(\boldsymbol{x})$ is the total component cost of the mooring system

M_{norm} is the mooring cost normalization constant

4.4.1.2. Constraints

The constraints for this optimization problem are chosen to ensure that the mooring system preforms appropriately. The constraints are developed using the same tiered constraint method outlined in [1] to avoid running more computationally expensive analysis on designs that are poor. Many of these constraints are based on the IEC/ABS guidelines for building and classing floating offshore wind turbines. At a high level the constraints that are applied are as follows:

1) A geometric feasibility constraint is implemented to avoid analyzing designs where the line lengths for a certain mooring radius yield nonsensical designs (i.e., $g_1(\boldsymbol{x})$).

2) Next, the FOWT platform periods are estimated so that designs which do meet minimum natural period requirements and would likely have resonance issues due to the wave loading are not analyzed (i.e., $g_2(\boldsymbol{x})$, $g_3(\boldsymbol{x})$ and $g_4(\boldsymbol{x})$).

3) Designs which pass the simplest constraints are applied with a mean load at 0 and 180-deg to determine the mean positions. This is used to determine the mooring system geometry and ensure that the synthetic section does not contact the seabed. (i.e., $g_5(\boldsymbol{x})$).

4) Designs which pass constraints (1) – (3) are subjected to DLC 6.1 simulations to determine the maximum and minimum loads in the mooring system and assess constraints requiring these values (i.e., $g_6(\boldsymbol{x}) - g_7(\boldsymbol{x})$).

This methodology modifies the previous work done in [1] by including an additional layer to the constraint screening process. This new layer, $g_5(\boldsymbol{x})$, is a preliminary OpenFAST run that is used to determine the mean position of the platform. These runs are done by using modified OpenFAST input files with increased quadratic damping for the translational and rotational degrees of freedom by factors of 10 and 100 respectively. A flowchart of the constraint handling process with the added layer of screening is presented in Figure 4.3.

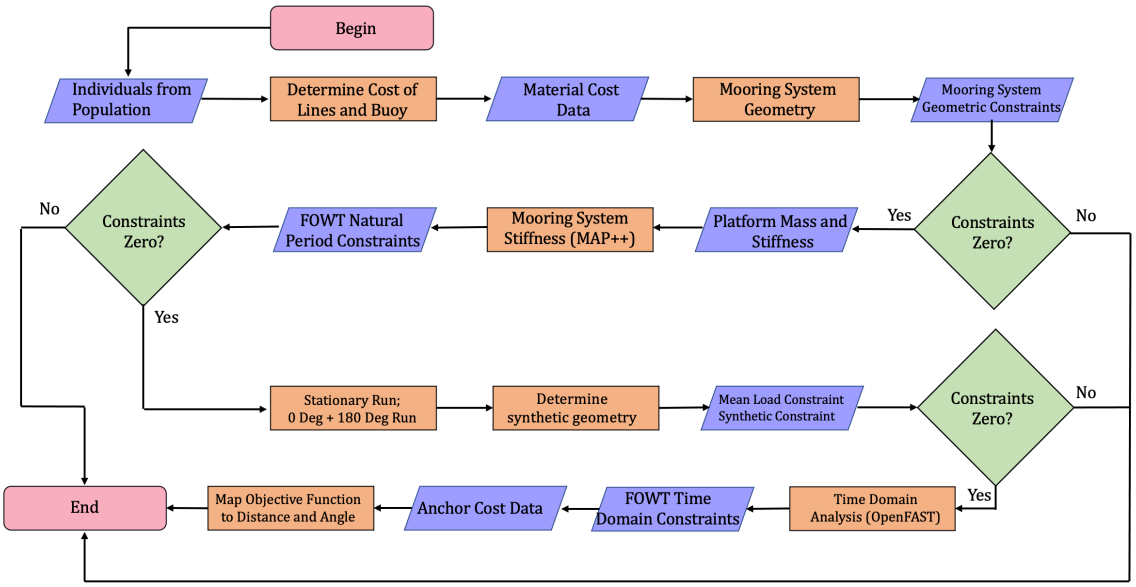

Figure 4.3. Constraint Screening Flowchart with Mean Offset Constraints

The first layer of the of the constraint screening chart is identical to that of the previous work [1] so only a short description will be provided. The purpose of this constraint is to eliminate especially egregious designs where the line lengths are either far too short or too long

to have a functional mooring system. The upper bound of line length is a line that descends straight from the fairlead to the seafloor and then horizontally to the anchors as there will be no stiffness due to the geometry of the mooring system. The other extreme is the situation where the line length is too short to be functional. In this case it if a line is less than 85% of straight-line anchor to fairlead distance the design will be thrown out. This number should be updated based on the mooring line materials selected. A schematic of the geometry as described is provided in Figure 4.4. The geometric constraints as implemented in the optimization routine are presented in Equation (4.4.).

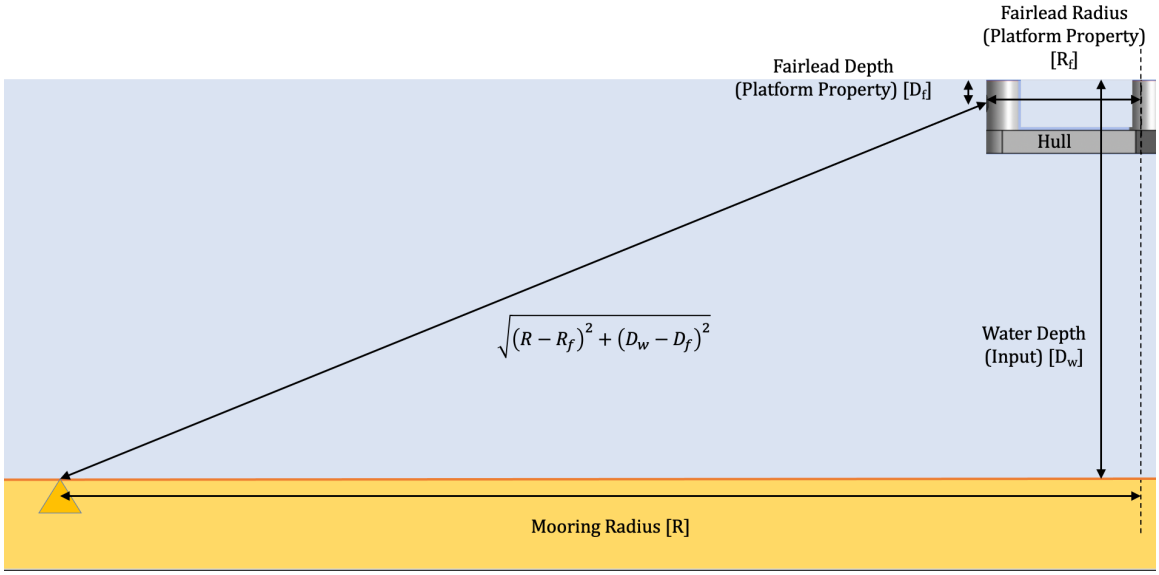

Figure 4.4. Geometric Constraint Check

$$\text{If:} \quad L_T \leq 0.85\sqrt{\left(R - R_f\right)^2 + \left(D_w - D_f\right)^2} \tag{4.4.}$$

$$\text{Then:} \quad g_1 = 100\frac{0.85\sqrt{\left(R - R_f\right)^2 + \left(D_w - D_f\right)^2} - L_T}{0.85\sqrt{\left(R - R_f\right)^2 + \left(D_w - D_f\right)^2}} + 46$$

$$\text{Else If:} \quad \left(R - R_f\right) + \left(D_w - D_f\right) \leq L_T$$

$$\text{Then:} \quad g_1 = 100\frac{L_T - [\left(R - R_f\right) + \left(D_w - D_f\right)]}{[\left(R - R_f\right) + \left(D_w - D_f\right)]} + 46$$

$$\text{Else:} \quad g_1 = 0$$

Where: R_f is the distance from the center of the platform to the fairlead connection point
D_w is water depth
D_f is the depth from the mean water line (MWL) to the fairlead connection point
L_T is the total line length

The next constraints presented are the natural period constraints. The purpose of these constraints is to determine which designs have resonance issues which are likely to affect the response of the platform in the time domain. In this way expensive time-domain simulations can be avoided by analyzing the mooring system quasi-statically using the open source software MAP++ [13].

MAP++ is a quasistatic mooring system solver which is not ideal for time domain simulations but is computationally efficient. The solver works by solving the catenary equations for each portion of the line individually forcing the loads at the connections between materials to be in equilibrium. MAP++ also allows users to determine the 6x6 linear mooring system stiffness matrix which can be used in conjunction with Equations (4.5.) – (4.7.) to estimate the FOWT natural periods.

$$T_{n\_\text{heave}} = \frac{2\pi}{\sqrt{\frac{k_{33} + k_{33\text{Mooring}}}{m_{\text{platform}} + a_{33}}}} \tag{4.5.}$$

If: $T_{n\_\text{heave}} \leq T_{\text{heave\_min}}$

Then: $g_2 = 30\frac{T_{\text{heave\_min}} - T_{n\_\text{heave}}}{T_{\text{heave\_min}}} + 16$

Else: $g_2 = 0$

Where: k_{33} is the platform heave stiffness
$k_{33\text{Mooring}}$ is the mooring system heave stiffness
m_{platform} is the mass of the platform
a_{33} is the infinite period added mass of the platform in heave
T_{n_heave} is the platform heave natural period
$T_{\text{heave\_min}}$ is the minimum acceptable platform heave period

$$T_{n\_\text{pitch}} = \frac{2\pi}{\sqrt{\frac{k_{55} + k_{55\text{Mooring}}}{I_{\text{platform}} + a_{55}}}} \tag{4.6.}$$

If: $T_{n\_\text{pitch}} \leq T_{\text{pitch\_min}}$

Then: $g_3 = 30\frac{T_{\text{pitch\_min}} - T_{n\_\text{pitch}}}{T_{\text{pitch\_min}}} + 16$

Else: $g_3 = 0$

Where: k_{55} is the platform pitch stiffness
$k_{55\text{Mooring}}$ is the mooring system pitch stiffness
I_{platform} is the platform pitch inertia
a_{55} is the infinite period added inertia of the platform in pitch
T_{n_pitch} is the platform pitch natural period
$T_{\text{pitch\_min}}$ is the minimum acceptable platform heave period

$$T_{n\_\text{surge}} = \frac{2\pi}{\sqrt{\frac{k_{11\text{Mooring}}}{m_{\text{platform}} + a_{11}}}} \tag{4.7.}$$

If: $T_{n\_\text{surge}} \leq T_{\text{surge\_min}}$

Then: $g_4 = 30\frac{T_{\text{surge\_min}} - T_{n\_\text{surge}}}{T_{\text{surge\_min}}} + 16$

Else If: $T_{n\_\text{surge}} \geq T_{\text{surge\_max}}$

Then: $g_4 = 30\frac{T_{n\_\text{surge}} - T_{\text{surge\_max}}}{T_{\text{surge\_max}}} + 16$

Else: $g_4 = 0$

Where: $k_{11\text{Mooring}}$ is the mooring system surge stiffness
a_{11} is the infinite period added mass of the platform in surge
T_{n_surge} is the platform pitch natural period
$T_{\text{surge\_min}}$ is the minimum allowable surge period
$T_{\text{surge\_max}}$ is the maximum allowable surge period

The heave and pitch constraint (g_3 and g_4) are nearly identical to the heave and pitch constraints presented in [1]. The main difference is the addition of a surge natural period constraint. This constraint aims to screen out mooring systems that are overly stiff or compliant before moving onto the time domain simulations.

The biggest difference between the formulation of the constraints and those developed in [1] is the inclusion of a new layer where simulations are run to determine the mean position of the FOWT at rest and due to both 0 and 180-deg loading. The loading in this case consists of the mean load due to the current, second order wave loading and turbine thrust. In the OpenFAST [13] coordinate system 0-deg is defined as positive surge behind the FOWT. The 0 and 180-deg loading will induce the maximum and minimum extensions in the mooring line respectively. In the previous work the tension in the synthetic section was required to not go below 2% of the line MBS based on axial fatigue failure for other materials. This was an overly-conservative estimate and has been replaced with a new constraint that requires the synthetic section of the mooring line to be kept off the seafloor. To determine this the position of the connection points

between the chain and synthetic sections of the line are determined and used in conjunction with the catenary equation to obtain the geometry of the synthetic section.

The catenary equations from the MAP++ user manual [14] and implemented into the code are presented in Equations (4.8.) – (4.10.). Equations (4.8.) and (4.9.) give the profile of the line given the horizontal force at the fairlead connection and the vertical force at the anchor. The vertical force at the anchor is related to the vertical force at the fairlead through Equation (4.10.)

$$x(s) = \frac{H}{\omega}\left\{\ln\left[\frac{V_a + \omega s}{H} + \sqrt{1 + \left(\frac{V_a + \omega s}{H}\right)^2}\right] - \ln\left[\frac{V_a}{H} + \sqrt{1 + \left(\frac{V_a}{H}\right)^2}\right]\right\} + \frac{Hs}{EA} \tag{4.8.}$$

$$z(s) = \frac{H}{\omega}\left[\sqrt{1 + \left(\frac{V_a + \omega s}{H}\right)^2} - \sqrt{1 + \left(\frac{V_a}{H}\right)^2}\right] + \frac{1}{EA}\left(V_a s + \frac{\omega s^2}{2}\right) \tag{4.9.}$$

$$V_a = V - \omega L \tag{4.10.}$$

Where: ω is the wet weight of the line
s is the unstretched position along the line
$x(s)$ is the horizontal position of the line
$z(s)$ is the vertical position of the line
H is the horizontal fairlead force
V is the vertical fairlead force
EA is the line Stiffness
V_a is the vertical force at the anchor
L is the length of the line

In general, with a mooring line the position of the fairlead relative to the anchor is known instead of having knowledge of the forces at the fairlead. Substituting Equation (4.10.) into (4.9.) and (4.8.) while also making the substituting $s = L$ will lead to Equation (4.11.) and (4.12.). These two equations can then be iteratively solved for the horizontal and vertical forces at the fairlead given the relative location of the fairlead and anchors. Once these forces are known Equations (4.11.) and (4.12.) can be used to determine the geometry of the mooring line.

$$x_f = \frac{H}{\omega}\left\{\ln\left[\frac{V}{H} + \sqrt{1 + \left(\frac{V}{H}\right)^2}\right] - \ln\left[\frac{V - \omega L}{H} + \sqrt{1 + \left(\frac{V - \omega L}{H}\right)^2}\right]\right\} + \frac{HL}{EA} \tag{4.11.}$$

$$z_f = \frac{H}{\omega}\left[\sqrt{1 + \left(\frac{V}{H}\right)^2} - \sqrt{1 + \left(\frac{V - \omega L}{H}\right)^2}\right] + \frac{1}{EA}\left(VL - \frac{\omega L^2}{2}\right) \tag{4.12.}$$

Where: x_f is horizontal excursion from the anchor to the fairlead
z_f is the vertical excursion from the anchor to the fairlead

Last, the location of the top and bottom connection points of the synthetic sections are then determined from the stationary, 0-deg, and 180-deg OpenFAST [13] runs. In Open Using Equations (4.8.) – (4.12.) the synthetic geometry is determined for these 3 loading scenarios. Equation (4.13.) is then used to ensure that the synthetic section for each different loading scenario is at least 1.0 meter off the seafloor. This could be increased to a larger distance from the seafloor to ensure a more conservative design if necessary.

$$z_{\min} = \min\left[z_i(s)\right] \tag{4.13.}$$

If: $z_{\min} < z_{\text{syn\_allowable}}$

Then: $g_5 = \left| 10\,\frac{z_{\text{syn\_allowable}} - z_{\min}}{z_{\text{syn\_allowable}}} \right| + 6$

Else: $g_5 = 0$

Where: $z_{\min}$ is maximum depth of the synthetic section of the mooring line
z_i is the vertical position of line in the stationary, 0 deg, and 180 deg loading case
$z_{\text{syn\_allowable}}$ is the allowable synthetic distance from the seafloor

The final constraints are the DLC 6.1-time constraints to ensure that the mooring lines can withstand the dynamic loading. These constraints are identical to those implemented in [1] although the methods to derive the mean tensions are different. For this DLC the environmental loading is directed at the front leg of the FOWT and corresponds to 0-deg. The DLC is defined by the wind and wave parameters measured at a lease site off the coast of New York State. In

the previous work a modified OpenFAST executable compiled to allow nonlinear tension strain relationships to model the line were used. In this work the tension in the line is determined using the ABS upper-lower bound stiffness model [15] for modelling synthetic mooring lines is used. The methodology for determining the maximum tension in the lines is detailed in Section 4.4.5. The constraints for the maximum line tension in the chain and synthetic section of the mooring line are presented in Equations (4.14) and (4.15) respectively.

$$\text{If:} \quad F_{f\_\text{chain}}\, \mathrm{T}_{\text{fairlead\_max}} \geq \mathrm{MBS}_{\text{chain}} \tag{4.14.}$$
$$\text{Then:} \quad g_6 = 3\frac{F_{f\_\text{chain}}\, \mathrm{T}_{\text{fairlead\_max}} - \mathrm{MBS}_{\text{chain}}}{\mathrm{MBS}_{\text{chain}}}$$
$$\text{Else:} \quad g_6 = 0$$

Where: $\mathrm{T}_{\text{fairlead\_max}}$ is the maximum tension at the fairlead
F_{f_chain} is chain fatigue factor
$\mathrm{MBS}_{\text{chain}}$ is the minimum breaking strength of the chain

$$\text{If:} \quad F_{s\_\text{syn}}\mathrm{T}_{\text{syn\_max}} \geq \mathrm{MBS}_{\text{syn}} \tag{4.15.}$$
$$\text{Then:} \quad g_7 = 3\frac{F_{s\_\text{syn}}\mathrm{T}_{\text{syn\_max}} - \mathrm{MBS}_{\text{syn}}}{\mathrm{MBS}_{\text{syn}}}$$
$$\text{Else:} \quad g_7 = 0$$

Where: $\mathrm{T}_{\text{syn\_max}}$ is the maximum tension at the fairlead
F_{s_syn} is the ABS synthetic factor of safety for a synthetic mooring line
$\mathrm{MBS}_{\text{syn}}$ is the minimum breaking strength of the synthetic mooring line

The factors multiplying and constants added to the constraint values ensure that a design that fails earlier on in the design process will always have a larger constraint value than a design that fails later in the process. This system is setup to ensure that worse designs are screened out by the optimizer and better designs are left in the mating pool [1]. The main goal of this constraint screening process is to weed out ineffective designs in a computationally efficient

manner. Both the possible values of constraint violations for each constraint as well as the cumulative computational time required to evaluate each constraint is illustrated in Figure 4.5.

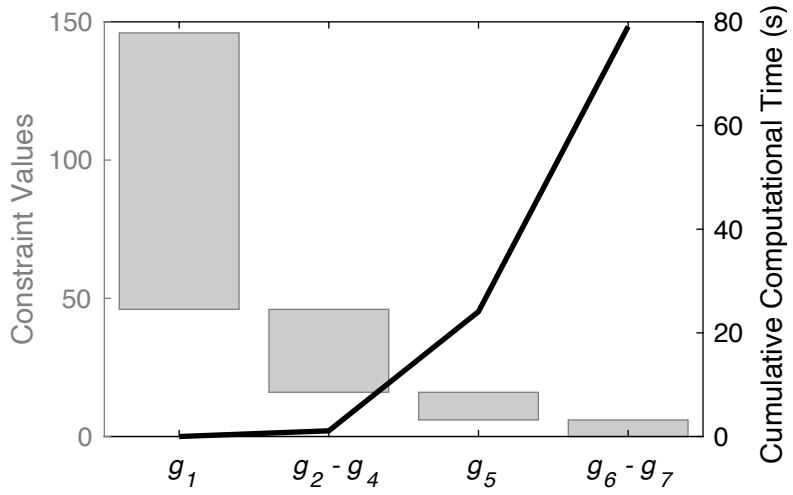

Figure 4.5. Constraint Violation Value and Cumulative Computational Time

This procedure is very effective for reducing computational time required to determine the performance of a mooring system. The constraint violations for the first 200 generations of the optimization are shown in Figure 4.6. Over the first 200 generations designs have been determined to be ineffective before needing to run a DLC 6.1-time domain simulation about 60% of the time. Overall, the constraint screening methodology developed is effective and leads to substantial time savings.

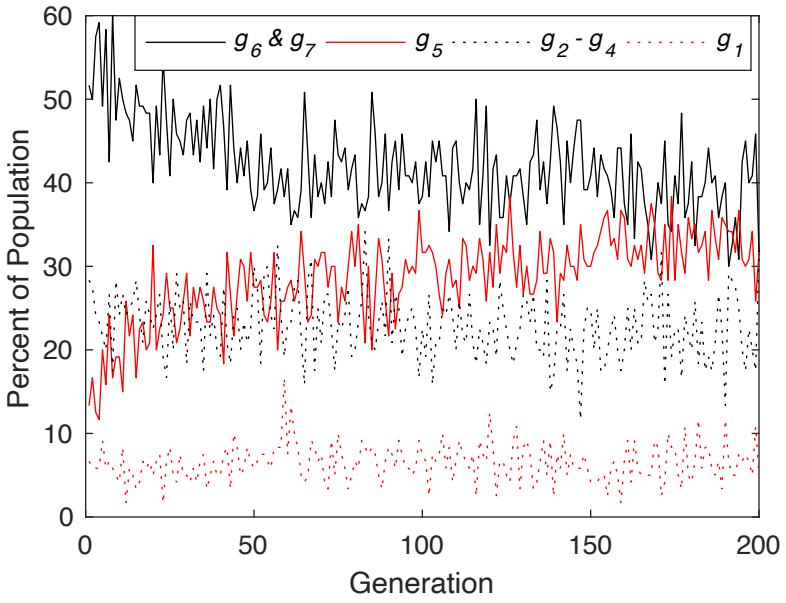

Figure 4.6. Constraint Violations for the First 200 Generations

4.5. Optimization Inputs

The inputs needed to perform the optimization in this study are presented in the following sections. Section 4.5.1. outlines the mooring system which includes the geometry of the mooring system and the mooring line inputs including both mechanical properties and cost data. This section also lays out the procedure which for estimating the cost of the anchors which is a substantial cost of a mooring system. Section 4.5.2. provides the inputs needed to model the IEA 15-MW FOWT [16] used in this study. This includes the geometry of the platform to model the hydrodynamic loading on the hull and the gross properties of the platform, tower, and rotor nacelle assembly (RNA). Sections 4.5.3. and 4.5.4. outline the design requirements and the environmental loading respectively. Lastly section 4.5.5. outlines the ABS upper-lower bound stiffness

modelling method used to model the stiffnesses of the synthetic mooring lines and the quadratic damping coefficients and OpenFAST timesteps to perform the OpenFAST simulations.

4.5.1. Mooring System

The geometry of the mooring system to be optimized is illustrated in Figure 4.7. For this work a water depth of 56m was selected, this being typical of an intermediate water depth site. This depth dictated some of the other elements of the optimization problem, namely the length of the bottom chain. The bottom chain section was required to be 20m more than the water depth in order to ensure that hookup between the synthetic section of the line and chain section would be feasible. In addition, this mooring system has a buoy of variable size to ensure that the synthetic section is kept off the seafloor. The optimizer was able to select mooring configurations without a buoy if a taut synthetic system was the optimal design. This design also includes 10m of chain at the fairlead connection point so the mooring lines can be ratcheted to the correct installed pretension.

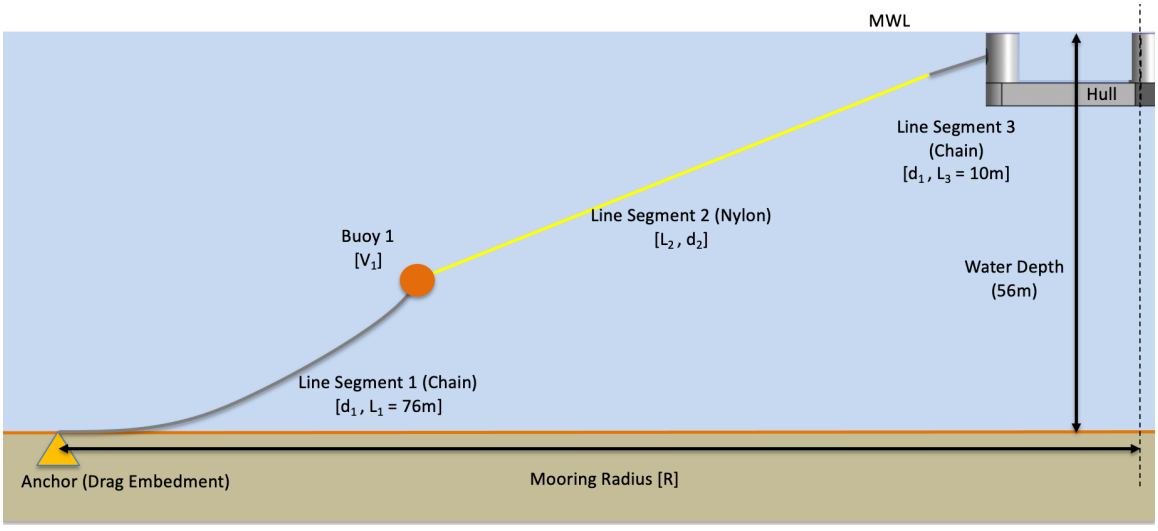

Figure 4.7. Mooring System Geometry

Table 4.1. contains the Mooring System properties. This table contains both the properties of the mooring system, and the properties that can be selected by the optimization routine. Some properties such as the fairlead connection points are driven by the platform geometry. The mooring systems for this design optimization were modeled in the OpenFAST module MoorDyn [17].

Table 4.1. Mooring System Properties

Number of mooring lines	3
Angle of mooring lines (0° aligned with positive surge axis downwind of the turbine; positive defined as counter-clockwise)	60°, 180°, 300°
Depth to anchors below SWL (water depth)	56 m
Depth to fairleads below SWL	14 m
Radius to anchors from platform centerline	Design Variable
Radius to fairleads from platform centerline	58 m
Unstretched chain length (Leader)	10 m
Unstretched chain length (Anchor)	76 m
Unstretched synthetic length	0.42 - 0.65 (105 m – 260m)
Synthetic line diameter	175 mm – 240 mm
Chain diameter	135 mm – 178 mm
Buoy displaced volumed	0 m^3 – 10 m^3

The stiffnesses and breaking strengths of the chain and synthetic lines, which are based on commercially-available products, are presented in Figure 4.8. The specific gravity of the synthetic lines is 1.15 and the mass density of steel chain is 8050 kg/m^3. The specific gravity of the buoyancy module is 0.5. The nondimensionalized stiffness for the chain and synthetic mooring components is provided in Table 4.2.

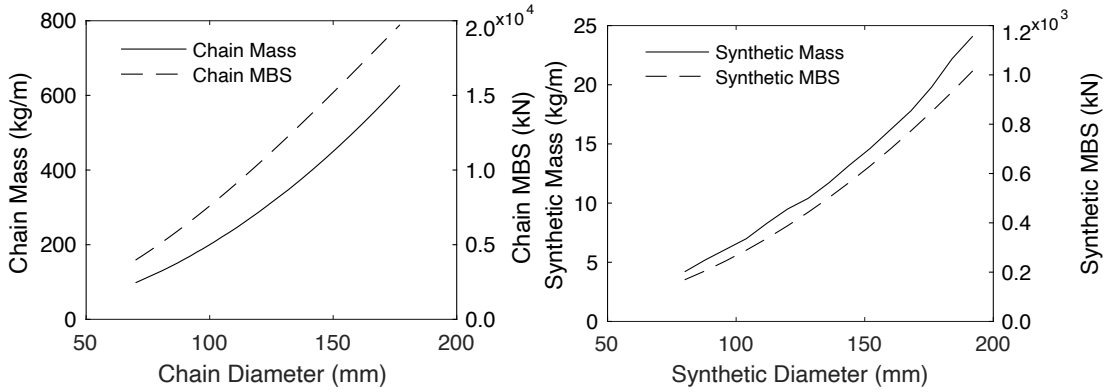

Figure 4.8. Dry Chain Mass and Chain Load Capacity (left) and Dry Synthetic Mass and Synthetic Load Capacity (right)

Table 4.2. Material Nondimensionalized stiffness

Material	**Stiffness**
Steel chain	43 × MBS
Synthetic (quasi-static stiffness)	5 × MBS
Synthetic (dynamic stiffness)	10 × MBS

The material cost data used to estimate the mooring cost is provided Table 4.3. The material costs provided are based on cost estimates provided by manufacturers for the Aqua Ventus I project which is managed by the University of Maine. The material costs are first determined based on the masses of the buoy, chain, and synthetic components. After the time domain simulations are run the cost of the anchor is added to complete the cost of the mooring system components.

Table 4.3. Mooring System Component Costs

Material	**Cost (USD/kg)**
Steel chain	1.50
Synthetic	17.00
Buoy	22.30
Anchor	155.00
Mooring Cost Normalization Constant	3.3×10^4

A major inclusion in this work is factoring in the cost of the anchor to the mooring system. The problem with estimating the cost of the anchor is that it can only be determined after a time domain simulation has been run. To contrast the rest of the cost of the other mooring system components can be determined ahead of time. The anchor considered in this work is a Vryhof Stevmantis Mk 5 drag embedment anchor [18]. The Ultimate holding capacity of this anchor is related to the weight of the anchor by Equation (4.16.).

$$\mathrm{UHC} = AW^{.92} \tag{4.16.}$$

Where: UHC is the ultimate holding capacity of the anchor (in mT)
W is the weight of the anchor (in mT)
A is a parameter that depends on soil and can vary from 24 to 110 (lower for mud/silt; higher for sand and hard clay)

Drag embedment anchors are primarily designed to hold horizontal loads at the seafloor. Guidance from the API however does allow there to be slight vertical loads provided that the appropriate load reduction factors are used. The load reduction factors for a given load relative to the seafloor recommended by the API [19] are provided in Table 4.4. The angle at the seafloor is determined from the OpenFAST simulations by tracking the vertical position of the node closest to the anchor. Rearranging Equation (4.16.) and applying the appropriate safety factors and load reduction factors yields a relationship between maximum anchor tension and anchor weight shown in Equation (4.17.).

$$W = e^{\ln\left(\frac{F_{S\_\mathrm{Anch}}T}{R_f A}\right)/.92} \tag{4.17.}$$

Where: F_{S_Anch} is the anchor safety factor
R_f is the mudline angle reduction factor

Table 4.4. Reduction Factor vs. Mudline Angle

Mudline Angle (Deg.)	0	5	10	15	20
Reduction Factor	1.0	.98	.95	.89	.81

4.5.2. Description of the Turbine

For this study the IEA 15-MW reference turbine developed by NREL and UMaine was used [16]. This turbine is not a commercially-available system, instead it is a baseline next-generation FOWT that provides researchers a consistent model to develop upcoming technologies. The floating foundation for the IEA 15-MW system was developed by the University of Maine and referred to as the VolturnUS-S system. The geometry of the VolturnUS-S system is shown in Figure 4.9.

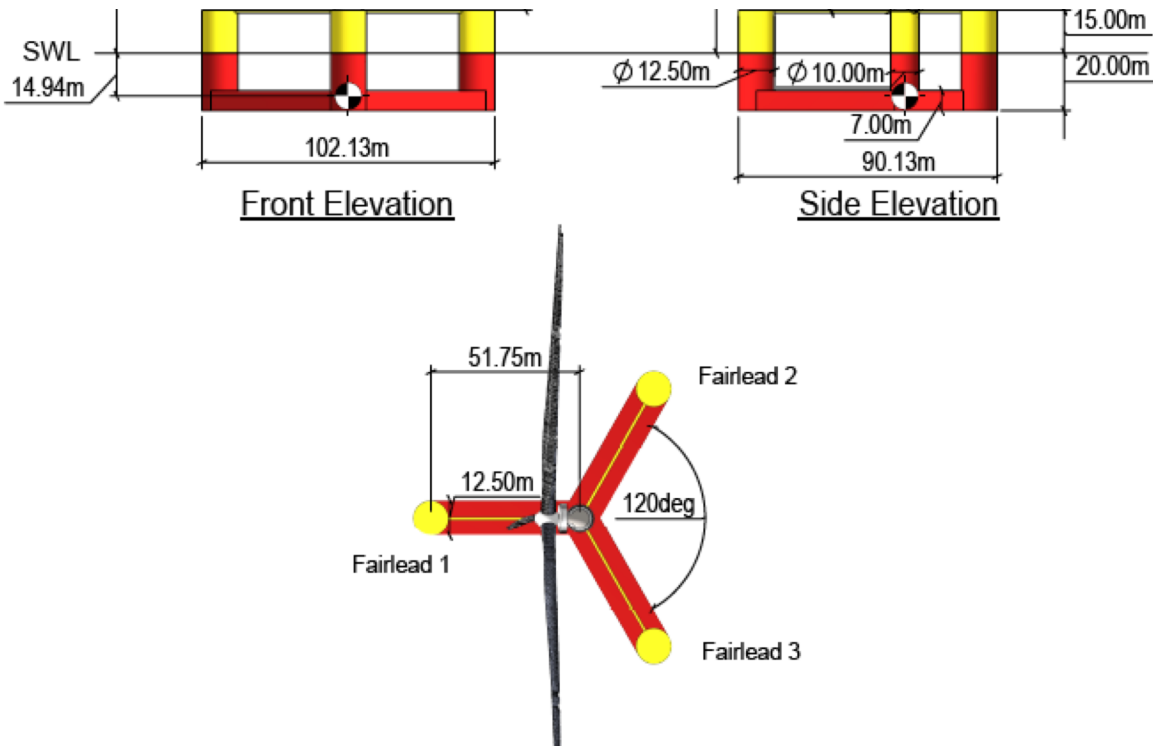

Figure 4.9. 15-MW VolturnUS-S Platform Geometry [16]

The geometry of the platform can be used in conjunction with the code WAMIT [20] to determine both the hydrodynamic coefficients of the platform, and the hydrostatics due to the center of buoyancy and waterplane area of the platform. To determine the hydrostatic stiffness of the FOWT due to the center of gravity the locations of the platform and FOWT center of gravities and the masses must be known. In addition, these masses and locations are needed to perform time domain analysis. The gross properties of the IEA 15-MW reference turbine supported by the VolturnUS-S hull are provided in Table 4.5. The IEA 15-MW FOWT OpenFAST model is free and readily available for research programs.

Table 4.5. IEA 15-MW Floating Reference Turbine Gross Properties

Total Draft	20.0 m
Platform Mass, Including Ballast	1.784×10^7 kg
Displacement	2.02×10^4 m^3
Center of Mass (CM) Location Below SWL Along Platform Centerline	14.94 m
Platform Roll Inertia About CM	1.251×10^{10} kg-m^2
Platform Pitch Inertia About CM	1.251×10^{10} kg-m^2
Platform Yaw Inertia About CM	2.367×10^{10} kg-m^2
Hub Height Above SWL	150 m
Total Tower Top Mass	991,000 kg
Tower Mass	1.263×10^6 kg
Tower CM above SWL	56.50 m

4.5.3. Design Criteria

The design criteria for this work are based on both the recommended ABS, IEC and API [21] [22] [23] criteria as well as well as well as other design work done at the University of Maine. Both the anchor factor of safety for a non-redundant system and the synthetic material breaking factor of safety come from ABS guidance. The minimum chain factor of safety is based on a preliminary design that was checked to ensure that it would survive the DLC 1.2 fatigue conditions for 25 years. This factor of safety is much lower than the fatigue factor that

was used in [1] which is likely due to the environmental loading conditions and the 15-MW turbine. In the previous work the turbine was a 6-MW subjected to a larger wave environment. In this case the wave environment is smaller, and it is also significantly smaller relative to the platform size leading to much smaller loads induced by the waves as compared to the mean load on the system.

There are also design requirements to ensure that the natural period of the platform is staying outside of the wave energy region. The number selected is 18 s for the minimum heave period and 25 s for the minimum pitch period consistent with the previous work. In this work an additional constraint was also added to check the surge period of the system. The surge period is deemed to be acceptable over a wide range from 55 s to 350 s. Any mooring systems that leads to a surge period outside of that range are likely to be unnecessarily soft or stiff, foregoing the need to run time domain.

The last design requirements are for ensuring that the synthetic mooring line is kept off the seafloor and the soil parameter for sizing of the anchor. For this work, a comprehensive geotechnical analysis of the soil conditions is not available. As a result, a conservative soil parameter which reflects soft soil conditions was used to estimate the size the anchor. The other design requirement is that the synthetic section of the line must be at least 1.0 meter off the seafloor. This is driven by the ABS requirement that the synthetic must not contact the soil. Larger clearance values could be considered to yield more conservative designs. The design requirements for this study are summarized in Table 4.6.

Table 4.6. IEA 15-MW Design Requirements

Synthetic Minimum Breaking Factor of Safety	2.18
Chain Minimum Breaking Factor of Safety	3.30
Anchor Factor of Safety (Non-Redundant)	1.8
Soil Parameter	50
Maximum Synthetic Depth from SWL	55
Maximum Platform Surge Period	350 s
Minimum Platform Surge Period	55 s
Minimum Platform Heave Period	18 s
Minimum Platform Pitch Period	25 s
Allowable Synthetic Distance to Seabed	1 m

4.5.4. Environmental Loading

The environmental loading for this work is based on a lease site situated off the cost of New York. The significant wave height and peak period for this site are 8.4 m and 11.65 s respectively and are calculated based on DNV Guidelines [24]. Based on these two parameters the shape factor which describes the JONSWAP spectrum can also be estimated. The DNV also outlines a procedure in which the mean drift force on a floating structure can be estimated using the JONSWAP spectrum and the diagonal terms of the difference frequency quadratic transfer function [25]. The load on the platform due to the current loading is determined by multiplying the surge term of the quadratic damping function corresponding to the 15-MW VolturnUS-S platform by the squared velocity of the current at the site. Lastly the mean load on the turbine due to the wind velocity is determined based on the 15-MW IEA turbine thrust in the parked configuration due to the windspeed at the site. The environmental loading on the FOWT at the site is summarized in Table 4.7.

For these simulations the mean load due to the wave, current and wind loading is applied to the platform. This is done to increase the speed of the simulations which makes the problem computationally feasible as was done in [1]. Given sufficient computational resources the

OpenFAST simulations could be setup to compute the low frequency wave loading, current loading, and aerodynamic loading on the FOWT. To do this the difference QTF has to be initialized in OpenFAST and to explicitly compute the aerodynamic loading on the turbine smaller timesteps would be needed to resolve the motions.

Table 4.7. IEA 15-MW FOWT Environmental Loading

Wave Loading			
JONSWAP Spectrum	H_s (m)	T_p (s)	γ
	8.4	11.65	3.09
Mean Load due to Second-order Wave Effects	Mean Load (kN)		
	64.2		
Current Loading			
Mean Load due to Current	Current Velocity (m/s)	Mean Load (kN)	
	1.39	1780	
Wind Loading			
Mean Load due to Wind	Wind Velocity (m/s)	Mean Load (kN)	
	39	896	

Three 1-hour OpenFAST simulations were run to test the assumption that the mooring line tensions can be captured by applying a mean load for the second-order difference frequency wave loading, current, and drag on the turbine. This was done by comparing simulations with the mean load approximation with a turbulent wind field and second-order wave difference frequency load. In both cases the current was applied as a mean load. The results of these simulations are shown in Table 4.8. The mean fairlead tensions in the lead line are about 6% higher with the mean load approximation when compared to the simulations with second order waves and turbulent wind. The standard deviation of the tension is about 30% lower for the mean load approximation than the simulations with turbulent wind and second order waves. This indicates there is some low frequency dynamics of the platform due to the turbulent wind and second order waves that contribute to larger mooring line tensions. This low frequency

surge motion leads to the mean load approximation underpredicting the maximum mooring line tension by about 16%.

Table 4.8. Mean Load Approximation vs. Turbulent Wind and Second-order Waves

	Mean Tension		STD Tension		Max Tension (kN)		Min Tension	
	MLA	TW + SOW	MLA	TW + SOW	MLA	TW + SOW	MLA	TW + SOW
Seed A	3298	3132	537	686	5477	6350	1403	835
Seed B	3295	3096	509	668	4912	5679	1888	1285
Seed C	3296	3095	504	660	5039	5422	1571	1378

MLA – Mean Load Approximation
TW + SOW – Turbulent Wind and Second-order Waves

A time domain simulation of the lead fairlead mooring line tension response is provided in Figure 4.10. The time series shows the largest discrepancy in the maximum tension in Table 4.8. during Seed A which occurs around 3110 s. The time series data shows that the mean mooring line tension is captured well with the mean load approximation. There is however low frequency motion that is not captured that leads to the mooring line dynamic tensions being underpredicted. A 16% underprediction is reasonable for the purposes of screening the mooring design space, but with the right computational resources it would be possible to include second order waves and turbulent wind into the optimization routine.

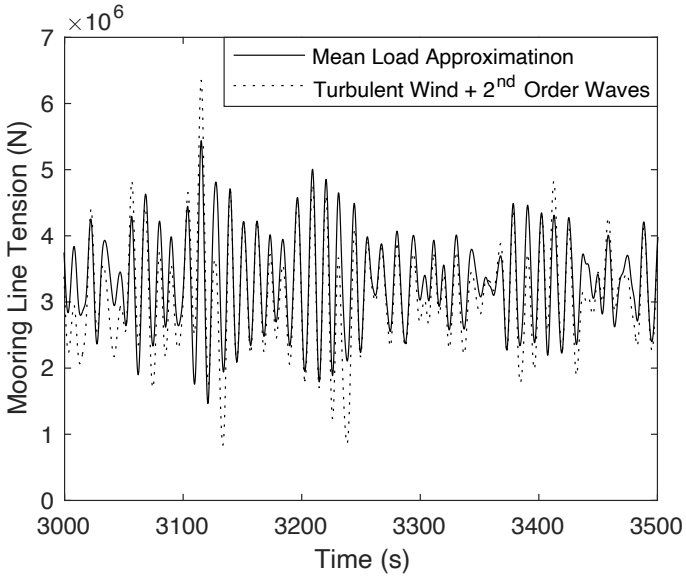

Figure 4.10. Mooring Line Tension Time History Comparison between the Mean Load Approximation used and Turbulent Wind and Second-Order Wave Forces

4.5.5. Modelling approach to extrapolate the maximum loads

The modelling approach used for these simulations is based on the ABS guide to synthetic moorings and the previous work. As outlined in the ABS guide to synthetic moorings synthetic lines have both a quasi-static and dynamic stiffness [15]. The quasi-static stiffness is used to find the pretension of the system and is used to determine both the mean offsets of the platform and the mean mooring line tensions. To perform the dynamic simulations the dynamic line stiffness is used, and the initial length of the line is adjusted to match the pretension from the static simulation for the quasi-static line stiffness. Once the pretension has been matched a dynamic simulation is run with the dynamic stiffness. The response amplitudes from this simulation are taken and added to the mean tension found for the static-simulation. This methodology is consistent with what is outlined by the ABS. At this point the maximum tension peaks of the ABS derived tension time history are extracted and the maximum tension that would occur for the 24 1-hour simulations is estimated based on the GEV fit of the first 1000s consistent with [1].

The seed selected to generate the wave time series from the JONSWAP Spectrum was selected in a way consistent with the method outlined in [1]. For this work 24 random pairs of seeds were generated. It was found that extrapolating the first 1000s of Seed 22 is within 1% of the design value determined from the mean of the maximum fairlead tensions. Seed 22 corresponds to Seed 1 of -853383955 and Seed 2 of 1133687019 in the HydroDyn Input Files. The methodology used to estimate the maximum tension in the line is illustrated in Figure 4.11.

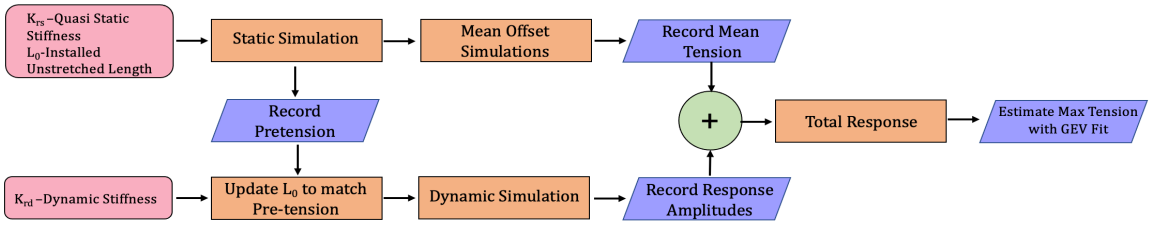

Figure 4.11. Modelling Approach to estimate the Maximum Loads

To determine the mean offsets in a timelier manner both the linear and quadratic damping coefficients in the HydroDyn input files are adjusted to increase damping. This results in an overdamped system that will reach both steady state displacements and mooring line tensions more quickly. In the original IEA 15-MW files the only source on linear damping is the damping coefficients from the potential flow analysis. To enhance the damping in the model for the mean offset simulations the linear damping matrix shown in Equation (4.18.) is implemented in OpenFAST.

$$\boldsymbol{B}_{\text{lin}} = \frac{Ns}{m}\begin{bmatrix} 5\times10^{5} & 0 & 0 & 0 & 0 & 0 \\ 0 & 5\times10^{5} & 0 & 0 & 0 & 0 \\ 0 & 0 & 1\times10^{7} & 0 & 0 & 0 \\ 0 & 0 & 0 & 1\times10^{10}\text{m}^2 & 0 & 0 \\ 0 & 0 & 0 & 0 & 1\times10^{10}\text{m}^2 & 0 \\ 0 & 0 & 0 & 0 & 0 & 1\times10^{9}\text{m}^2 \end{bmatrix} \tag{4.18.}$$

The quadratic damping matrix is also augmented for the mean offset simulations. The order of magnitude for the surge and sway degrees of freedom are increased by a factor of 10. The quadratic damping for the heave degree of freedom as well as all the rotational degrees of freedom is increased by a factor of 100. The rest of the components of the quadratic matrix are left unchanged. The modified quadratic damping matrix used for the mean offset simulations is provided by Equation (4.19.).

$$\boldsymbol{B}_{\text{quad}} = \frac{Ns^2}{\text{m}^2}\begin{bmatrix} 9.22\times10^6 & 0 & 0 & 0 & -8.92\times10^6\text{m}^2 & 0 \\ 0 & 9.22\times10^6 & 0 & 8.92\times10^6\text{m}^2 & 0 & 0 \\ 0 & 0 & 2.30\times10^8 & 0 & 0 & 0 \\ 0 & 8.92\times10^6\text{m}^2 & 0 & 1.68\times10^{12}\text{m}^3 & 0 & 0 \\ -8.92\times10^6\text{m}^2 & 0 & 0 & 0 & 1.68\times10^{12}\text{m}^3 & 0 \\ 0 & 0 & 0 & 0 & 0 & 4.80\times10^{12}\text{m}^3 \end{bmatrix} \quad (4.19.)$$

To run the OpenFAST DLC 6.1-time domain simulations used extract the fairlead tension amplitudes only the linear damping due to the potential flow analysis is used, and the quadratic damping matrix is left unmodified. The unmodified IEA 15-MW quadratic damping is provided in Equation (4.20.).

$$\boldsymbol{B}_{quad} = \frac{Ns^2}{m^2}\begin{bmatrix} 9.22\times10^5 & 0 & 0 & 0 & -8.92\times10^6m^2 & 0 \\ 0 & 9.22\times10^5 & 0 & 8.92\times10^6m^2 & 0 & 0 \\ 0 & 0 & 2.30\times10^6 & 0 & 0 & 0 \\ 0 & 8.92\times10^6m^2 & 0 & 1.68\times10^{10}m^3 & 0 & 0 \\ -8.92\times10^6m^2 & 0 & 0 & 0 & 1.68\times10^{10}m^3 & 0 \\ 0 & 0 & 0 & 0 & 0 & 4.80\times10^{10}m^3 \end{bmatrix} \quad (4.20.)$$

Lastly, the OpenFAST and MoorDyn settings used for both the mean offset and DLC 6.1 tension time history are presented in Table 4.9. In [1] a complex convergence study was performed to determine the relationship between the MoorDyn timesteps, OpenFAST timesteps and line discretization. For this mooring system configuration, a finer line discretization was needed to resolve the line geometry on the seafloor. The DLC 6.1 time-domain simulations tend to be more stable for this configuration which could be attributed to this system being semi-taut.

Table 4.9. OpenFAST and MoorDyn Discretization and Timesteps

OpenFAST Timestep (s)	MoorDyn Timestep (s)	Bottom Chain Discretization (segments)	Synthetic Section Discretization (segments)	Top Chain Discretization (segments)
0.125	0.001	14	70	2

4.6. Mooring Optimization Results

The multi-objective genetic algorithm optimization problem laid out in this study was run with a population of 140 individuals for 400 generations. The results from this run are presented below in two different sections. The first section aims to demonstrate the optimizer is working towards a converged solution by studying the formation of the mapped Pareto-front and the corresponding mooring radius-lowest cost relationship. The population will also be analyzed to ensure that the solutions obtained from this run are feasible and behaving as expected. The second section aims to explore the design space. This includes analyzing important trends across the population and examining in more detail designs at a variety of locations along mooring radius-lowest cost relationship.

4.6.1. Formation of the Mapped Pareto-front

To ensure that the optimizer is finding good designs with the objective function mapping method, the formation of the Pareto-front and mapped space needs to be examined to verify convergence and the solutions throughout the design space need to be inspected. The formation of the Pareto-front for the mapped objective function as well as the corresponding cost and mooring radius relationship are shown for generations 5, 20 and 240 in Figure 4.12. In generation 5 the Pareto-front of the mapped objective functions has many gaps and the trends in the mooring radius-lowest cost relationship are not clear. For example, at a radius of around 340m there are many solutions that have widely varying costs. At generation 20 it can be seen in the mapped Pareto front that feasible designs are starting to fill the gaps and the designs from 300m to 400m radius on the mooring radius-lowest cost plots are starting to trend towards cheaper designs. Finally, by generation 240 the mapped Pareto-front is finely filled in, and there is a clear trend between mooring radius and mooring system cost.

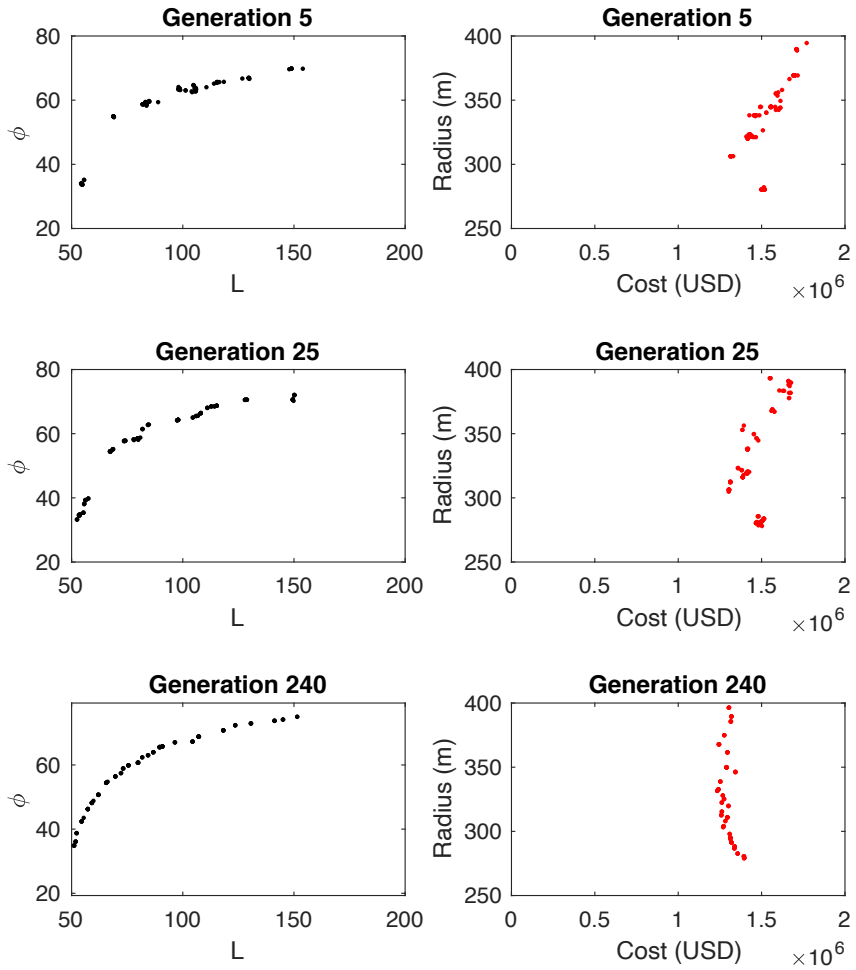

Figure 4.12. Development of the Mapped Pareto-Front and Corresponding Mooring Radius vs. Cost Relationship for Generations 5, 25, and 240

Although it is not something that is specified to be minimized in the optimization routine, it is expected that the material factors of safety will approach the constraint boundaries outlined in Table 4.6. in seeking low-cost mooring solutions. Any design that is above the target factor of safety is considered a feasible design, but one way to drive the cost down is to decrease the diameter of the materials. As the materials decrease in size so does their holding capacity and thus the factors of safety. Table 4.10. outlines both the synthetic and chain factors of safety for the mooring system across all the designs. The target factor of safety for the chain and the synthetic is 3.30 and 2.18 respectively. Across the entire population the average factor of safety

for the chain and synthetic is 3.32 and 2.19. These values are less than 1% over the target values. The maximum factors of safety in the population are 3.39 for the chain and 2.26 for the synthetic. These designs might not be considered completely converged, but even these values are only 3% and 4%, respectively above the target chain and synthetic factor of safety constraint values. There could also be other factors in the determining the size of the lines, for example, if extra stiffness is needed in the system due to the weight of the chain. Lastly the coefficient of variation for both population factors of safety are less than 1% which signals that there is not a lot of variability about the average factors of safety. These results indicate that the methodology outlined in this work is producing reasonable mooring system designs.

Table 4.10. Line Factor of Safety across the Entire Suite of Designs

Material	Target FoS	Average FoS	Max FoS	Min FoS	FoS COV
Chain	3.30	3.32	3.39	3.30	0.78%
Synthetic	2.18	2.19	2.26	2.18	0.62%

4.6.2. Exploration of the Design Space

The main objective of the optimization run was to determine the mooring radius-minimum cost relationship. This relationship is illustrated in Figure 4.13. The cost of the mooring system is constant around 1.25 million dollars from a mooring radius from 400 m to 300 m. These costs are just looking at component cost and other costs associated with a mooring system such as installation and maintenance costs are not considered. As the mooring radius decreases below 300 meters the cost of the mooring system consistently rises to around 1.4 million dollars. Overall, the minimum mooring cost is more or less constant with changing mooring radius. Further understanding of this trend requires investigation of the relationships between the design variables and mooring radius.

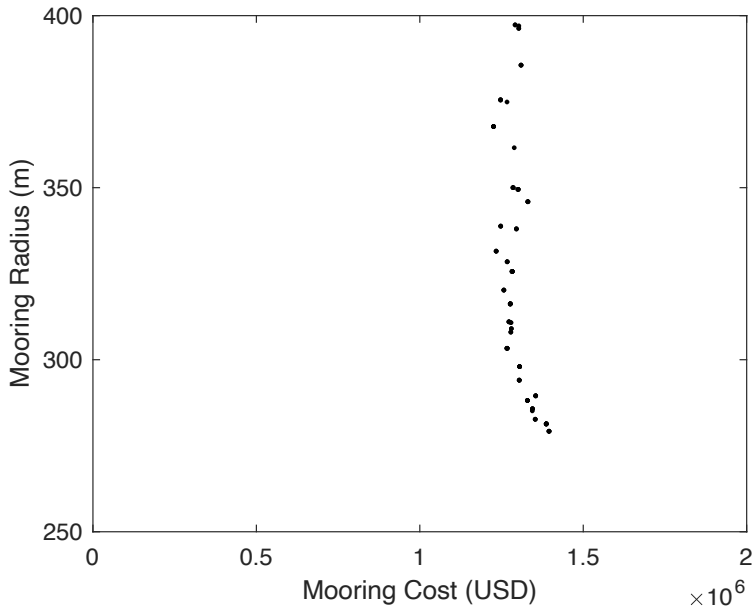

Figure 4.13. Mooring Radius vs Mooring Cost for Generation 400

Figure 4.14. shows the relationship between the mooring system radius and the synthetic line length. The lengths of both the top and bottom chain connection in this mooring configuration is fixed. As only the length of the synthetic can change it is logical that the length would increase with the mooring radius. Perhaps surprising is how linear this relationship is. This could suggest that there is a catenary action due to bottom chain geometry that is important to the dynamics of the FOWT which the optimizer aims to preserve.

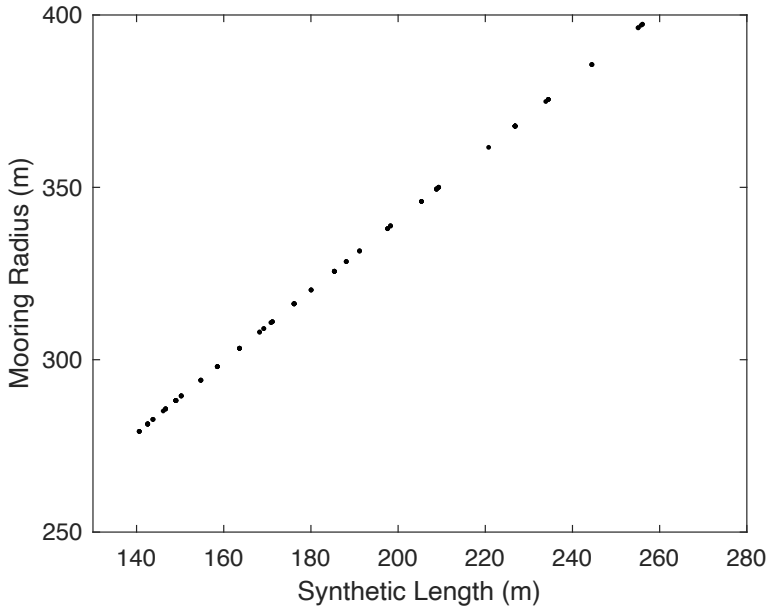

Figure 4.14. Mooring Radius vs. Synthetic Length

Figure 4.15. illustrates the relationship between the mooring radius and the buoy displaced volume. This graph illustrates a clear trend where buoy displaced volume decreases as mooring radius increases. The buoy displaced volume varies from around 7.25 m^3 to 4.6 m^3 for a mooring radius of 280 m to 400 m respectively. This is likely because a given FOWT surge displacement will likely require a larger buoy to keep the synthetic mooring line section off the seabed as the mooring radius is reduced. For a relatively large mooring radius at a similar surge displacement, a smaller buoy will be sufficient for keeping the mooring line off the seabed.

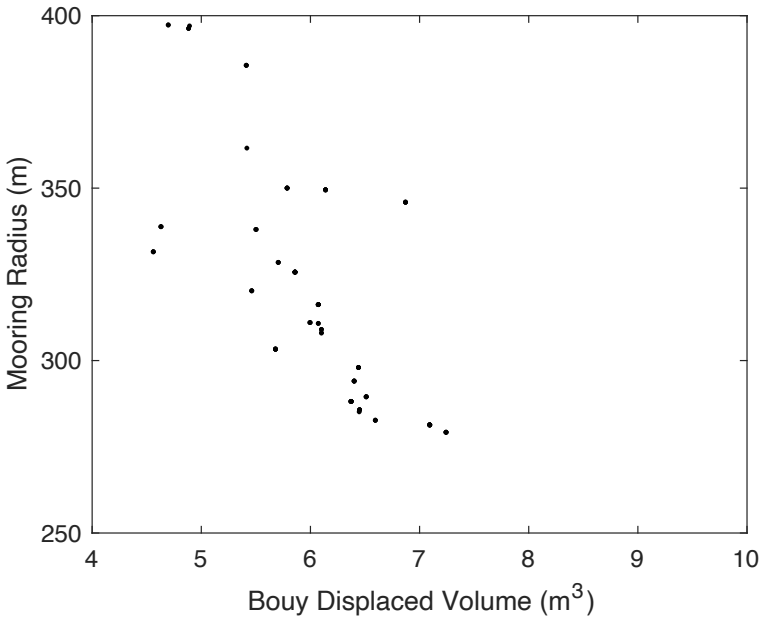

Figure 4.15. Mooring Radius vs. Buoy Displaced Volume

Figures 4.16. and 4.17. shows the relationship between mooring line radius and line diameter (chain diameter and synthetic diameter) respectively. These plots both illustrate a clear trend that line diameter decreases as mooring radius increases. Although these are the trends that were also observed in [1], there is much less of a change in line diameter in this work. The chain diameter only varies from 167mm to 154mm, and the synthetic diameter varies from 208mm to 195mm. As discussed in [1] this reduction is likely due to two factors. First as the line length increases the equivalent stiffness of the line decreases. This causes the lines to attract less load which ultimately lends itself to smaller materials. The second effect that could lead to this is that as the mooring radius increases the line is more horizonal as compared to the seafloor. This leads to the lines being loaded in a more efficient way. The major difference between the results from [1] and this work is the relatively small variation in line diameters. This is likely due to the large mean loading on the turbine and smaller dynamic loading due to the waves. The mean load in DLC 6.1 for the IEA 15-MW turbine is about 7.6 times larger than the mean load in the

similar case for the 6-MW VolturnUS system and associated environment that was analyzed [1]. In addition to the mean loads being larger the significant wave heights the 15-MW hull is subjected to are about 21% smaller than the sea state for the 6-MW hull. In addition, the 15-MW hull is larger relative to the same sea state a 6-MW turbine would be subject to. In conclusion the mean loads dominate and are constant regardless of mooring configuration. This leads to relatively similar line diameters.

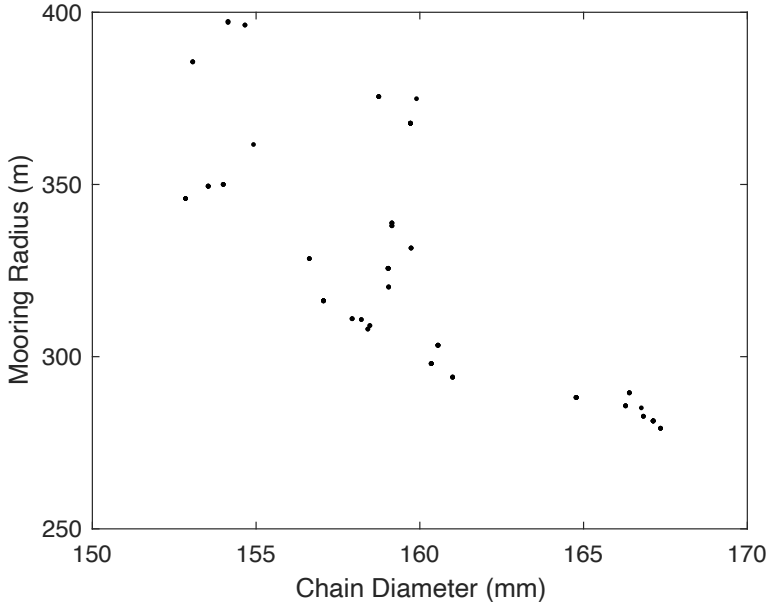

Figure 4.16. Mooring Radius vs. Chain Diameter

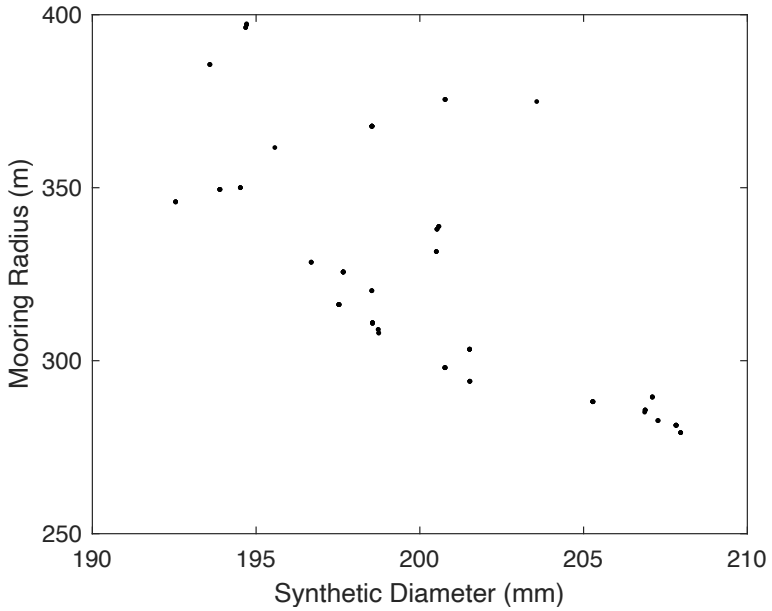

Figure 4.17. Mooring Radius vs. Synthetic Diameter

Plots illustrating the relationship between maximum fairlead tension and mooring radius as well as mean surge offset and mooring radius are provided in Figures 4.18. and 4.19. As the mooring radius increases from 278 m to 397 m the maximum fairlead tension decreases by about 15%. Over this same range the area of the synthetic line decreases by 18% which is very consistent with the mooring line maximum fairlead tension. Similarly, the mean offset of the platform increases by about 30% which suggests that the mooring system gains compliance as the radius increases. This increased compliance is what causes the larger radius mooring systems to attract less load and ultimately need smaller mooring line diameters.

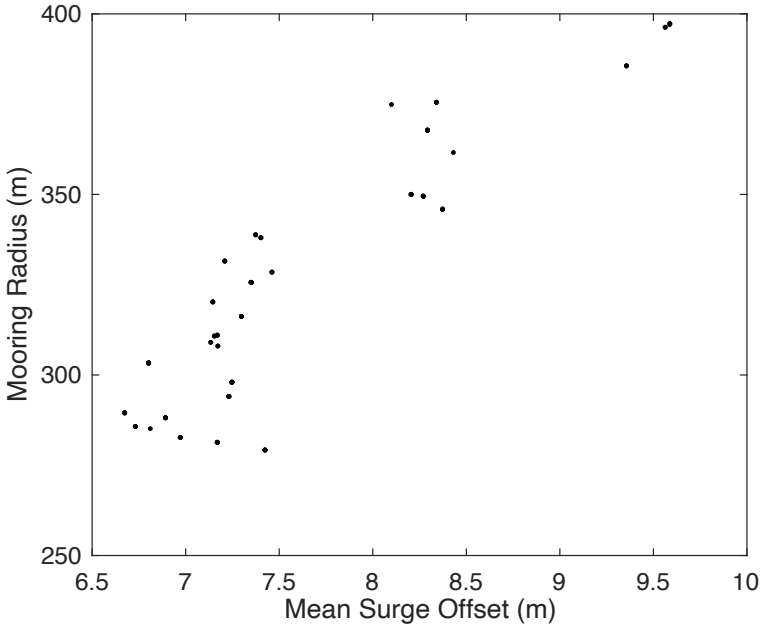

Figure 4.18. Mooring Radius vs. Mean Surge Offset

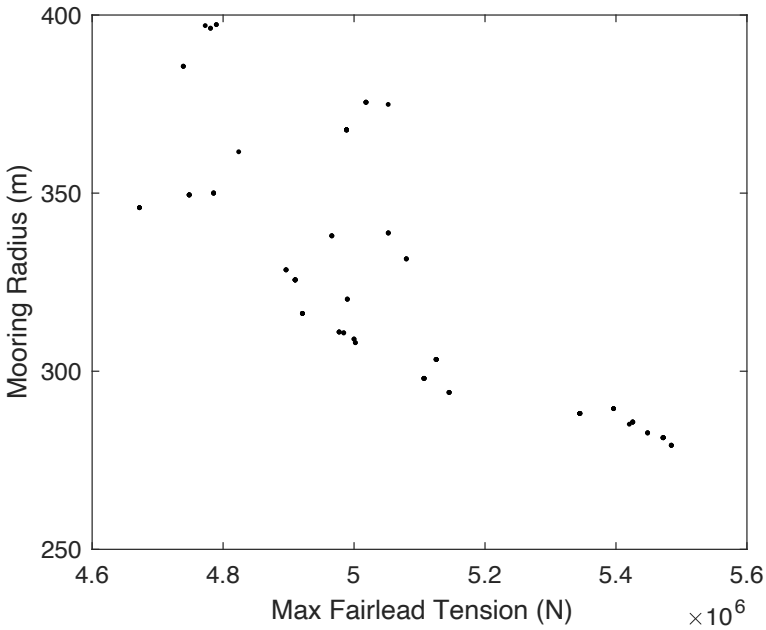

Figure 4.19. Mooring Radius vs. Maximum Fairlead Tension

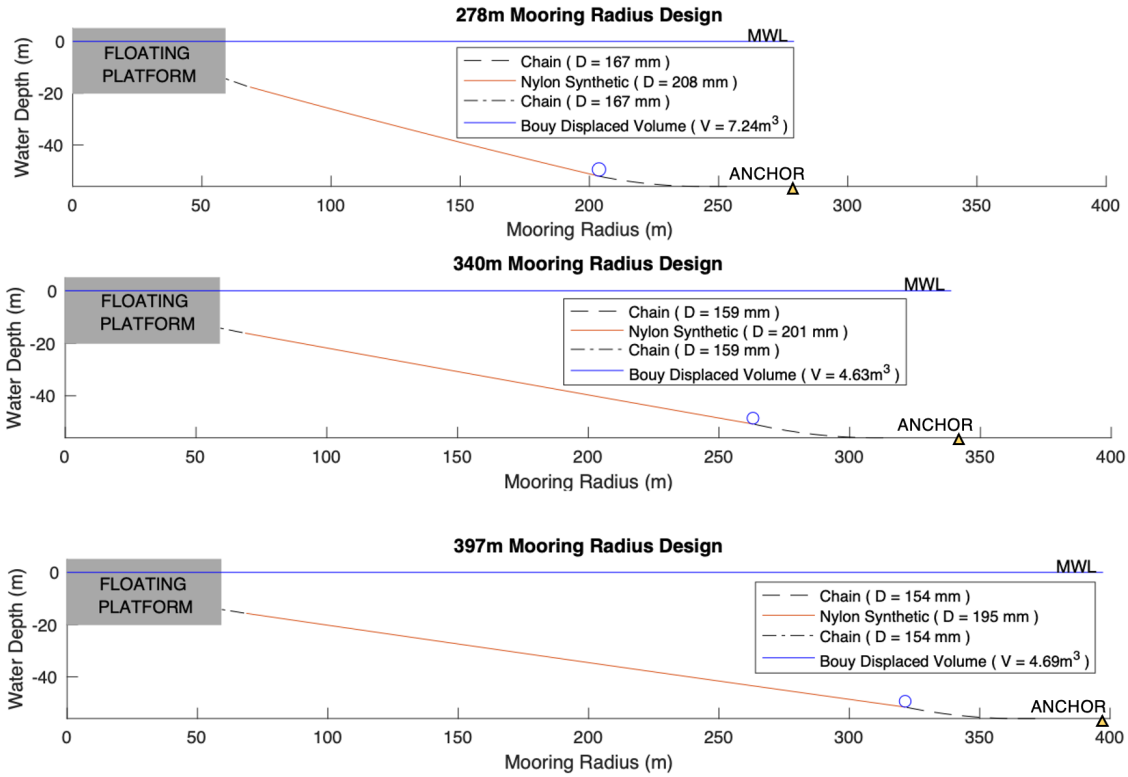

Figure 4.20. Illustrations of Mooring Systems at Different Radii along the Mooring Radius/Cost Relationship

Figure 4.20. illustrates the geometry of various mooring configurations found from the optimization routine along the mooring radius-cost relationship. The geometry selected by the optimizer for all these designs are similar with a taut synthetic section in the middle and a catenary shape in the mooring chain at the bottom with around 40m to 50m of chain on the seafloor. Each of these designs show the small reduction in mooring line diameters and the larger reduction in buoy size from the smallest radius design to the largest radius design.

The surge static offset curves and surge mooring stiffness curves are provided in Figure 4.21. The mooring system restoring force for positive surge offsets is very similar for the 278 m and 340 m radius design. This is consistent with both designs having a mean offset around 7.4 m in Figure 4.18. The mooring system stiffness for the 340 m radius design however begins to decrease for surge offsets greater than about 5 m which leads to the 340 m radius system

attracting less loads than the 278 m radius system. The stiffnesses for the 278 m radius system and the 397 m radius system decrease by about 25%. This is consistent with the mean surge offset increasing by 30% over the range of mooring radii in Figure 4.18.

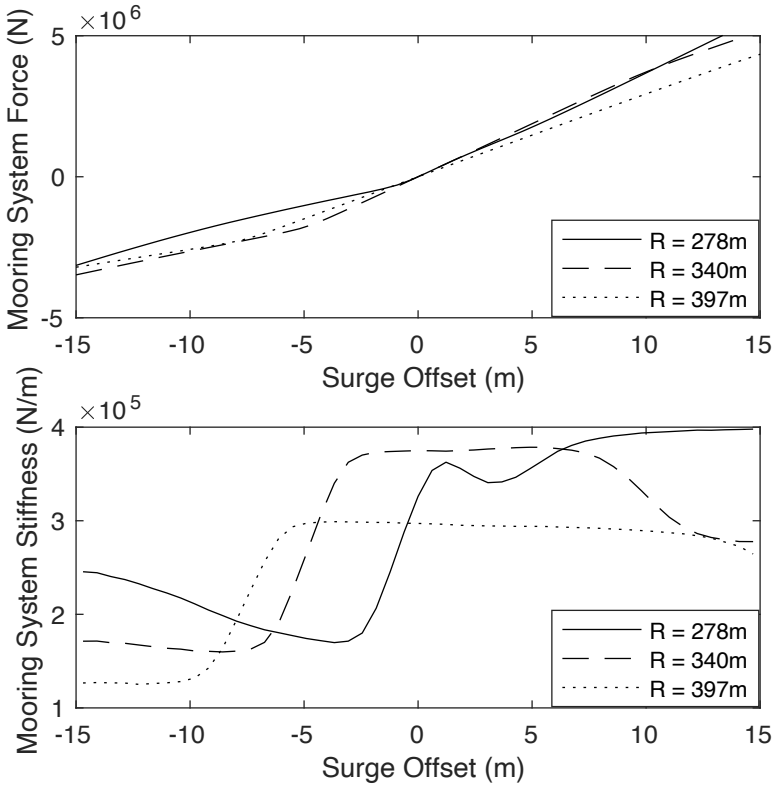

Figure 4.21. Mooring System Static Offset Curves and Mooring System Stiffness Curves for the Designs Presented in Figure 4.20.

The designs along the mooring cost-radius relationship stay mostly constant because as the costs for mooring materials decrease as the radius increases leading to a longer synthetic length. The savings on the material sizes are counteracted by the synthetic line section cost increase as longer lengths are needed. The cost breakdown for each mooring system illustrated in Figure 4.20 is provided in Table 4.11. As the radius increases the buoy cost between the largest and smallest mooring radius decreases by around 35%. Similarly, chain cost and anchor cost both reduce by about 15%. The cost of the synthetic increases by 37% due to the increased

line length at a larger mooring radius. Together this leads to a small cost savings of about 6.6% when the radius of the mooring system is increased from 278m to 397m.

Table 4.11. Mooring System Cost Breakdown at Different Radii along the Mooring Radius/Cost Relationship

Mooring Radius (m)	Total Cost (USD)	Buoy Cost (USD)	Synthetic Cost (USD)	Chain Cost (USD)	Anchor Cost (USD)
278	1,384,000	478,000	284,000	214,000	408,000
340	1,233,000	305,000	371,000	193,000	364,000
397	1,292,000	310,000	453,000	181,000	348,000

4.7. Conclusions

The main role of this work is to generalize an optimization methodology for determining the mooring system minimum cost-radius relationship for FOWT installations. Many of the techniques that were developed in a previous study [1] such as the tiered constraint methodology and the estimation of the maximum line tensions using the generalized extreme value fit were employed in this work. This study significantly introduced a more realistic mooring system constraints where a longer length of chain at the seafloor is necessary. In addition, the tool developed included the ABS-recommended approach for modelling the stiffness of synthetic materials and incorporated the pricing of anchors into the overall cost of the mooring system.

The key contribution in this work for enabling more broad applicability of this tool was the process of mapping mooring radius and mooring cost into new variables. For the previous 6-MW system [1] and the associated environmental inputs it was found that the mooring component cost and mooring radius were two objectives that were competing. In a situation where the variables of interest are not competing it is necessary to express the mooring cost and radius using new competing objective functions. This was done by mapping each design in the mooring radius-lowest cost space into a new space defined by a vector length and angle.

Overall, this new mapping approach along with more realistic mooring designs lead to a suite of low-cost designs for the 15-MW system over the range of mooring radii considered. It was found that as the radius increased the cost of the mooring system was held fairly constant around 1.25 million dollars. This was attributed to the increased synthetic line length counteracting any cost reductions due to slightly smaller line diameters, smaller buoys, and smaller anchors. The reduction in line diameters for this case was significantly different than the reduction seen with the 6-MW case. This is likely due to how different the loading is on these two different structures at their respective sites. The 15-MW mooring system must withstand a much higher mean load with relatively smaller dynamic loads induced by the waves when compared to the 6-MW turbine.

4.8. References

[1] West, W.; Goupee, A.; Hallowell, S.; Viselli, A. Development of a Multi-Objective Optimization Tool for Screening Designs of Taut Synthetic Mooring Systems to Minimize Mooring Component Cost and Footprint. *Modelling* 2021, *2*, 728-752. https://doi.org/10.3390/modelling2040039

[2] Gaertner, Evan, Jennifer Rinker, Latha Sethuraman, Frederik Zahle, Benjamin Anderson, Garrett Barter, Nikhar Abbas, Fanzhong Meng, Pietro Bortolotti, Witold Skrzypinski, George Scott, Roland Feil, Henrik Bredmose, Katherine Dykes, Matt Shields, Christopher Allen, and Anthony Viselli. 2020. *Definition of the IEA 15-Megawatt Offshore Reference Wind*. Golden, CO: National Renewable Energy Laboratory. NREL/TP-5000-75698. https://www.nrel.gov/docs/fy20osti/75698.pdf

[3] Xu, K.; Larsen, K.; Shao, Y.; Zhang, M.; Gao, Z.; Moan, T. Design and comparative analysis of alternative mooring systems for floating wind turbines in shallow water with emphasis on ultimate limit state design. *Ocean Eng.* 2021, *219*, 108377.

[4] Brommundt, M.; Krause, L.; Merz, K.; Muskulus, M. Mooring System Optimization for Floating Wind Turbines using Frequency Domain Analysis. *Energy Procedia* 2012, *24*, 289–296.

[5] Benassai, G.; Campanile, A.; Piscopo, V.; Scamardella, A. Optimization of Mooring Systems for Floating Offshore Wind Turbines. *Coast. Eng. J.* 2015, *57*, 1550021.

[6] Hall, M.; Goupee, A. Validation of a lumped-mass mooring line model with DeepCwind semisubmersible model test data. *Ocean Eng.* 2015, *104*, 590–603.

[7] Thomsen, J.B.; Ferri, F.; Kofoed, J.P.; Black, K. Cost Optimization of Mooring Solutions for Large Floating Wave Energy Converters. *Energies* 2018, *11*, 159.

[8] Pillai, A.C.; Thies, P.R.; Johanning, L. Mooring system design optimization using a surrogate assisted multi-objective genetic algorithm. *Eng. Optim.* 2019, *51*, 1370–1392.

[9] Li, L.; Jiang, Z.; Ong, M.C.; Hu, W. Design optimization of mooring system: An application to a vessel-shaped offshore fish farm. *Eng. Struct.* 2019, *197*, 109363.

[10] Ferreira, F.M.; Lages, E.; Afonso, S.M.B.; Lyra, P.R. Dynamic design optimization of an equivalent truncated mooring system. *Ocean Eng.* 2016, *122*, 186–201.

[11] Deb, K.; Pratap, A.; Agarwal, S.; Meyarivan, T. A Fast and Elitist Multiobjective Genetic Algorithm. *IEEE Trans. Evol. Comput.* 2002, *6*, 182–197.

[12] Goupee, A.J.; Vel, S.S. Multi-objective optimization of functionally graded materials with temperature-dependent material properties. *Mater. Des.* 2007, *28*, 1861–1879.

[13] Masciola, M. MAP ++ Documentation. 2018. Available online: https://map-plus-plus.readthedocs.io/_/downloads/en/latest/pdf/ (accessed on 1 October 2021).

[14] NREL. *OpenFAST Documentation Release v2.3.0*; National Renewable Energy Laboratory: Golden, CO, USA, 2020.

[15] ABS. *Guidance Notes on the Application of Fiber Rope for Offshore Mooring*; ABS: Spring, TX, USA, 2014.

[16] Allen, Christopher, Anthony Viselli, Habib Dagher, Andrew Goupee, Evan Gaertner, Nikhar Abbas, Matthew Hall, and Garrett Barter. *Definition of the UMaine VolturnUS-S Reference Platform Developed for the IEA Wind 15-Megawatt Offshore Reference Wind Turbine*. Golden, CO: National Renewable Energy Laboratory. NREL/TP-5000-76773.

[17] Hall, M. *MoorDyn User's Guide*; University of Maine: Orono, ME, USA, 2015.

[18] Demar/Vryhof. *Vryhof Guide to Anchoring; 2018*

[19] API. *API RP 2SK: Design and Analysis of Stationkeeping Systems for Floating Structures*; API: Washington, DC, USA, 2005.

[20] WAMIT. WAMIT R User Manual. 2020. Available online: https://www.wamit.com/manualupdate/v74_manual.pdf (accessed on 1 October 2021).

[21] API. *API RP 2SM: Recommended Practice for Design, Manufacture, Installation, and Maintenance of Synthetic Fiber Ropes for Offshore Mooring*; API: Washington, DC, USA, 2014.

[22] ABS. *Guide for Position Mooring Systems*; ABS: Spring, TX, USA, 2020.

[23] IEC. *IEC 61400-3 Design Requirements for Offshore Wind Turbines*; IEC: Geneve, Switzerland, 2019.

[24] DNV. *DNV RP-C205 Environmental Conditions and Environmental Loads,* DET NORSKE VERITAS AS, Høvik, Norway, 2014

[25] DNV. *Global Perfomance Analysis of Deepwater Floating Structures*; DNV: Bærum, Norway, 2004.

CHAPTER 5

CONCLUSIONS

This final chapter concludes the dissertation and provides a summary of key results. Section 5.1 summarizes the results in Chapter 2: A Floating Wind Turbine Model Test to Verify a MoorDyn Modification for Nonlinear Elastic Materials. Section 5.2 summarizes the results in Chapter 3: Development of a Multi-objective Optimization Tool for Screening Designs of Taut Synthetic Mooring Systems to Minimize Cost and Radius. Section 5.3 summarizes the results from Chapter 4: Determination of Minimum-Cost Synthetic Mooring Systems for Large Floating Wind Turbines Deployed in Intermediate Water Depths. Finally, Section 5.4 highlights some appropriate next steps for future work.

5.1. Summary of A Floating Wind Turbine Model Test to Verify a MoorDyn Modification for Nonlinear Elastic Materials

Chapter 2 of this dissertation highlights key results of a scale model test campaign in which a 6-MW FOWT was outfitted with a synthetic mooring system. Previously none of the mooring modules compatible within OpenFAST were capable of modeling materials such as a synthetic fiber ropes which can have highly nonlinear tension-strain responses and viscoelastic responses. One such mooring module, MoorDyn, was modified to allow nonlinear elastic mooring line tension-strain responses to be input via a lookup table. This modification also allows for simplified synthetic mooring line material modeling approaches, such as the ABS static-dynamic model to be implemented. Simulations utilizing OpenFAST with the modified MoorDyn module were then compared with experimental data generated in the Harold Alfond W^2 Wind Wave Lab at the University of Maine Advanced Structures and Composites Center. The simulation and experimental results were found to correlate well with one another.

The results generated show that the mooring module modifications are working as expected. The tensions in the line match very closely with experimental data for both the surge and sway static offset tests which ensures that OpenFAST is determining the tension in the mooring line properly. The damped natural periods determined from the experimental data and OpenFAST also agree well which provide confidence that the MoorDyn enhancements have been implemented properly as for these degrees of freedom the restoring force is strictly due to the mooring system.

There are however some minor differences in the line tension for dynamic loading, as illustrated by the white noise wave case and the DLC 1.6 loading. This is very likely due to the surge motion of the platform being slightly over-predicted as line tension and surge offset are strongly correlated. In the case of both surge RAO and the surge PSD plots the OpenFAST model over-predicts the experimental data in the linear wave region, but this is consistently observed across the results. As line tension and platform surge response are strongly correlated the over-prediction of the surge response leads to an over-prediction of line tension. One other difference between line tension in the OpenFAST model compared to the experiment is the lack of the low-frequency tension response in OpenFAST. It is more difficult to accurately model the second-order wave forces than it is to determine the platform responses due to linear waves. Unfortunately, in this case the forcing due to the second-order wave loading has not been captured adequately by OpenFAST, which in turn causes the low-frequency surge response to be under-predicted. The mean load caused by second-order wave forcing is likely under-predicted as well leading to the mean surge offset and mean line tension in OpenFAST to be lower than what was measured in the basin.

Although some of the simulated mean platform responses are smaller than the experimental data the dynamic response of the platform and line tensions are captured very well. The tensions calculated in OpenFAST due to the modifications made to MoorDyn only differ slightly from the experimental data with respect to the mean platform surge response and line tension. These results tend to indicate that this difference is due to the simulated platform motion in OpenFAST underpredicting the response the physical model. Overall, the tension simulated by OpenFAST tends to match the experimental data well, and the smaller simulated mean line tension is consistent with the simulated surge offset which indicates the MoorDyn enhancements are working as expected.

5.2. Summary of Development of a Multi-objective Optimization Tool for Screening Designs of Taut Synthetic Mooring Systems to Minimize Cost and Radius

Chapter 3 outlines the effort to implement a MOGA, NSGA II, for design optimization of synthetic mooring systems for FOWTs. The objective functions for this problem are fairly trivial, but a significant time investment was made ensuring the constraints implemented would lead to mooring designs that were realistic and adhered to the ABS/IEC design guidelines. To adequately capture the physics of a mooring system which can experience both geometric and material non-linearities it is imperative that time-domain simulations are run. Time-domain simulations are computationally expensive so the constraints are posed in such a way that inadequate designs can be screened out which prevents running time domain simulations unnecessarily. To make the problem computationally feasible on a normal desktop computer some concessions needed to be made such as reducing the number of simulations done, using fairly large timesteps and carefully selecting seeds which will produce line tensions representative of the true design value.

This method was then used to develop a set of Pareto-optimal designs which balance the footprint of the mooring system and the mooring system component cost. The Pareto-optimal solutions found from this optimization contained a gap in the front which was found to be a result of the designs in that area having constraint violations due to the tensions in the line being slightly too large for the materials load capacity. The lines would handle the internal load if both the synthetic and chain segments were increased in diameter by 3% however the cost increase from this resulted in a design that would be dominated by designs having a smaller component cost and radius.

A design that resulted in a small footprint was analyzed more in depth to determine if the 1000 s of data used to extrapolate the maximum tension was adequate. The seed used was carefully chosen based on a DLC 6.1 run for another synthetic mooring system. The candidate design mooring system was then subjected to the same DLC 6.1 simulations with the same seed as the initial analysis of the synthetic mooring system. The value obtained from the 1000 s of extrapolated data was within 2% of the ABS design value found by taking the mean of the maximum values of the six one-hour simulations. Overall, this methodology provides designs that balance mooring line cost and mooring footprint and would be a good starting point for performing a full suite of ABS/IEC simulations.

Ideally, for future work this method would be used without the performance enhancements needed to make it computationally feasible on the hardware available. This would be fairly easy to implement given a computer with more cores available for parallel processing as the computer used in this study was an average desktop computer with four cores. With adequate computational resources the OpenFAST time domain simulations could be run with fully turbulent wind fields

for the full 3600 s which at this point is not possible as it would require timesteps that are so small it would make the problem computationally infeasible with the resources available.

5.3. Summary of Determination of Minimum-Cost Synthetic Mooring Systems for Large Floating Wind Turbines Deployed in Intermediate Water Depths

Lastly, Chapter 4 generalizes an optimization methodology for determining the mooring system minimum cost-mooring radius relationship for FOWT installations. Many of the techniques that were developed in a previous study such as the tiered constraint methodology and the estimation of the maximum line tensions using the generalized extreme value fit were employed in this study. This study significantly introduced a more realistic mooring system constraints where a longer length of chain at the seafloor is necessary. In addition, the tool developed included the ABS-recommended approach for modelling the stiffness of synthetic materials and incorporated the pricing of anchors into the overall cost of the mooring system.

The most important work to generalize this tool was the process of mapping mooring radius and mooring cost into new variables. For the previous 6-MW system and the environmental inputs it was found that the mooring component cost and mooring radius were two objectives that were competing. In a situation where the variables of interest are not competing it is necessary to express the system using new competing objective functions. This was done by mapping each design in the mooring radius-cost space into a new space defined by a vector length and angle.

Overall, this new mapping approach along with more realistic mooring design constraints lead to good results for the 15-MW system. It was found that as the radius increased the cost of the mooring system components was held fairly constant around 1.25 million dollars. This was attributed to the increased synthetic line length counteracting any cost reductions due to slightly

smaller line diameters, smaller buoys, and smaller anchors. The reduction in line diameters for this case was significantly different than the reduction seen with the 6-MW case. This is likely due to how different the loading is on these two different structures at their respective sites. The 15-MW mooring system must withstand a much higher mean load with relatively smaller dynamic loads induced by the waves when compared to the 6-MW turbine.

5.4. Recommendations for Future Work

There are many ways the work presented in this dissertation could be expanded on for the future. One area is the modelling of synthetic fiber ropes within the design and analysis software. Chapter 2 of this dissertation improved the numerical tools by allowing general tension strain relationships for the mooring materials. In the future it would be ideal to have a model that accounts for the strain-rate dependent properties of the mooring materials. This could potentially be done by implementing the DNV's ratchet model into the software. For this to be implemented a significant effort would need to be made to generate an extensive data set of rope properties.

Another area for potential future work could be with the optimization procedures developed. In Chapters 3 and 4 only three-line configurations have been investigated. In the future more lines could be considered in as well as different configurations which account for the directionality of the environmental loading. This could involve non-symmetrical arrangements of the mooring lines, or mooring lines with different properties depending on the location relative to the environment. This would introduce new variables into the formulation so more computational power would be necessary to perform the analysis.

BIBLIOGRAPHY

ABS. *ABS Review Advances University of Maine's Innovative Floating Offshore Wind Concept*; ABS: Spring, TX, USA, 2017.

ABS. *Guide for Position Mooring Systems*; ABS: Spring, TX, USA, 2020.

ABS. *Guidance Notes on the Application of Fiber Rope for Offshore Mooring*; ABS: Spring, TX, USA, 2014.

ABS. *Guide for Building and Classing Floating Offshore Wind Turbine Installations*; ABS: Spring, TX, USA, 2015.

Allen, Christopher, Anthony Viselli, Habib Dagher, Andrew Goupee, Evan Gaertner, Nikhar Abbas, Matthew Hall, and Garrett Barter. *Definition of the UMaine VolturnUS-S Reference Platform Developed for the IEA Wind 15-Megawatt Offshore Reference Wind Turbine*. Golden, CO: National Renewable Energy Laboratory. NREL/TP-5000-76773.

API. *API RP 2SK: Design and Analysis of Stationkeeping Systems for Floating Structures*; API: Washington, DC, USA, 2005.

API. *API RP 2SM: Recommended Practice for Design, Manufacture, Installation, and Maintenance of Synthetic Fiber Ropes for Offshore Mooring*; API: Washington, DC, USA, 2014.

Arapogianni, A.; *et al.*, "Deep Water: The Next Step for Offshore Wind Energy," 2013.

Benassai, G.; Campanile, A.; Piscopo, V.; Scamardella, A. Optimization of Mooring Systems for Floating Offshore Wind Turbines. *Coast. Eng. J.* 2015, *57*, 1550021.

Brommundt, M.; Krause, L.; Merz, K.; Muskulus, M. Mooring System Optimization for Floating Wind Turbines using Frequency Domain Analysis. *Energy Procedia* 2012, *24*, 289–296.

Browning J. R., Jonkman J., and Robertson A., "The effects of second-order hydrodynamics on a semisubmersible floating offshore wind turbine ," *J. Phys. Conf. Ser*, vol. 524, p. 12094, 2014.

Coulling A. J., Goupee A. J., Robertson A. N., Jonkman J. M., and Dagher H. J., "Validation of a FAST semi-submersible floating wind turbine numerical model with DeepCwind test data," *J. Renew. Sustain. Energy*, vol. 5, no. 2, 2013.

Coulling A. J., Goupee A. J., Robertson A. N., and Jonkman J. M., "Importance of second-Order difference-Frequency wave-Diffraction forces in the validation of a fast semi-Submersible floating wind turbine model," *Proc. Int. Conf. Offshore Mech. Arct. Eng. - OMAE*, vol. 8, no. June, 2013.

Cummins W. E., “The Impulse Response Function and Ship Motions,” in *Symposium on Ship Theory*, 1962, p. 6.

Dagher, H.; Viselli, A.; Goupee, A.; Kimball, R.; Allen, C. *The VolturnUS 1:8 Floating Wind Turbine: Design, Construction, Deployment, Testing, Retrieval, and Inspection of the First Grid-Connected Offshore Wind Turbine in US*; University of Maine: Orono, ME, USA, 2017.

Davies, P.; Weller, S.D.; Johanning, L.; Banfield, S.J. A review of synthetic fiber moorings for marine energy applications. In Proceedings of the 5th International Conference on Ocean Energy, Halifax, NS, Canada, 4–6 November 2014; pp. 1–6.

Deb, K.; Pratap, A.; Agarwal, S.; Meyarivan, T. A Fast and Elitist Multiobjective Genetic Algorithm. *IEEE Trans. Evol. Comput.* 2002, *6*, 182–197.

Del Vecchio C., “Lightweight Materials for Deep Water Moorings,” University of Reading, 1992

Delmar/Vryhof. *Vryhof Guide to Anchoring; 2018*

DNV. *DNV RP-C205 Environmental Conditions and Environmental Loads,* DET NORSKE VERITAS AS, Høvik, Norway, 2014

DNV. *Global Perfomance Analysis of Deepwater Floating Structures*; DNV: Bærum, Norway, 2004.

Draxl, C., B.M. Hodge, A. Clifton, and J. McCaa. 2015. *Overview and Meteorological Validation of the Wind Integration National Dataset Toolkit* (Technical Report, NREL/TP-5000-61740). Golden, CO: National Renewable Energy Laboratory.

Draxl, C., B.M. Hodge, A. Clifton, and J. McCaa. 2015. "The Wind Integration National Dataset (WIND) Toolkit." *Applied Energy* 151: 355366.

Falkenberg E., Yang L., and Ahjem V., “SPRING-DASHPOT SIMULATIONS OF POLYESTER ROPES : VALIDATION OF THE SYROPE MODEL,” *Proc. ASME 2019 38th Int. Conf. Ocean. Offshore Arct. Eng.*, pp. 1–8, 2019.

Ferreira, F.M.; Lages, E.; Afonso, S.M.B.; Lyra, P.R. Dynamic design optimization of an equivalent truncated mooring system. *Ocean Eng.* 2016, *122*, 186–201.

Flory, J. F., Banfield, S. J., Ridge, I. M. L., Yeats, B., Mackay, T., Wang, P., Hunter, T., Johanning, L., Herduin, M., & Foxton, P. (2016). Mooring systems for marine energy converters. In J. Zande, & B. Kirkwood (Eds.), *OCEANS 2016 MTS/IEEE Monterey, OCE 2016* [7761007] IEEE, Institute of Electrical and Electronics
Engineers. https://doi.org/10.1109/OCEANS.2016.7761007

Gaeta M. G., Segurini G., Moreno A. M., and Archetti R., "Implementation and validation of a potential model for a moored floating cylinder under waves," *J. Mar. Sci. Eng.*, vol. 8, no. 2, 2020.

Goupee, A.J.; Vel, S.S. Multi-objective optimization of functionally graded materials with temperature-dependent material properties. *Mater. Des.* 2007, *28*, 1861–1879.

Hall, M. *MoorDyn User's Guide*; University of Maine: Orono, ME, USA, 2015.

Hall M. and Goupee A., "Validation of a lumped-mass mooring line model with DeepCwind semisubmersible model test data," *Ocean Eng.*, vol. 104, pp. 590–603, 2015.

Haslum H. A., "Simplified methods applied to nonlinear motion of spar platforms," Norwegian Univeristy of Science and Technology, Trondheim, 2000.

IEA. *IEA Wind TCP Annual Report 2020;* International Energy Agency: Paris, France, 2020.

IEC. *IEC 61400-3 Design Requirements for Offshore Wind Turbines*; IEC: Geneve, Switzerland, 2019.

Koo B. J., Goupee A. J., Kimball R. W., and Lambrakos K. F., "Model Tests for a Floating Wind Turbine on Three Different Floaters," *J. Offshore Mech. Arct. Eng.*, vol. 136, no. 2, p. 020907, 2014.

Li, L.; Jiang, Z.; Ong, M.C.; Hu, W. Design optimization of mooring system: An application to a vessel-shaped offshore fish farm. *Eng. Struct.* 2019, *197*, 109363.

Lopez-pavon C., Watai R. A., Ruggeri F., Simos A. N., and Souto-iglesias A., "Influence of Wave Induced Second-Order Forces in Semisubmersible FOWT Mooring Design," vol. 137, no. June, pp. 1–10, 2015.

Martin H. R., Kimball R. W., Viselli A. M., and Goupee A. J., "Methodology for Wind/Wave Basin Testing of Floating Offshore Wind Turbines," 2014.

Masciola, M. MAP ++ Documentation. 2018. Available online: https://map-plus-plus.readthedocs.io/_/downloads/en/latest/pdf/ (accessed on 1 October 2021).

Musial, W., Parker, Z., Fields, M., Scott, G., Elliott, D., and Draxl, C. *Assessment of Offshore Wind Energy Leasing Areas for the BOEM Massachusetts Wind Energy Area*. United States: N. p., 2013. Web. doi:10.2172/1118096.

NREL. *OpenFAST Documentation Release v2.3.0*; National Renewable Energy Laboratory: Golden, CO, USA, 2020.

NREL. *2019 Offshore Wind Technology Data Update*; National Renewable Energy Laboratory: Golden, CO, USA, 2020.

Pillai, A.C.; Thies, P.R.; Johanning, L. Mooring system design optimization using a surrogate assisted multi-objective genetic algorithm. *Eng. Optim.* 2019, *51*, 1370–1392.

Qualysis, "QTM Version: 2.15," 2017

Thomsen, J.B.; Ferri, F.; Kofoed, J.P.; Black, K. Cost Optimization of Mooring Solutions for Large Floating Wave Energy Converters. *Energies* 2018, *11*, 159.

US Department of Energy. *Offshore Wind Market Report: 2021 Edition*; US Department of Energy: Washington, DC, USA, 2021.

Viselli, A.M.; Forristall, G.Z.; Pearce, B.R.; Dagher, H.J. Estimation of extreme wave and wind design parameters for offshore wind turbines in the Gulf of Maine using a POT method. *Ocean Eng.* 2015, *104*, 649–658.

WAMIT. WAMIT R User Manual. 2020. Available online: https://www.wamit.com/manualupdate/v74_manual.pdf (accessed on 1 October 2021).

Ward, J. C., Fowler M. J., Viselli A. M., Goupee A. J., and Dagher H. J., "Design and Validation of a Multi-Scale Model Floating Offshore Test Wind Turbine." Nov-2018.

Weller, S. D., Johanning, L., Davies, P., & Banfield, S. J. (2015). Synthetic mooring ropes for marine renewable energy applications. *Renewable Energy*, *83*, 1268–1278. https://doi.org/10.1016/j.renene.2015.03.058

West, W.M.; Goupee, A.J.; Allen, C.; Viselli, A.M. Floating Wind Turbine Model Test to Verify a MoorDyn Modification for Nonlinear Elastic Materials. *J. Offshore Mech. Arct. Eng.* 2021, 1–41.

West, W.; Goupee, A.; Hallowell, S.; Viselli, A. Development of a Multi-Objective Optimization Tool for Screening Designs of Taut Synthetic Mooring Systems to Minimize Mooring Component Cost and Footprint. *Modelling* 2021, *2*, 728-752. https://doi.org/10.3390/modelling2040039

West, W.; Design and Modelling of Synthetic Mooring Systems for Floating Offshore Wind Turbines. Master's Thesis, University of Maine, Orono, ME, USA, 2019.

West, W.M., Goupee, A.J., Viselli, A.M., and Dagher H. J., "The Influence of Synthetic Mooring Line Stiffness Model Type on Global Floating Offshore Wind Turbine Performance The Influence of Synthetic Mooring Line Stiffness Model Type on Global Floating Offshore Wind Turbine Performance," *J. Phys. Conf. Ser.*, 2020.

Wichers J., “Slowly Oscillating Mooring Forces in Single Point Mooring Systems,” in *Second International Conference on Behaviour of Off-Shore Structures*, 1979.

Xu, K.; Larsen, K.; Shao, Y.; Zhang, M.; Gao, Z.; Moan, T. Design and comparative analysis of alternative mooring systems for floating wind turbines in shallow water with emphasis on ultimate limit state design. *Ocean Eng.* 2021, *219*, 108377.

BIOGRAPHY OF THE AUTHOR

William West was born and raised in Maine. He attended high school at the Maine School of Science and Mathematics in Limestone Maine graduating in 2013. After graduating high school Will began pursuing a degree in Mechanical Engineering at the University of Maine. After graduating in 2017 Will had the opportunity to join the offshore wind research group at the University of Maine's Advanced Structures and Composites Center. In 2019 Will was awarded a Master of Science Degree in Mechanical Engineering.

In his free time Will is an avid sport climber. His favorite place to climb is in Rumney, New Hampshire with partners Emily and Winniford Tomak. During his years as a graduate student, great friends were made, good times were had, and lessons were learned in this important place. Will is a Candidate for the Doctor of Philosophy Degree in Mechanical Engineering in May 2022.

Cold War 5.14a Rumney, NH